WIDE-BAND PERFECT METAMATERIAL ABSORBER FOR SOLAR CELL APPLICATIONS

A THESIS SUBMITTED TO THE BOARD OF GRADUATE PROGRAMS

OF

MIDDLE EAST TECHNICAL UNIVERSITY, NORTHERN CYPRUS CAMPUS

BY

PATRICK RUFANGURA

IN PARTIAL FULFILLMENT OF THE REQUIREMENTS

FOR

THE DEGREE OF MASTER OF SCIENCE

IN

SUSTAINABLE ENVIRONMENT AND ENERGY SYSTEMS

AUGUST 2015

Approval of the Board of Graduate Programs

_____
Prof. Dr. Tanju Mehmetoğlu
Chair person

I certify that this thesis satisfies all the requirements as a thesis for the degree of Master of
Science.

_____
Assoc. Prof. Dr. Ali Muhtaroğlu
Program Coordinator

This is to certify that we have read this thesis and that in our opinion it is fully adequate, in scope and quality, as a thesis for the degree of Master of Science.

_____
Assoc. Prof. Dr. Cumali Sabah
Supervisor

Examining Committee Members

Assoc. Prof. Dr. Cumali Sabah	Electrical and Electronics Engineering Dept. METU NCC	_____
Assist. Prof. Dr. Volkan Esat	Mechanical Engineering Dept. METU NCC	_____
Assist. Prof. Dr. Soydan Redif	Electrical and Electronics Engineering Dept. European University of Lefke	_____

I hereby declare that all information in this document has been obtained and presented in accordance with academic rules and ethical conduct. I also declare that, as required by these rules and conduct, I have fully cited and referenced all material and results that are not original to this work.

Name, Last name: Patrick Rufangura

Signature :

ABSTRACT

WIDE-BAND PERFECT METAMATERIAL ABSORBER FOR SOLAR CELLS APPLICATIONS

Patrick Rufangura

M.Sc. Sustainable Environment and Energy Systems Program

Supervisor: Assoc. Prof. Dr. Cumali Sabah

Global adoption of solar photovoltaic (PV) cells as a sustainable substitute to fossil fuel technologies has been impeded by its low efficiency. Generally, efficiency of these devices strongly depends on their ability to absorb radiations of electromagnetic waves incident on them. Their low absorptivity provides a challenge. Metamaterials (MTM) based solar cells offer an opportunity for increasing the system efficiency by enhancing the total absorbed solar radiation incident on solar PV cells. In this thesis a wide-band MTM absorber for solar cell application is proposed. The thesis first explains theories, properties and applications of metamaterials. Different absorber designs, including dual-bands and tunable wide-band perfect MTMs, are then proposed, characterized and numerically discussed. Absorption rates of more than 99% are numerically achieved for all the presented designs. Furthermore, a novel absorber is proposed, where a nearly perfect absorption is gained with a wide-band absorption response of more than 90%, covering a wide frequency range of 98 THz. Thermal and theoretical characterizations of the proposed metamaterial absorber unit cell are also discussed. Lastly, graphene monolayer sheet is integrated to the proposed wide-band MTM perfect absorber structure in order to improve its absorption capability.

Keywords: Metamaterial, perfect absorber, wide-band, solar cells application

ÖZ

GÜNEŞ PİLİ UYGULAMALARI İÇİN GENİŞ-BANTLI METAMALZEME SOĞURUCUSU

Rufangura Patrick

Yüksek Lisans, Sürdürülebilir Çevre ve Enerji Sistemleri Programı

Tez Yöneticisi: Doç. Dr. Cumali Sabah

Sürdürülebilir bir teknoloji olan güneş pili (fotovoltaik) sistemlerinin, fosil yakıt teknolojilerinin yerini alarak dünya tarafından kabul edilmesi, düşük enerji verimlilikleri sebebiyle engellenmiştir. Genel olarak bu aygıtların verimlilikleri, üzerlerine düşen elektromanyetik radyasyonları soğurma yeteneklerine güçlü bir şekilde bağlıdır. Düşük emicilikleri bu konuda çözülmeyi bekleyen bir sonun teşkil etmektedir. Meta malzeme (MTM) tabanlı güneş pilleri, üzerlerine düşen toplam güneş radyasyonunun emilimini artırarak, güneş pillerinin sistem verimliliğini yükseltme imkânı sunmaktadırlar. Bu tezde, güneş pili uygulamaları için, geniş-bantlı MTM soğurucusu tasarlanmıştır. Tez ilk olarak, meta malzemelerle ilgili teorileri, meta malzemelerin özelliklerini ve uygulamalarını ele almıştır. Çift-bantlı ve ayarlanabilir geniş bantlı MTM soğurucu tasarımlarını da içeren farklı meta malzeme soğurucusu tasarımları yapılmış ve bu tasarımların özellikleri sayısal olarak incelenmiştir. Tüm tasarımlar için emicilik oranları 99% ‘’un üzerinde olarak elde edilmiştir. Ayrıca, 90%’ın üzerinde soğurma kapasitesine sahip, 98 THz frekans aralığını kapsayan, geniş-bantlı, yeni bir MTM soğurucu tasarımı yapılmıştır. Tasarlanan MTM soğurucusun termal ve teorik nitelendirilmesi de ayrıca tartışılmıştır. Son olarak, önerilen geniş-bantlı MTM soğurucusunun birim hücresinin soğurma yeteneğini artırmak için bu soğurucunun üzerine tek katmanlı tabaka halinde grafen eklenmiştir.

Anahtar kelimeler: Meta malzeme, Mükemmel soğurucu, Geniş-bant, Güneş pili uygulamaları

DEDICATION

I dedicate this dissertation to the Almighty God who gave me strength and enablement to complete this work, my late father, family and my fiancée for all their inconsiderable support and encouragement.

ACKNOWLEDGEMENTS

As a graduate student at METU, writing a dissertation has being one of the biggest tasks to accomplish before graduation and is always characterized by many responsibilities and challenges which are not easy to accomplish alone. In this dissertation, there are people to whom I owe many thanks to due to their immeasurable contributions.

First of all, I sincerely want to thank my thesis supervisor, Assoc. Prof. Dr. Cumali Sabah who sharpened my interest in metamaterial absorber designs. I cannot afford to forget his impact in my life in the area of scientific research and writing. As a young researcher, his encouragement and support brought me this far thus, we were able to produce this thesis, conference and journal papers which I would not have achieved without his help. I would like also to thank Assist. Prof. Dr. Furkan Dincer for his help on understanding the theoretical modeling of metamaterial absorber. I cannot forget to mention other colleagues in the metamaterial research group; Batuhan Mulla and Mehmet Ustunsoy for their companionship and constructive ideas during this research.

Secondly, gratitude goes to my thesis committee members: Assist. Prof. Dr. Volkan Esat and Assist. Prof. Dr. Soydan Redif for their encouragement, constructive criticisms and suggestions in producing this dissertation without forgetting all my instructors from SEES program. To them, I say thank you.

Thirdly, I would like to acknowledge the Government of Rwanda for their incredible financial support during this two years of my master's studies in METU. Without their help I would not have been in Middle East Technical University, Northern Cyprus Campus and not to talk about thesis writing.

I would like to thank my family for their prayers, support, love and encouragement during my studies, without their provision of my basic education and ethics I would not have reached this far. Many thanks to my father whom God called few months ago, he was my role model and my best advisor towards academic excellence, I cannot forget his statement "very good, but you can do better than this" which was his message anytime he saw my academic transcript.

I also want to acknowledge my beautiful fiancée Bona Uwera for her prayers, support, encouragement and patience during these two years.

Finally, I would like to thank my fellow graduate students in Sustainable Environment and Energy Systems program, Okoye Onyeka Chiemeka, Samuel Asumadu-Sarkodie, Meisam Mohseni and Keunwon Song an alumnus from PSIR department in METU for their help in proofreading this dissertation. In this list I would like to add my best companions Pradeep Jayaweera and my roommate Furkan Ercan for their encouragement during this work.

TABLE OF CONTENTS

ETHICAL DECLARATION iii

ABSTRACT iv

ÖZ v

DEDICATION vi

ACKNOWLEDGEMENTS vii

TABLE OF CONTENTS ix

LIST OF FIGURES xiii

NOMENCLATURE xvii

CHAPTER 1

INTRODUCTION 1

1.1. Metamaterials 1

1.2 Historical Realization of Artificial Materials and Metamaterials 2

1.3. Properties of Materials: Left Hand Materials and Right Hand Materials 3

1.4. Electromagnetic Wave and Materials Interaction: Maxwell's Equations 5

1.5 Electronic Properties of Materials 8

1.6. Optical Properties of Dielectrics and Metals 10

1.7. Applications of Metamaterials 13

CHAPTER 2

METAMATERIALS ABSORBER AND APPLICATION IN DIFFERENT FREQUENCIES RANGE 16

2.1 Introduction 16

2.2. Metamaterials Perfect Absorber in Microwave and Terahertz (THz) Frequency Regime 18

2.3. Metamaterials Perfect Absorber in Infrared and Visible Frequencies Regime 20

CHAPTER 3

DESIGNING A PERFECT METAMATERIALS ABSORBER 23

3.1. Selection of a Numerical Simulation Software 23

3.1.1. Finite Element Method (FEM) 24

3.1.2. Finite Difference Time Domain (FDTD) 24

3.1.3. The Finite Integration Technique (FIT) 25

3.1.4. Validation of FIT Simulation Package 26

3.2. Selection of Geometrical Parameters and Materials 28

CHAPTER 4

DUAL BAND PERFECT METAMATERIAL ABSORBER FOR SOLAR CELLS APPLICATIONS 30

4.1. Resonator Based Dual Band Perfect Metamaterial Absorber for Solar Cell Application 30

4.1.1. Introduction 30

4.1.2. Design and Simulation 32

4.1.3. Results and Discussion 33

4.1.4. Conclusions 42

4.2. A Novel Patches Based Dual-Band Perfect Metamaterial Absorber for Solar Cell Applications 43

4.2.1 Introduction 43

4.2.2 Designing, Simulations and Discussion 44

4.2.3. Conclusions 52

CHAPTER 5

POLARIZATION INSENSITIVE TUNABLE PERFECT METAMATERIAL ABSORBER FOR SOLAR CELLS APPLICATIONS 53

5.1. Structure Design and Geometric Parameters 53

5.2. Simulation and Discussion of Results 54

CHAPTER 6

THE PROPOSED WIDE-BAND PERFECT METAMATERIAL ABSORBERS FOR SOLAR CELL APPLICATIONS 61

6.1. Introduction 61

6.2. Wide Band Perfect Metamaterial Absorber for Solar Cell Application 61

6.2.1. Structure Design and Simulation 61

6.2.2. Results and Discussion 63

6.2.3. Geometry Parametric Study 64

6.2.4. Polarization Angles, Fields and Surface Currents Distributions Analysis 67

6.3. Theoretical Characterisation of the Proposed Wide Band Metamaterial Absorber Using Interference Theory 71

6.3.1. Introduction 71

6.3.2. Extended Interference Theory Model 73

6.4. Thermal Characterization of the Proposed Wide-Band Perfect Metamaterial Absorber 78

6.5. Finite Integration Technique versus Finite Element Method 80

6.6. Conclusions 82

CHAPTER 7

GRAPHENE BASED WIDE BAND PERFECT METAMATERIAL ABSORBER FOR SOLAR CELLS APPLICATIONS 83

7.1. Introduction 83

7.2. Evolution of Graphene Material 84

7.3. Properties of Graphene 85

7.3.1. Electronic and Optical Properties of Graphene 85

7.3.2. Mechanical Properties of Graphene 86

7.4. Applications of Graphene 86

7.4.1. Application in Nanoelectronic Devices 86

7.4.2. Application in Transparent Conductive Films 87

7.4.3. Applications in Sensors 87

7.4.4. Applications in Energy Storage Devices and Solar Cells and Fuel Cells 87

7.5. The Current State of Art in Graphene Application: Graphene Based Metamaterial Absorbers 88

7.6. Wide-Band Graphene Based Perfect Metamaterial Absorber 89

7.7. Conclusion 93

CHAPTER 8

CONCLUSIONS 94

8.1. The conclusions of the thesis 94

8.2. Future work 96

BIBLIOGRAPHY 97

LIST OF FIGURES

Figure 1-1. Geometrical representation of propagation of incident electromagnetic wave in Right and Left handed medium. 5
Figure 1-2. Geometric representation of S ,k, H and E in: (a) Right handed materials and (b) Left handed materials. 8
Figure 1-3. Energy band gab diagram for Conductor, Semiconductor and Insulator. The dashed black line between the conduction and valence bands represent Fermi energy level (E_F) [18]. 9
Figure 1-4. Invisible cloak: Photo by Brian Dodson [25]. 14
Figure 1-5. Electromagnetic wave moving in negative refractive index. 15
Figure 3-1. First metamaterial perfect absorber proposed by Landy et al. [47]. (a) electric resonator(copper), (b) cut wire(copper), (c) axes indicating the direction of propagation of Transverse Electric and Magnetic Wave and (d) simulated results by Landy et al using FDTD (blue, green, and red line represent transitivity, reflection and absorption coefficient, respectively), (e) simulated results with FIT based simulation software. 27
Figure 4-1. (a) A unit cell of the proposed perfect MTM absorber; (b) top view of the proposed design without glass on the top. 33
Figure 4-2. The Simulated absorption and reflection coefficients of the proposed MTM in visible spectrum (450 THz-700 THz). 34
Figure 4-3. (a) A unit cell of the proposed design without ground metallic sheet and intermediate dielectric spacer (b) simulation results of a modified structure. 35
Figure 4. 4. Simulated absorption and reflectance characteristics of the proposed MTM unit cell in Ultraviolet (UV) spectrum range (800 THz-1500 THz). 37
Figure 4-5. Simulated absorption and reflectance characteristics of the proposed MTM unit cell in Infrared (IR) spectrum range (3 THz-450 THz). 37
Figure 4-6. Simulated absorption rate of a designed MTM unit cell in visible spectrum range (450 THz-700 THz) for different geometrical parameters: (a). the structure's periodicity 'x', (b) radius of resonator 'a' and ' b' and (c) thickness "k" of the resonator. 39

Figure 4-7. Simulated absorption coefficient of the proposed structure in visible spectrum range (450 THz-700 THz) for: (a) different polarization angles (b) TM incident wave, (c) TE incident wave. 40
Figure 4-8. Simulated Electric fields distribution for a designed MTM at the resonant frequencies, (a) 543.75.5 THz and (b) 663.5 THz. 41
Figure 4-9. Simulated surface currents distribution of a designed MTM at the resonant frequencies, (a). 543.75 THz and (b). 663.75 THz, respectively. 41
Figure 4-10. (a) Perspective view of the proposed MTM structure unit cell with its geometric parameters, (b). Top view of the proposed design with additional patches on the top of each other. 44
Figure 4-11. (a) Absorption and reflection coefficient of the proposed MPA structure, (b) Absorption rates for the design with additional patches (P) at the top layer (1P-5P). 46
Figure 4-12. A validation of absorption characteristics of the proposed MPA structure using two different software (FIT and FEM based Software) the resonant frequency of 613.4 THz and 700.1 THz. 47
Figure 4-13. (a) Absorption result for different periodicity 'a' for the proposed MPA. (b) Absorption result for different values of thickness of the dielectric spacer 'z'.... 48
Figure 4-14. Electric fields distribution for the proposed MPA structure at 613.4 THz and 701.1 THz, respectively. (a) & (b) Perspective view, (c) and (d) back side view. 50
Figure 4-15. Surface currents distribution of the proposed MPA structure at (a) 613.4 THz and (b) 701.1 THz. 50
Figure 4-16. (a) Simulated absorption rated for different TE polarization angle (ϕ). (b) Simulated absorption rate for different TM polarization angle (ϕ). (c) Simulated absorption results for different incident angle (θ) of EM wave (oblique incident radiation). 52
Figure 5-1.The proposed MPA unit cell. (a) Isometric view and (b) top view (Patches) 54
Figure 5-2. Simulated absorption and reflection rates at resonance frequency of 614.4 THz. 55

Figure 5-3. (a) Front of view of electric field distribution, (b) back view of electric field distribution, and (c) surface current distributions of the proposed MPA design at the resonance frequency of 614.4 THz. 56
Figure 5-4. Absorption characteristics of a proposed MPA unit cell for different dielectric thicknesses‘t’ of dielectric spacer. 57
Figure 5-5. Simulated absorption characteristics of the proposed MPA structure with different patches’ geometric parameters: (a) different values of patches’ periodicity ‘b’, (b) different patches thickness ‘k’. 58
Figure 5-6. Simulated absorption characteristics of a proposed MPA for different incident angles: (a) TE incident wave (θ), TM incident wave (ϕ), and (c) simulated absorption characteristics of the proposed MPA for different polarization angles (γ) of EM wave. 59
Figure 6-1. (a) A unit cell of the proposed perfect metamaterial absorber, (b) Top view of the proposed MPA unit cell (showing resonators)..... 63
Figure 6-2. Simulated absorption rate of the proposed wide band MPA unit cell. (a) Wide band perfect absorption, (b) simulated absorption rate for each ring. 64
Figure 6-3. Simulated absorption results for the proposed wide-band MPA unit cell under different dimension of geometric parameter: (a) different dielectric thickness ‘t’, (b) different thicknesses of resonator ‘k’, (c) different length of structure periodicity ‘x’ and (d) different thickness ‘n’ of a glass layer. 67
Figure 6-4. Simulated absorption characteristics of the proposed MPA structure under different polarization angles and angles of incident EM radiations. (a) TE polarization (θ), (b) TM polarization (α), and (c) different incident angles (∅) of incidence electromagnetic radiations. 68
Figure 6-5. Electric fields distribution for the proposed MPA unit cell at the resonant frequencies of: (a) 565.15 THz, (b) 582.5 THz and (c) 598.75 THz. 69
Figure 6-6. Surface current distributions for the proposed MPA unit cell at the resonant frequencies of: (a) 565.15 THz, (b) 582.5 THz and (c) 598.75 THz 70
Figure 6-7. Multiple reflection and interference theory model..... 73
Figure 6-8. A unit cell of the proposed MPA structure. (a) Coupled model (for numerical simulation) , (b) Decoupled model (for interference theory). 76

Figure 6-9. (a) S-parameters for the decoupled model, (b) Phase angle for S-parameters 77
Figure 6-10. Absorption results for coupled (conventional metamaterial) and decoupled (interference theory) model. 77
Figure 6-11. Absorption characteristics of the proposed wide-band MPA structure at difference value of temperature (100 K-400 K)..... 80
Figure 6-12. (a) The proposed wide-band metamaterial unit cell in FEM simulator, (b) the absorption characteristics of the proposed structure from FIT and FEM. 81
Figure 7-1. Structures representation of some carbon's allotropes including graphene [108]. 83
Figure 7-1. Growth in graphene related researches for a decade (2004-2013) after its discovery [110]..... 84
Figure 7-3. (a) A unit cell of the proposed metamaterial structure with graphene integrated, (b) comparison between enhanced absorption bandwidth using graphene and the results without graphene, (c) comparison between simulation results of the proposed wide-band MTM absorber with graphene using FIT and FM based solvers. 91
Figure 7-4. Absorption characteristics of the proposed graphene based wide-band MPA structure under different geometric parameters. (a) Different value of graphene periodicity 'x', (b) Different thickness 'n' of graphene sheet..... 92

NOMENCLATURE

PV	Photovoltaic
MTM	Metamaterials
METU	Middle East Technical University
PSIR	Political Science and International Relations
μ	Magnetic permeability
ε	Electric permittivity
n	Index of refraction
D	Electric flux density or electric displacement ($C.m^{-2}$)
B	Magnetic flux density (T)
E	Electric field ($V.m^{-1}$)
H	Magnetic field ($A.m^{-1}$)
ω	Angular frequency (Hz)
k	Wave number
K	Extinction coefficient
c	Speed of light ($m\ s^{-1}$)
$\vec{S}$	Poynting vector
ITO	Indium Tin Oxide
W	Tungsten or Wolfram
EM	Electromagnetic
e	Charge of electron ($1.60217657 \times 10 - 19$ C)
Γ	Damping Constant
ω_p	Plasma frequency
ε_0	Permittivity free space (8.85×10^{-12} F/m)
$R(\omega)$	Frequency dependent reflection coefficient
$A(\omega)$	Frequency dependent absorption coefficient
$T(\omega)$	Frequency dependent transmission coefficient
$Z(\omega)$	Frequency dependent impedance
MPA	Metamaterial perfect absorber
$FWHM$	Full Width at Half Maximum

SRR	Split Ring Resonator
TE	Transverse Electric
TM	Transverse Magnetic
VCD	Vibrational Circular Dichroism
ERR	Electric Ring Resonator
FBW	Frequency Bandwidth
PIMNIM	Perfect Impedance Matched Negative Index Material
FIT	Finite Integration Technique
CST	Computer Simulation Technology
FEM	Finite Element Method
FDTD	Finite Difference Time Domain
PDEs	Partial Differential Equations
δ	Skin depth (m)
GaAs	Gallium Arsenide
UV	Ultraviolet
IR	Infrared
Au	Gold
TL	Transmission line
β	Debye temperature (K)
T	Absolute temperature (K)
σ	Electric conductivity (s m^{-1})
ρ	Electric resistivity
C	Carbon
h	Plank's constant ($6.62606957 \times 10^{-34} m^2 kg\ s^{-1}$)
LED	Light Emitting Diode
FET	Field Effect Transistor
TCFs	Transparent Conductive Films
LCDs	Liquid Crystal Displays
OLEDs	Organic Light Emitting Diodes
k_B	Boltzmann's constant ($1.3806 \times 10^{-23}\ m^2 kg\ s^{-2} K^{-1}$)
μ_c	Chemical potential (V)
τ	Electron relaxation time (s)

PBC	Periodic boundary condition

CHAPTER 1

INTRODUCTION

Augmentation of energy demand and scarcity of its resources is one of the major problems the World is facing at the present time. Energy is a key component for industrial and economic development of every country. Even though, fossil fuels continue to supply the needed energy, environmental concern for utilization of fossil fuels in electricity generation, uncertainty on the reserves and continuous increase in global oil prices are core factors for adoption of reinforcing renewable energy technologies. Nuclear energy seemed to be another alternative energy. However, two huge accidents, Chernobyl nuclear plant, Russia, 1986, and Fukushima Daiichi nuclear power accident, Japan 2011, ended the expectation for future nuclear energy advancement [1-2]. Solar energy proved to be one of the best solutions to all the uncertainties linked with energy [3-4]. Solar photovoltaic (PV) cells which are devices for direct conversion of solar radiation into electricity, is among the best technologies to harvest these resources [5-8]. On the other hand, the efficiency of PV has been one of the major problems impeding its global adoption as a sustainable substitute to fossil-fuel-based technologies. Metamaterials (MTM) based solar cells ranked among the new technologies towards increasing the system efficiency by enhancing the absorption coefficient of solar PV cells.

1.1. Metamaterials

Normally, natural materials consist of a combination of individual atoms and molecules which are joined together in a chemical process called bonding. The interaction between natural materials and light (electromagnetic radiation) gives rise to three distinct phenomena: First, when solar radiations hit a material, some of them are absorbed which is called “Absorption”. Secondly, some portion of these radiations which are not absorbed by the materials reflected back by the contact medium to the atmosphere (or environment) which is called “Reflection phenomenon”. Then lastly the portion of radiations which are neither absorbed nor reflected is characterized as

transmittance coefficient. Absorption, reflection and transmission properties of natural materials depend on their atomic/molecular characteristics [9].

Currently, there has been a great deal of interest in creating electromagnetic-based materials from a non-natural sub-wavelength material known as "Metamaterials (MTM)" in order to exhibit extraordinary electromagnetic properties not able to find in nature and different to the conventional materials. Basically, the concept of MTM is derived from the replacement of the natural materials with artificial materials of a much smaller size than the given light wavelength. The interesting properties of MTM are achieved from the degree of the skillfulness of its structure (geometry, shape, orientation and size) while its chemical composition plays a very thin role.

1.2 Historical Realization of Artificial Materials and Metamaterials

Metamaterials emerged later (five decades) after the Second World War. The realization of artificial materials started at the end of 19th century (1898) when Jagadis first performed his experiment on twisted structures' geometries which was basically an artificial element called chiral as the present time researchers call it [10]. Early in 20th century (1914), Lindell et al. [11] created a chiral media by inserting several randomly oriented small wire helices in a host medium. Subsequently, in 1948, Kock [12] also designed a light weight microwave lens by manipulating the conducting spheres, period strips as well as tailoring the effective refractive index of the artificial media. Due to the advancement in science of materials, more synthetic materials were invented which presented unconventional properties. Based on the experiment performed by Lord Rayleigh in 1887 on the periodic multilayers, photonic materials had been developed through the use of the photon of light which led to the creation of photonic crystals [13]. However, the boasting finding achieved in 1968, when Veselago theoretically explored the propagation of plane-wave in a medium of both negative dielectric permittivity (ε) and magnetic permeability (μ) [14]. In his study, he found the group velocity of the given monochromatic plane wave to be propagating in the direction opposing the Poynting vector (energy flux) when travelling in medium (material) of simultaneously negative ε and μ, which is not the case for conventional

material where the group velocity always propagates in a direction parallel with energy flux.

Naturally, the chromatic dispersion (or group velocity dispersion) strongly depends on electric permittivity and magnetic permeability of the materials (medium) through which it is travelling. To explore the extraordinary behavior of materials with simultaneous negative ε and μ, Vaselago suggested three hypotheses. First, he assumed the properties of a material to remain unchanged regardless of simultaneous change of signs of electric permittivity and magnetic permeability. Second, he supposed that existence of materials with negative ε and μ might be in contrast with the fundamental laws of nature (physics). Third, he admitted that if materials with simultaneously negative ε and μ exist, there might have been some properties different from those of positive properties. Due to this mysterious concept, Vaselago's idea had to wait for a couple of decades till 1999 when Smith et al. [15] experimentally constructed and demonstrated existence of the first material with both negative electric permittivity and magnetic permeability. In their study, Smith and his research group also predicted the existence of negative refractive index, which later was explained by Sir Pendry a professor from University of Cambridge [16]. Following these works numerous research groups have turned their attention in this field for different applications. To this days, there are plenty of publications about MTMs for applications in microwave, infrared, THz frequencies and optical spectrum regime of light.

1.3. Properties of Materials: Left Hand Materials and Right Hand Materials

The interaction of a material and electromagnetic wave (light) is affected hugely by the electromagnetic properties like; electric permittivity and magnetic permeability. Usually, electric permittivity and magnetic permeability play a crucial role in the propagation of electromagnetic waves in a medium. This is due to the fact that they are only parameters which are present in the dispersion equation [14]. The electric permittivity defines the interaction between electric field and the contacted medium while magnetic permeability determines how the material reacts to an applied magnetic field and this can be described by the following dispersion relations.

$$k^2 = \varepsilon\mu\omega^2 \tag{1.1}$$

where k and ω describe wave number and frequency of electromagnetic wave, respectively. The relation (1.1) between wave vectors, angular frequency and index of refraction (n) can be transformed and becomes (1.2) and (1.3).

$$n = \sqrt{\varepsilon\mu} \tag{1.2}$$

$$\frac{k}{\omega} = n \tag{1.3}$$

It's obvious from relations (1.1) and (1.2), that changing sign of ε and μ has no impact on these equations. Vaselago explained these by saying that if changing the signs of ε and μ has no impact on equation (1.1) and (1.2), the materials with both negative ε and μ may not exist or even if they exist they must have properties different from those of conventional materials. To explain this he illustrated two concepts. First 'Right handed materials' which are materials or medium in which the monochromatic waves travel in conventional path way and obey Snell's law of refraction [17]. In right handed materials wave vector k, electric field E and magnetic field H also obey the right hand rule. Secondly, he postulated the concept of "Left handed materials" which are the materials or the medium in which monochromatic waves flow in unconventional path way of wave propagation resulting from the simultaneously negative signs of ε and μ in that medium. In such medium the wave vector and energy flux (Poynting vector) travel in opposite direction. In Figure 1-1 the geometrical representation of incident EM in Right and Left handed medium is displayed.

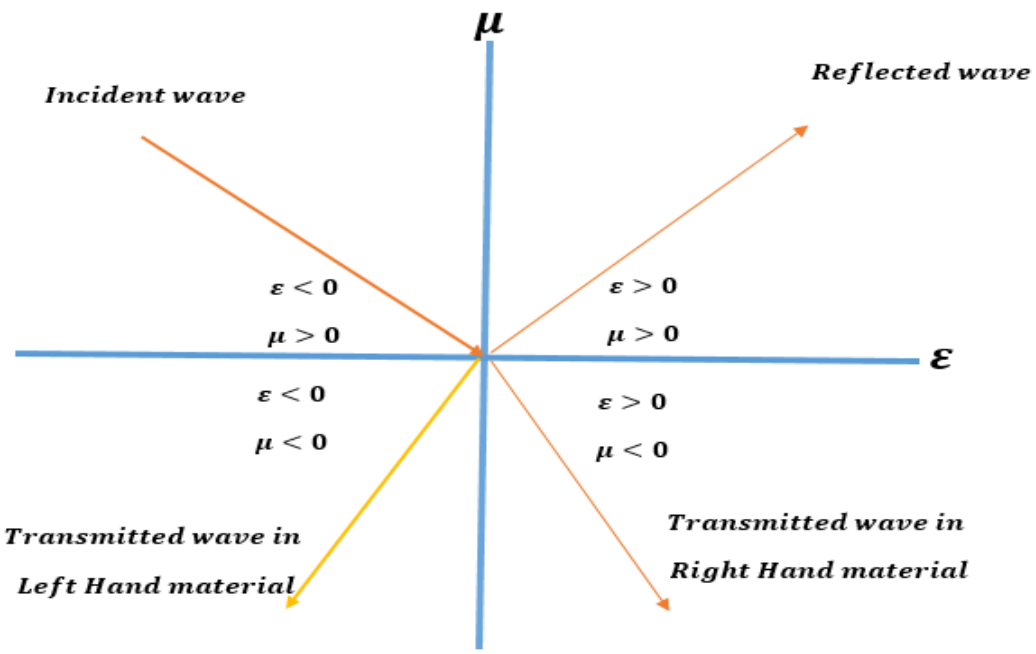

Figure 1-1. Geometrical representation of propagation of incident electromagnetic wave in Right and Left handed medium.

1.4. Electromagnetic Wave and Materials Interaction: Maxwell's Equations

The best way to understand the interaction of light wave and matter and the impact of signs of ε and μ on the propagation properties of materials, is to study Maxwell's equations (1.4-1.7) in an isotropic medium which is controlled by the behavior of a wave in a medium.

$$\nabla . \vec{D} = 0 \tag{1.4}$$

$$\nabla . \vec{B} = 0 \tag{1.5}$$

$$\nabla \times \vec{E} = -\frac{\partial \vec{B}}{\partial t} \tag{1.6}$$

$$\nabla \times \vec{H} = \frac{\partial \vec{D}}{\partial t} \tag{1.7}$$

where D is electric flux density or electric displacement (C/m^2), B is magnetic flux density (T or Vs/m^2), E electric field (V/m) and H is magnetic field (A/m).

In homogeneous isotropic medium, electric and magnetic flux density (D and B) are given by relations (1.8) and (1.9).

$$\vec{D} = \varepsilon\vec{E} \tag{1.8}$$

$$\vec{B} = \mu\vec{H} \tag{1.9}$$

From relation (1.8) & (1.9) Maxwell's equations in isotropic medium become (1.10) & (1.13),

$$\nabla.\varepsilon\vec{E} = 0 \tag{1.10}$$

$$\nabla.\mu\vec{H} = 0 \tag{1.11}$$

$$\nabla \times \vec{E} = -\mu\frac{\partial\vec{H}}{\partial t} \tag{1.12}$$

$$\nabla \times \vec{H} = \varepsilon\frac{\partial\vec{E}}{\partial t} \tag{1.13}$$

In the case of a plane monochromatic wave where electric and magnetic fields are expressed as indicated in relations (1.14) & (1.15);

$$\vec{E}(\omega,\vec{k}) = \vec{E}_0 e^{i(\vec{k}\,\vec{Z}-\omega t)} \tag{1.14}$$

$$\vec{B} = \vec{B}_0 e^{i(\vec{k}\,\vec{Z}-\omega t)} \tag{1.15}$$

Using these relations, Maxwell's equations can be rearranged to become (1.16) and (1.17).

$$\vec{k} \times \vec{E} = -\frac{\omega}{c}\mu H \tag{1.16}$$

$$\vec{k} \times \vec{H} = \frac{\omega}{c}\varepsilon\vec{E} \tag{1.17}$$

with $\vec{k}$, ω, and c representing wave vector, angular frequency of electromagnetic wave and speed of light in free space, respectively. The permittivity and permeability of materials are usually expressed in complex function.

$$\varepsilon(\omega) = \varepsilon'(\omega) + i\varepsilon''(\omega) \tag{1.18}$$

$$\mu(\omega) = \mu'(\omega) + i\mu''(\omega) \tag{1.19}$$

Index of refraction of a material can also be represented in complex function ($\tilde{n}$) as in (20).

$$\tilde{n} = n + iK \tag{1.20}$$

where K designates the extinction coefficient of electromagnetic wave in matter.

As it can be observed schematically in Figure 1-2(a), for a plane monochromatic wave in isotropic medium $\vec{k}$, $\vec{H}$ and $\vec{E}$ are always perpendicular to each other while $\vec{H}$ and $\vec{E}$ are in phase. One can see that simultaneous change of signs of electric permittivity and magnetic permeability affect the signs of (1.16) and (1.17). In Figure 1-2 wave vector, magnetic field, electric field and Poynting vector are geometrically described. If the signs of ε and μ are both positive, equations (1.16) and (1.17) remain unchanged "Right-handed material". But when the signs of ε and μ are simultaneously negative, both equations (1.16) and (1.17) change accordingly "Left-handed material". The behavior of electromagnetic wave travelling in right and left hand material can be defined mathematically by equations for energy flux / Poynting vector (1.21), and wave vector as it is described in Figure 1-2.

$$\vec{S} = \vec{E} \times \vec{H} \tag{1.21}$$

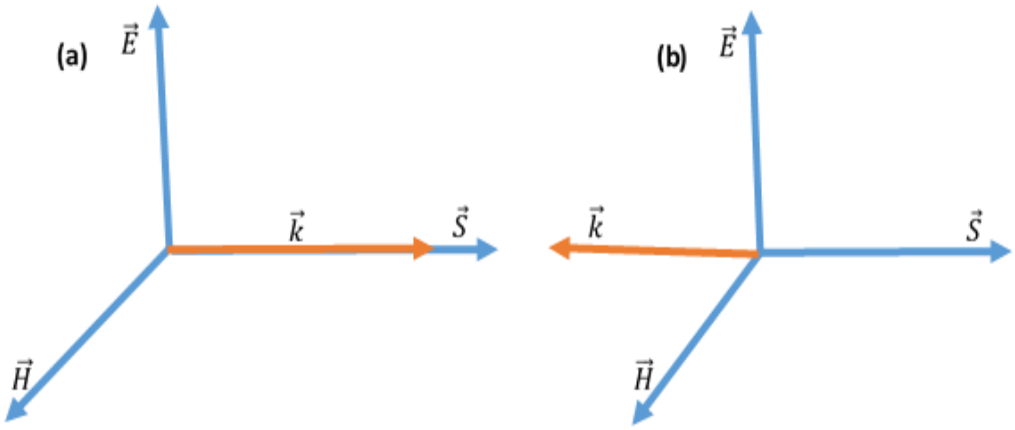

Figure 1-2. Geometric representation of $\vec{S}$,$\vec{k}$, $\vec{H}$ and $\vec{E}$ in: (a) Right handed materials and (b) Left handed materials.

Based on (1.21) in electrodynamics, Poynting vector $\vec{S}$ and the fields $\vec{E}$ and $\vec{H}$ have to obey the right hand rule and energy must flow in the same direction with wave vector $\vec{k}$. On the other hand; in left handed materials, the two vectors $\vec{k}$ and $\vec{S}$ propagate in the opposite directions. Therefore, because vector $\vec{k}$ shows the direction of phase velocity; in the left handed substances energy flows in the opposite direction of the phase velocity. In other word left handed materials are called "negative group velocity materials" [14].

1.5 Electronic Properties of Materials

Metamaterials as the engineered materials, are made from arrangement of artificial unit structures ("metal-atoms/ metal-molecules") which are fashioned from already existing substances and arranged in a periodic shape. The combination of those unit structures form a new material which displays extraordinary properties different from its elementary constituents. Consequently, the response of a metamaterial structure to the electromagnetic wave and its behavior depend entirely on the MTM unit cell (composite materials and their arrangement in a unit cell). Thus, when designing metamaterials, the selection of materials to use and their physical properties (Optical and electronic properties) need to be well considered in order to understand the suitable material for the intended design, application and the wavelength range of interest. Basically, in electronics there are three kinds of materials: insulator/dielectrics, semiconductors and conductors/metals. These material classifications are grounded on

their conductivity characteristics which are explained by energy band structure or electronic energy levels [6, 18]. Electronically every material consists of two basic energy bands; valance and conduction bands separated by an empty space. The conduction band is at the highest energy level and usually empty, whereas valence band is at lowest energy level and partially filled with electrons. The empty space between these two bands is called "band gap or forbidden band" and plays an important role in conductivity capability of materials. In Figure1-3, electronic energy level for conductor, semiconductor and insulator are schematically represented. In conductors/metals the conduction band and valance band are overlapped. Consequently, at a very small applied electric field (small biased voltage) electrons from valence band easily jump to conduction band (metals are good conductors of electricity). The band gap in a semiconductor is larger than that of conductor and smaller than insulator's band gap, thus, more applied electric field is required to move electrons from valence band to conduction band in semiconductors than in conductors. Dielectric, on the other hand, has a huge band gap compared to the other two. Therefore, electrons cannot do that and require much more energy to jump the empty space between the valence band and conduction band, then dielectric are unable to allow flow of electric current (bad conductor of electricity).

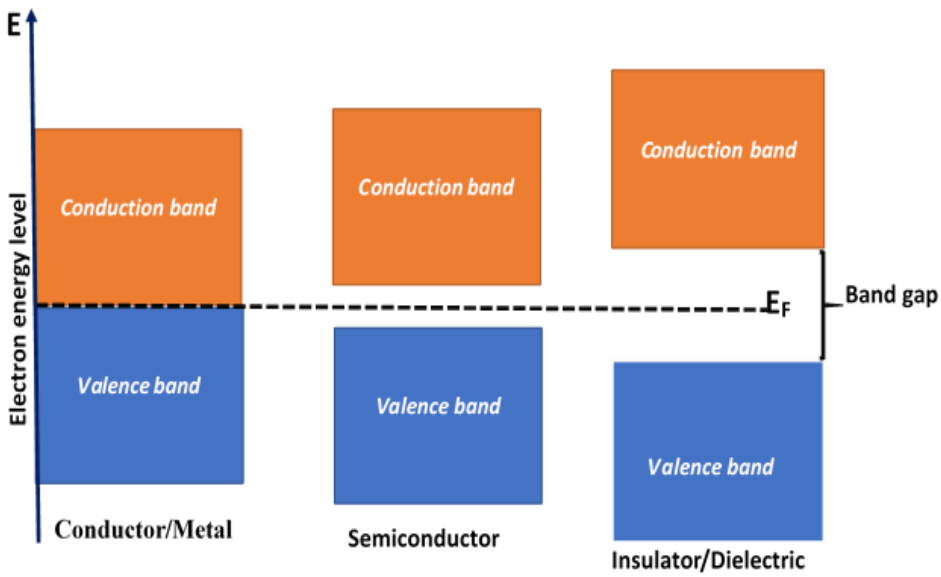

Figure 1-3. Energy band gab diagram for Conductor, Semiconductor and Insulator. The dashed black line between the conduction and valence bands represent Fermi energy level (E_F) [18].

It is not worthwhile enough to classify materials based on their electronic energy bands levels which is due to the fact that some substances behave like metal substances when viewed electronically while optically act as dielectrics. Indium tin oxide (ITO) is one example of those compounds which electronically reacts as a metal substance (outstanding electrical conductivity), while optically behaves like a dielectric material (with excellent optical transparency) and these properties make ITO to be widely used in transparent electrodes in the display and lighting domain. Some metals also display such behavior, like tungsten/ wolfram (W) which is naturally a metal and is used to conduct current in the light bulbs' filaments, but it behaves similar to the lossy dielectric material in visible spectrum range with a positive dielectric constant [18]. Due to their tiny band gap, semiconductor materials, are mostly used in metamaterials designs in the place of dielectric materıals because they are easy to be used in manipulating the propagation path of electromagnetic waves and where it can behave as a lossy/absorber layer or a loss-free substrate depending on the range of the wavelength of interest.

1.6. Optical Properties of Dielectrics and Metals

Since metamaterials are artificially man-made materials formed by periodic arrangement of unit structures of metal and dielectrics arrays, before taking a step forward to design a metamaterial, it is worthwhile to understand first the properties and physical characteristics of its material composition. Generally, in optic industries dielectric materials are widely used elements for fabrication of many optical devices. This is because of the great role played by dielectric materials to effectively control propagation path of electromagnetic wave. Every dielectric material is characterized by its dielectric constant as it is stated in relations (1.8) and (1.9) from the previous section in this chapter. In the process of designing a metamaterial for optical frequency ranges, it is advisable to select a dielectric material which is transparent in this frequency range, failing to do so leads to significant loss of resonance photons in a dielectric and it affects the performance of the designed metamaterial. As described in [18], dielectric constant as a function of frequency can be characterized by Helmholtz–Drude model (1.22).

$$\varepsilon(\omega) = 1 + \sum_i \frac{S_i \omega_i^2}{\omega_i^2 - \omega^2 - i\omega\gamma i} \tag{1.22}$$

With ω_i symbolizing resonance frequency of the ith mode, γ_i and S_i representing the damping constant and the strength of ith mode, in order. On the other hand, metals are not often used in optical components as dielectric materials do, but in metamaterial technology, metals have great importance, due to the fact that they join together with dielectric materials in order to control electromagnetic properties of devices (metamaterial based devices). Similar to dielectric materials, when making selection of the suitable metals in the process to design metamaterials for optical or visible frequency applications they are some important elements to be carefully considered. The reaction of metallic substrates always change depending on the wavelength of the interested electromagnetic wave. Here is to say for instance: the transmittance of certain metals where majority of metallic elements hold high reflection coefficient (low transmittance). The metals of this kind do not allow transmission or propagation of EM wave with contact medium unless its thickness is much smaller that the "skin depth/optical penetration depth" [19]. As it was explained above in Figure 1-3, the reactions and characteristics of metals arise from the disposition of their electron energy level. Since in metals the conduction band and valence band overlap, any incident radiation that hits its surface is enough to excite electron from valence band to conduction; as a result all the light which is able to interact with a metallic layer is totally absorbed (vanish) before penetrating a very long distance (mostly order of tens of nanometers and roughly 50 nm in a visible range). Similar to dielectric materials, the physics behind interaction of light and metal can be explained well by using the dielectric function. The electromagnetic characteristics of metals are hugely governed by the free movement of electrons inside the metals crystalline lattice. In this case, Lorentz Harmonic model is extended for metal, with electrons considered to move spontaneously in the metal lattice without any restoring force to bring them back. At this instance (standard Lorentz Model), the resonance frequency is zero. "Drude free electron model" relation (1.23) is normally used for the motion of electrons in metals, where electron motion is always connected with the incident electric field.

$$m\frac{\partial^2 \vec{r}(t)}{\partial t^2} + m\Gamma\ \frac{\partial \vec{r}(t)}{\partial t} = -e\overrightarrow{E_0}e^{-i\omega t} \tag{1.23}$$

With m and e, Γ , $\vec{r}$ symbolizing the effective mass, charge of electron, damping constant and displacement of the electron from its initial position, respectively. Through algebraic adjustment, the displacement vector can be rearranged to become (1.24).

$$\vec{r}(t) = \frac{e\,\overrightarrow{E_0}\,e^{-i\omega t}}{m(\omega^2 + i\Gamma\,\omega)} \tag{1.24}$$

Mathematical manipulation of equation (1.8) and (1.24) gives the frequency dependency dielectric function relation for metals as in (1.25).

$$\varepsilon(\omega) = 1 - \frac{\omega_p^2}{\omega^2 + i\,\Gamma\,\omega} = 1 - \frac{\omega_p^2}{\omega^2 + \Gamma^2} + i\frac{\omega_p^2\Gamma}{\omega(\omega^2 + \Gamma^2)} \tag{1.25}$$

where ω and ω_p represent frequency of electron and plasma frequency to which electron charge density oscillate, correspondingly. The plasma frequency is given by the relation (1.26), where n and ε_0 represent total number of electrons per unit volume and permittivity of free space, respectively.

$$\omega_p = \left(\frac{ne^2}{\varepsilon_0 m}\right)^{\frac{1}{2}} \tag{1.26}$$

The Drude model in (1.25), consider only free electrons, however, not all electrons in metals are free because some are bound electrons. Even though most of metals' properties tremendously rely on their free electrons reaction, when dealing with visible frequencies and other high frequencies, the bound electron contributions must be taken into consideration. The standard Lorentz model with consideration of bound electrons can be expressed as (1.27).

$$\varepsilon_{ib}(\omega) = 1 + \frac{\omega_d^2}{\omega_0^2 - \omega^2 - i\gamma\omega} \tag{1.27}$$

where ω_0 representing the oscillation frequency of bound electron at an applied electric potential, while γ and ω_d represent density and damping factor of bound electrons, in order.

From the above relations, the final Drude model of metals with inclusion of interband bound electrons together with free electrons is:

$$\varepsilon(\omega) = \varepsilon'(\omega) + i\varepsilon''(\omega) = \varepsilon_{ib}(\omega) + 1 - \frac{\omega_p^2}{\omega^2 - i\Gamma\omega} \tag{1.28}$$

Additionally interband transition has effect on dielectric function for both high and low frequency electromagnetic wave. It is in this case that, when working at low frequencies far from interband resonance, the term $\varepsilon_{ib}(\omega)$ in relation (1.28) must be replaced by ε_∞.

$$\varepsilon(\omega) = \varepsilon'(\omega) + i\varepsilon''(\omega) = \varepsilon_\infty - \frac{\omega_p^2}{\omega^2 + \Gamma^2} + i\frac{\omega_{p\Gamma}^2}{\omega(\omega^2 + \Gamma^2)} \tag{1.29}$$

The theories, measurement and experimental data and other optical properties of metal are discussed more in detail in [18, 20-23].

1.7. Applications of Metamaterials

Due to their interesting electromagnetic properties, discovery and development of metamaterials brought huge potential applications in electromagnetic research industries such as in optics, communications and energy harvesting sectors. This section discuss about some example applications linked to metamaterials.

First applications of MTMs is realization of perfect invisible cloak. Metamaterials concept is capable of controlling electromagnetic fields which led to a novel breakthrough, namely, “invisible cloak.” Based on the idea of light bending and coordinate transformation Pendry et al. proposed the first perfect invisible cloak [24].

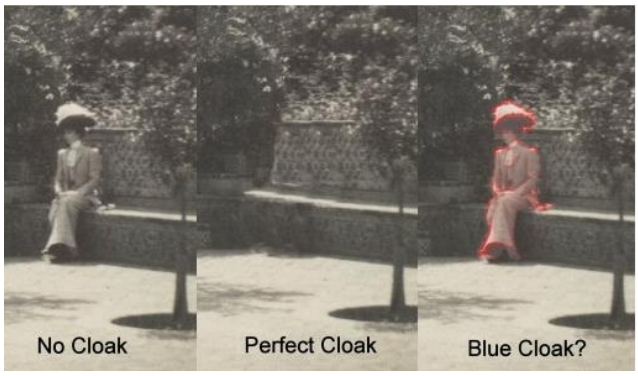

Figure 1-4. Invisible cloak: Photo by Brian Dodson [25].

This concept is mostly used in military domain where cloaked devices like military jet, car and wearing are made to be inhibited or completely prevented from electromagnetic waves (such as radar and other remote sensing devices) emission, as a result the object can be hidden in it and remains undetectable [26-28].

Second potential use of MTMs is their incredible role in developing excellent sensors and antennas [29-36]. Based on surface plasmonic resonance, metamaterials are used to create more sensitive guide modes. Typically, the phenomenon of surface plasmon happens at the interface between metal and dielectric. This phenomenon is strongly affected by the index of refraction of a contacted medium together with the penetration of evanescent depth field [37]. Therefore; a change in the index of refraction of a dielectric alters the propagation constant of the surface plasmon. By applying coupling condition, this leads to the modification of the characteristics of electromagnetic wave coupled with the surface plasmon.

Perfect lens or superlens are another potential application of MTMs. Owing negative electric permittivity and magnetic permeability simultaneously, metamaterials, led to the development of superlens. Professor Sir John Pendry from Imperial College, London, in 2000 using the theory of negative refractive index and metamaterials theory developed the first superlens which was able to break optical diffraction limit. Moreover, resolution of the images and underneath the diffraction limit are made possible by both propagating and evanescent waves [38].

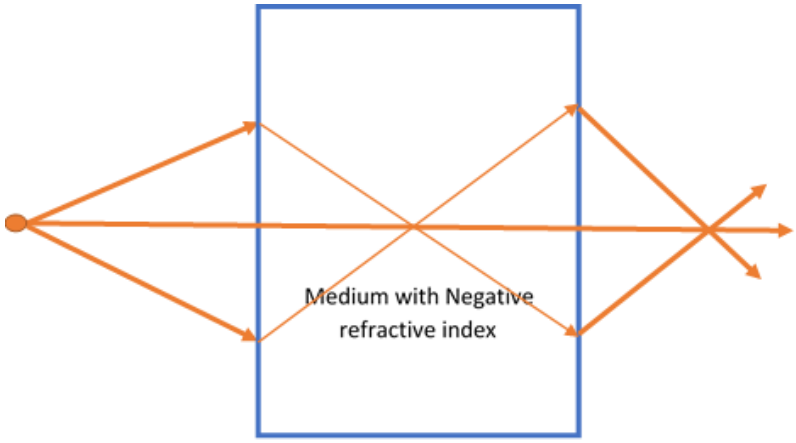

Figure 1-5. Electromagnetic wave moving in negative refractive index.

CHAPTER 2

METAMATERIALS ABSORBER AND APPLICATION IN DIFFERENT FREQUENCIES RANGE

2.1 Introduction

The development of metamaterial has brought about improvement of the absorption coefficient of many devices and has also led to the discovery of other newly high absorber devices [39]. As an artificial material, electromagnetic properties of MTM structure such as electric permittivity and magnetic permeability can be altered through careful arrangement of the metamaterial's geometrical parameters (shape and size) [40, 41].

Normally, the absorption coefficient of a metamaterial is determined by two basic parameters as it is described in relation (2.1).

$$A(\omega) = 1 - R(\omega) - T(\omega) \tag{2.1}$$

where, $R(\omega)$ and $T(\omega)$ represents frequency dependent transmission and reflection coefficients, respectively.

In order to eliminate transmission coefficient, the MTM structure needs to be designed in a way that the imaginary parts of their effective electric permittivity and magnetic permeability are large enough. This is because, they are the only parameters contributing to the loss in metamaterials [42]. Two methods are commonly used to cancel out the transmission losses. The first method utilizes a combination of multiple layers in the metamaterials design in order to block the transmission of EM waves. The second method employs a metallic ground plane with thickness much greater than its skin depth in the working frequency in order to reflect back the transmitted wave [43-44]. Once the transmission losses are eliminated, reflection rate is the remaining threat impeding the achievement of perfect absorption. The reflection rate of a MTM structure can be minimized by controlling its geometrical parameters which leads to the modification of the structure's properties (effective electric permittivity and magnetic permeability) and also regulate the structure impedance. At resonance

frequency, the impedance of MTM structure matches the free space impedance which happens at high absorption rate and very minimum reflection rate (perfect absorption is gained at this moment).

$$Z(\omega) = \sqrt{\frac{\mu(\omega)}{\varepsilon(\omega)}} \tag{2.2}$$

where, $Z(\omega)$ represents the impedance of the MTM unit cell.

Most of MTM absorber designs are made by a combination of metallic layers (conducting electric resonators) and a dielectric substrate embedded in them. The metallic layer/ conducting electric resonators are responsible for the electric resonance through the excitation of electric field, while the dielectric substrates are responsible for the magnetic response that arise from the excitation of antiparallel current on the side of the dielectric substrate. Another important factor needed to be considered, which has much impact on the absorption characteristics of MTM absorber is its response towards the polarized EM waves and its ability to absorb radiations that strikes the resonator's surface at different incident angles [45-46].

Presently, MTM structures which display single, dual and multiple-bands with excellent absorption rate of about a unit (perfect absorption) have been numerically and experimentally achieved in different frequency ranges of electromagnetic wave spectrum. The word perfect in metamaterial absorber research generally used for all metamaterial designs which offer absorption coefficient more than 99%. The first metamaterial perfect absorber (MPA) was proposed by Landy et al. [47] in 2008. They designed a single narrow-band MPA to operate at a frequency ranging from 9 GHz to14 GHz and they managed to achieve a narrow-band with absorption rate of 99% at the resonant frequency of 11.65 GHz which resulted from the strong coupling of the electrical and magnetic resonances.

The work by Landy et al. served as a platform for several research papers that followed in the field of MPA, where currently, lots of research work on MPA have been conducted in almost all the spectrum range of EM wave.

2.2. Metamaterials Perfect Absorber in Microwave and Terahertz (THz) Frequency Regime

In this section, different research works on MPA for microwave and terahertz (THz frequency ranges of electromagnetic wave and their related applications will be discussed.

The first MPA structure proposed by Landy et al. was to operate in microwave frequency range and it had the potential applications in imaging resolutions and application on other devices like bolometers. The unit cell of their MTM structure were made of two metallic layers (electric resonator and cut wire) and a dielectric substrate separating them. The electric ring resonator were responsible for electric coupling while magnetic coupling were produced by antiparallel currents resulted from joining the center wire of electric resonator with a cut wire in parallel plane detached by the dielectric substrate. Moreover, by changing the geometry of the cut wire and electric resonator they were able to modify magnetic resonance of their structure. Their simulation results showed the absorption rate of 99% at 11.65 GHz at resonant frequency with full width at half maximum (FWHM) of 4% with respect to the resonant frequency and they experimentally obtained absorption rate of 88% at the same resonant frequency.

One year later, Costas M.Soukoulis et al. from University of Crete (Greece) numerically and experimentally proposed a wide angle and polarization insensitive chiral metamaterial absorber to operate in microwave frequency regime [42]. Their MPA structure were composed of a ground metallic plane covered with a dielectric substrate. They covered the top of the dielectric space with split ring resonators (SRRs) which generated electromagnetic fields response. Their simulation results for different polarization angle (0° to 70°) provided absorption rate of above 90% for both TE and TM waves and 98% for TE wave at all radiations ranging from normal (0°) incident angle to 60°. Subsequently in 2010, Y. Feng et al. [48] numerically and experimentally proposed a polarization modulation scheme of electromagnetic wave through reflection of tunable metamaterial reflector/absorber which was made by coupling the resonators in a metamaterial unit cell with microwave diodes. The geometrical

parameters of their design permitted them to electrically control the polarization state of electromagnetic wave by applying different modulation signals on the diode. Their proposed MTM structure was reported as a good candidate for fabrication of ellipsometry, Vibrational Circular Dichroism (VCD) spectroscopy and also manufacturing of devices for telecommunication purpose. In 2011, J. Zhou et al. [49] from Tsinghwa University (Beijing in China) based on destructive interference proposed an extremely broadband metamaterial absorber for microwave frequency regime. By using multilayers SRRs feature composite metamaterial they made an appropriate dispersive index of refraction which was capable to induce successive antireflection at a wide frequency band. Numerically they achieved a strong absorption bandwidth of about 60 GHz for the frequency ranging from 0 GHz to 70 GHz. Their design had potential application in designing and optimization of transmittance devices and fabrication of broadband absorber in stealth technology [49]. Furthermore, dual and multiple-bands metamaterial absorbers for Microwave frequency regime were proposed such as the one presented by Long Li et al. [50] and Y. P. Lee et al. [51]. In their report, Li et al. presented a metamaterial design which consisted of a periodic arrangement of tetra arrow resonators (operating at three different resonant modes) disposed at the top of a dielectric substrate and a metallic ground plane. When they adjusted the geometry of their MTM unit cell, dual-bands (at 6.16 GHz and 7.9 GHz with 99% absorption rate) with polarization independency and wide angle absorber was obtained. But in reference [51] a metamaterial absorber for microwave frequency was proposed, which was made of the arrangement of donut-shape resonator and ground metallic plate with a dielectric material sandwiched between the two. By using numerical simulation and experimental verification; multiple-bands with near a 100% absorption rate were achieved and the absorption capability of their MPA structure was independent of incident angles for both TE and TM waves.

Furthermore, metamaterials absorber development goes beyond microwave frequency regime to terahertz. In 2008 Tao et al. [52], numerically and experimentally proposed the first metamaterials absorber in terahertz frequency regime which provided a single-band with absorption rate of 98% at 1.12 THz and 70% at 1.3 THz from numerical simulation and experimental characterization, respectively. The realization of the first MTM absorbers in THz frequencies brought great interest for the manufacturing of

narrow-band and low thermal mass absorbers which are important components in the fabrication of thermal sensors. In the article [53], they also designed, fabricated and characterized a metamaterial absorber (absorption rate of 97% at 1.6 THz) with higher flexibility and presented ability to keep high absorption rate for a wide angle of incident in terahertz frequencies. Their MPA design proved to be a potential candidate for nonplanar applications. In 2012, Chen [54] employed interference theory to develop a narrow band metamaterial absorber with nearly a unit absorption rate at 1 THz. In addition, metamaterial absorber designs with dual-bands, triple-bands and broadband response in microwave and terahertz frequencies range were proposed [55-58].

2.3. Metamaterials Perfect Absorber in Infrared and Visible Frequencies Regime

With the continual advancement in the study of metamaterial absorbers, researchers have been able to design MPA in higher frequency ranges (Infrared and Visible frequencies). Padilla et al. [59] demonstrated the first metamaterial absorber to exhibit perfect absorption in infrared region of EM wave. Their MPA structure experimentally revealed excellent absorption rate of 97% at a wavelength of 6 μm which agreed with their results from numerical simulation. They were able to achieve this result by designing a metamaterial structure which consisted of periodic combination of metallic cross resonator (ERR), dielectric spacer and a ground metallic plane (to prevent transmission of EM radiation). The cross resonator were responsible for strong uniform electric field resonance and a slight magnetic resonance where through trimming metallic ground plane with the top cross resonator, antiparallel currents were generated which produced strong magnetic field resonance. By adjusting the metamaterial structure geometric parameters, impedance of their MPA design were able to match the one for free space, thus the reflection were minimized to the negligible value and almost a perfect absorption was obtained [59]. Their designs have potential application in hyperspectral subsampling imaging. Subsequently, Avitzour et al. [60] in 2009 also published a research paper on metamaterial perfect absorber in infrared range where by using an anisotropic perfect impedance matched negative index material (PIMNIM) technique, they managed to gain nearly a 100% absorption rate. Their MPA structure gave the same results for the wide range of incident angle

for infrared radiation and their MPA design offered a great opportunity in fabrication of infrared imaging and coherent thermal sources. Several works on MPA in infrared radiation frequencies have been realized with different absorption characteristics and divers applications [61-66].

Developing metamaterial absorber for a visible spectrum of EM wave has been a challenging task to achieve compared to other frequency ranges. This is because of the ability of metamaterial absorbers to respond to the incoming EM radiations which always depend on its effective electric permittivity, and magnetic permeability and these parameters must appear homogeneous for the incident EM radiation in order for a MTM structure to perfectly absorb all incident radiations. As a result, the unit cell of metamaterial absorber needs to be much smaller (subwavelength) than the wavelength of interest and this causes fabrication challenges in visible frequency range where a unit cell must be in the range of tens of nanometers. Despite the fabrication issues of MPAs in visible region, some works have been realized in this range and lots of applications associated with MPAs structure have been proposed. Most of the metamaterial absorbers in visible range are designed using three basic techniques: surface plasmon technique, structure grating and periodic arrangement of nanoparticles structure [67]. In surface plasmon technique, the perfect absorption in visible frequency is achieved from the localized surface plasmon resonance which results from coupling the top layer (resonators) and the ground metallic plane of the MTM structure. Duan et al. [68], proposed a polarization insensitive and wide angle broadband metamaterials absorber with absorption nearly a unit in visible frequency range using surface plasmon technique. Their metamaterial design consisted of two metallic sheets (gold) separated by Kerr dielectric spacer. By choosing the ground metallic layer of thickness greater than its skin depth in visible frequency they succeeded in eliminating radiation losses associated with transmission to the ground plane. Thus, in order to maximize the absorption of their unit structure, they enhanced the transmission of the top layers (resonators) which was achieved through two mechanisms: first, excitation of surface plasmon polaritons (resulting from periodic arrangement of the subwavelength structures) and second, localized surface plasmon resonances which resulted from the size, shape, orientation and geometry of the structure. With these two mechanisms, impedance of their MTM structure matched

that of free space at resonance frequency and they were able to gain four nearly perfect absorptions. The broadband MPA unit cell by Duan et al., offered potential applications in solar cell, thermal detector imaging and so on [68]. Subsequently, Wu et al [69] proposed a metamaterial based integrated plasmonic absorber/emitter to be utilized for solar thermal photovoltaic energy harvesting in visible frequencies regime. L. Mo et al. [70] in 2014 also proposed enhanced broadband absorber. In their study, gold absorbers were designed both theoretically and experimentally based on plasmonic tapered coaxial holes and the absorption of 93% with polarization independent which was theoretically achieved in visible frequency region. In addition, the metamaterial absorbers with perfect absorption coefficient and broadband absorption which also keeps the same value of absorptivity for a wide range of incident angle for EM wave were also proposed and discussed in [71-73].

CHAPTER 3

DESIGNING A PERFECT METAMATERIALS ABSORBER

The previous chapters elaborated the properties of metamaterials and the important parameters which contribute to their superior properties. One of the most important steps in the process of designing perfect metamaterial absorber structures is the selection of their size, shape and geometrical orientation (geometrical parameters) for any intended metamaterial absorber unit cell. The reason is that the absorption characteristics of metamaterial absorber relies much on its geometric disposition rather than its materials chemical composition. The Drude model [18], plays a crucial role in the selection of the appropriate materials for metamaterial absorber design. Another vital step in the process of designing a metamaterial absorber is the decision on which numerical simulation software to use for characterization and designing a MTM absorber unit cells. Lots of computer software are commercially available on the market and each software presents its own advantages and limitations in the process of designing metamaterial absorbers. In this thesis, a Finite Integration Technique (FIT) based computational software is used for the design and characterization of the proposed metamaterial absorber. However, in order to validate the simulation results from FIT technique, another numerical simulation software which uses Finite Element Method (FEM) has been employed for one of the proposed designs.

3.1. Selection of a Numerical Simulation Software

In the study of electromagnetic field problems, the selection of an appropriate numerical simulation package to be used for that particular issue is a vital step. Thus, the decision on the numerical package software needs to be made carefully paying attention to the type of electromagnetic wave problem understudied and the frequency range of interest. Three basic criteria are considered in the selection of software packages for electromagnetic field problems: the memory requirement, the geometrical modelling accuracy and, the numerical solver and the time taken by the solver to complete the simulation. Several numerical solvers for simulation of electromagnetic wave problems are commercially available on the market, but each solver presents its own advantages and disadvantages depending on the type of EM

wave problems intended to solve. The methods which are widely used for numerical analyses of electromagnetics are but not limited to: Finite Element Method (FEM), Finite Difference Time Domain technique (FDTD), Modal methods and Finite Integration Technique [75].

3.1.1. Finite Element Method (FEM)

FEM is a numerical method for comprehending approximation solutions to the boundary value problems of partial differential equations (PDEs). This technique works in a way that the continuous domain is substituted by the subdomains (finite elements) and it uses interpolation functions to represent unknown function [75]. Advantages of FEM is that it has a high geometrical flexibility in modeling curvilinear geometric structures with no uniform material parameters, is also easy to modify, and dynamic. The drawbacks with this method are:

- High memory requirements, as a results it is not easy to find a suitable solver with this method.
- Problematic in discretization of time harmonic Maxwell's equations.
- Limitation in computing fast iterative solver such as flop to computing Maxwell's equations at higher frequency regime [75].

3.1.2. Finite Difference Time Domain (FDTD)

FDTD is a numerical analysis method used to solve electromagnetic fields problems which was invented by Yee [76]. FDTD method is a part of grid differential numerical modeling technique and approximates all spatial and temporal derivatives of the time dependent Maxwell's equations using finite difference expressions. Advantages of FDTD are:

- FDTD is free from matrix which means that it is not necessarily dependent on iterative solver.
- FDTD is easy and simple to use and it allows parallel computation which is an important factor for simulation of 3D structures at higher speed with higher accuracy.

The disadvantage of FDTD is that, it necessitates the whole computational domain to be gridded with the grid discretization sufficiency enough for resolution of both smallest geometrical structure and smallest electromagnetic wavelength in the model. This leads to a very long computational time. As a results, this technique is not a better choice for computation of very small structures.

3.1.3. The Finite Integration Technique (FIT)

FIT method transforms the integral form of Maxwell's equation into a linear systems of equations. FIT is a suitable method for modeling of homogenous medium and is closer to FDTD technique where both methods utilizes Yee Cartesian mesh [76].

FIT discretizes the integral form Maxwell's equations into a pair of interlocked discretization grids. This is to say that the structure after being analyzed is discretized into mess cells which splits up the calculation domain into several grid cells. This mesh given by the computer user while the simulation software sets a second orthogonal grid to the first one created by the user and the overall description of the system is given by the two. Afterward, the scattering parameter and far field radiation pattern results of the systems can be obtained and analyzed.

FIT method has one of the best accuracy modeling technique and is easy to implement. It allows effectiveness parallel computing and offers more accurate results for computation of complex designs and is flexible for geometrical modeling. The weakness of this method is that, it uses Yee Cartesian mesh which causes complication in computation of non-orthogonal complex designs.

In this thesis, FIT method has been employed for all numerical simulations, which is mainly due to the fact that this technique is simple to operate, more flexible and offers more accurate results for simulation of 3-D EM wave structure problems. Besides, FIT method has been used by many researchers in their analysis of electromagnetic wave problems at different frequency ranges of solar spectrum and has been proven to offer the better results [75, 77-79].

3.1.4. Validation of FIT Simulation Package

Throughout this thesis FIT based simulation package is being used for numerical modeling of metamaterial absorber structures. In order to validate the software, a metamaterial absorber which was numerically and experimentally proposed by Landy et al [42] has been redesigned and characterized with FIT based numerical solver.

In the modelling of their MPA unit cell, Landy et al used a commercial FDTD solver Microwave Studio by Computer Simulation Technology (CST); by applying appropriate boundary conditions "perfect electric along $\hat{y}\hat{z}$-plane, perfect magnetic along $\hat{x}\hat{z}$-plane and the waveguide ports on the other boundaries" they created a near perfect absorber metamaterial which displayed absorption rate of 99% from numerical simulation and experimentally obtained absorption rate of 88% at the resonant frequency of 11.65 GHz. Their MPA structure (geometry and materials composition) is replicated in this thesis by using FIT based simulation software, and with the use of the same boundary conditions. In Figure 3-1, a unit cell of MPA proposed by Landy et al. is geometrically represented along with its simulation results. Their unit cell geometric parameters (in mm) are: $a_1 = 4.2$, $a_2 = 12$, W = 4, G = 0.6, t = 0.6), cut wire dimensions (L = 1.7, H = 11.8).

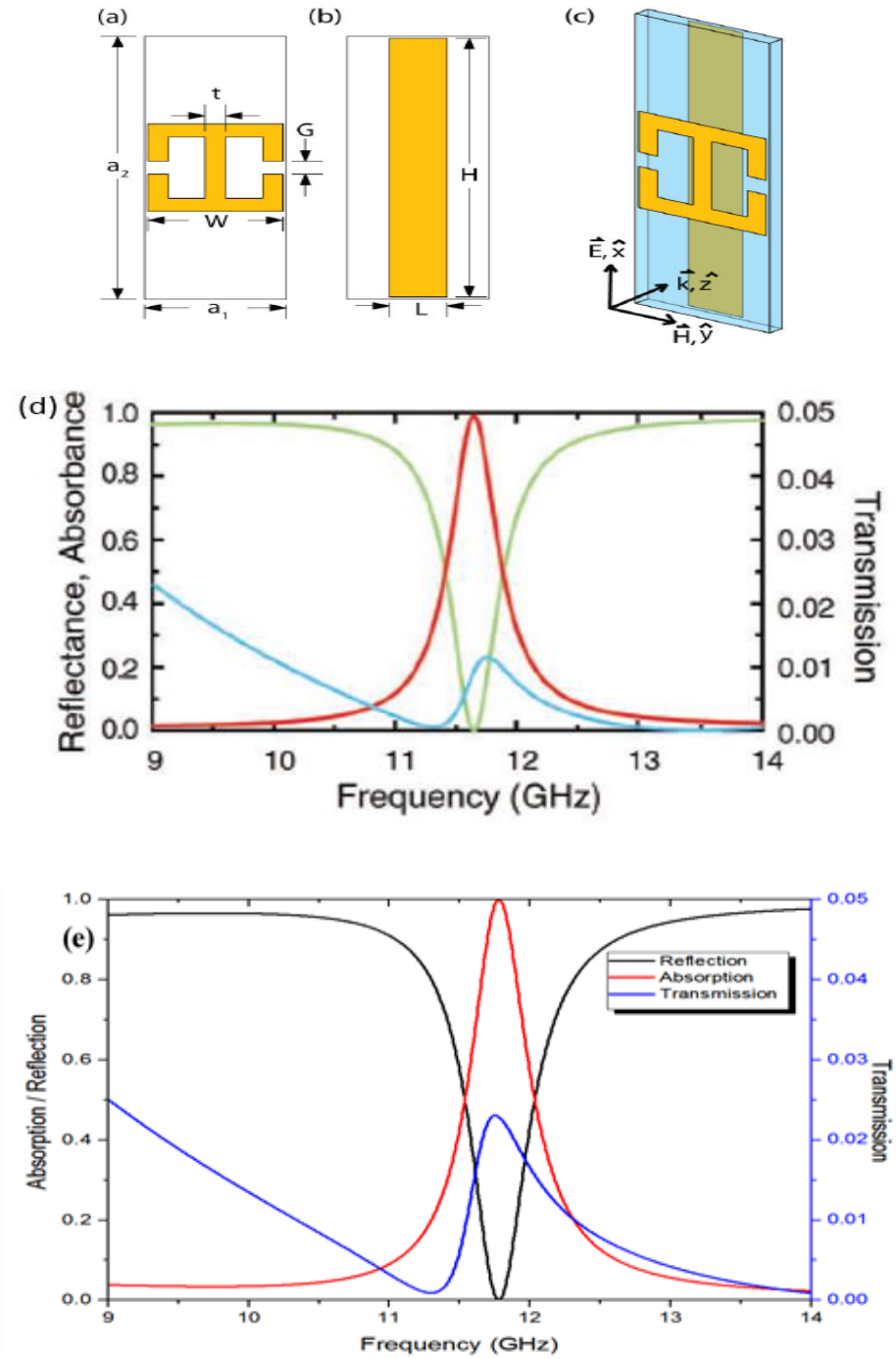

Figure 3-1. First metamaterial perfect absorber proposed by Landy et al. [47]. (a) electric resonator(copper), (b) cut wire(copper), (c) axes indicating the direction of propagation of Transverse Electric and Magnetic Wave and (d) simulated results by Landy et al using FDTD (blue, green, and red line represent transitivity, reflection and absorption coefficient, respectively), (e) simulated results with FIT based simulation software.

Similar to the results obtained by Landy et al, a narrow single-band absorption rate of about 99% with frequency bandwidth (FBW) of about 4% is gained at the resonant frequency of 11.7GHz. Despite a small shift (0.05GHz shift to the right) observed from the central frequency, the simulation results for both method (FDTD based solver by Landy et al and FIT based solver used in this thesis) offer similar results which is a confirmation of the exactness of the numerical solver used in this thesis.

3.2. Selection of Geometrical Parameters and Materials

The selection of the geometrical parameters (size, shape and orientation) for an intended metamaterial design is another important step after deciding on the suitable type of software to employ in the study of metamaterial absorbers. This is because the interaction of metamaterial absorber with electromagnetic wave and their response rely strongly on the values of $\varepsilon(\omega)$ and $\mu(\omega)$ and these parameters are dependent on the size, orientation, and the shape of the MTM structure and the wavelength of interest. Consequently, $\varepsilon(\omega)$and $\mu(\omega)$ are accountable for electromagnetic fields resonance in a MTM designs. This is one of the reasons why several scholars define metamaterial as unnaturally occurring materials whose properties are derived from its geometry instead of its materials chemistry composition. Therefore, depending on the purpose of the metamaterial structure to be designed, the resonators (electric ring resonators "ERR" and split ring resonators "SRR") size or average surface roughness must always be much smaller than the wavelength under consideration ($L \ll \lambda_0$) in order to overcome the scattering parameter effects [67, 80]. Widely used resonators are made of a very thin size noble metal sheet such as gold, silver and others metallic elements (aluminum, lead, copper and so on). MPA as a composite structure, consists of more than two layers (combination of metallic layers and dielectric spacer), thus after selection of geometric parameters and appropriate material for the resonators; one needs to determine the geometry and materials characteristics of dielectric layer and the ground plane substrate. In many MPA designs, the ground plane are made of metallic based materials which play the role to preventing the escape of EM radiation to space (transmission losses) by reflecting back the radiations to the dielectric layer

instead. In order to eliminate these losses, a metallic ground plane of thickness much greater than its skin depth or penetration depth (δ) is normally used.

$$\delta = \frac{c}{\omega \times \tilde{k}(\omega)} \tag{3.1}$$

where, c represents the velocity of light, ω is angular frequency of EM wave and $\tilde{k}$ is the extinction coefficient while δ represents the skin depth. As the main duty of ground metallic is to avoid any escape of radiations back to the space; once it is well selected, the dielectric spacer and resonator are the only remaining layers to be observed carefully. Thus, by choosing a very good dielectric lossy material and carefully coupling the top resonator with ground plane, absorption rate can be enhanced and even reach about a unit (perfect) absorption at the moment where the MTM structure's impedance matches the free space impedance ($Z(\omega) = Z_o(\omega)$). Besides, the selection of a dielectric material and its geometric size are subject to the EM wave frequency ranges of interest. This is because every dielectric material has strength and weakness vis-à-vis the wavelength to be exploited and depending on the intended application. For example, when one wants to design an optical metamaterial, the selected dielectric material must appear transparent for all radiations in the wavelength range under consideration [18].

CHAPTER 4

DUAL BAND PERFECT METAMATERIAL ABSORBER FOR SOLAR CELLS APPLICATIONS

Metamaterial absorbers demonstrated ability to be one of the best candidates to enhance the absorption capabilities of solar cells. From the time a first metamaterial absorber was realized by Landy to this day, several studies about metamaterial absorbers have been conducted. The challenge still existing is that most of those MPA designs are designed to work in low frequency ranges such as microwave frequencies, terahertz frequencies and infrared frequencies regime which cause limitation in their applications. Another challenge is that majority of them display narrow bands response which impede their effective use in solar energy harvesting devices.

In this chapter, dual-bands perfect metamaterial absorber structures for solar cell applications are proposed and discussed. The first structure is designed using the resonator as a source of electric and magnetic fields resonance while electromagnetic resonance for the second proposed dual- bands MPA design created by periodic arrangement of the patches on the top of a dielectric spacer.

4.1. Resonator Based Dual Band Perfect Metamaterial Absorber for Solar Cell Application

4.1.1. Introduction

Resonators “electric ring resonator (ERR)” and “split ring resonator (SRR)” are the widely used techniques for designing and fabrication of perfect metamaterial absorbers [54, 81-83]. This is because they help in controlling propagation path of electromagnetic wave, where by well placing them on the top of a dielectric spacer yield electromagnetic resonance which causes absorption of incident EM radiations while also preventing reflection of radiations back to the space. The only drawback with the use of resonators is that they are not easy to fabricate mostly when the intended MTM structure is to operate in short wavelength (visible and far infrared) where their thickness are of order of tens of nanometers.

In this thesis a new resonator based dual-bands perfect MTM absorbers for solar cell applications is suggested. The proposed design, offers two high peaks absorption in visible frequency regime. By well toiling the geometrical parameters of the proposed MPA unit cell enhancement of absorption rate is achieved. The MPA structure unit cell consists of metal-dielectric- and a glass lossy on the top of gold layer embedded a dielectric material. Geometrical parameters and materials properties of the proposed design are manipulated in order to gain dual - bands nearly perfect absorption at the resonant frequencies.

Naturally, when EM radiations hit the surface of solar cells, three different phenomenon take place. Some of the radiations are reflected back to the space, others are absorbed by the cells while others are transmitted through the cells to the space. For the case of high frequencies range; the scattering parameters which are the function of electric fields are defined to help understanding the physics behind these mechanism [84].

$$S_{11} = \frac{\int port\ 1\left((E_c - E_1).E_1^*\right)dA1}{\int Port1\ (E_1.E_1^*)dA1} \tag{4.1}$$

$$\mathrm{S}_{12} = \frac{\int \mathrm{port}\ 1\left((\mathrm{E_c} - \mathrm{E}_1).\mathrm{E}_1^*\right)\mathrm{dA1}}{\int \mathrm{Port2}\ (\mathrm{E}_2.\mathrm{E}_2^*)\mathrm{dA2}} \tag{4.2}$$

where, E_c is the computer electric field on the port, $E_1$and E_2 are the electric field on ports 1 (input port) and port 2 (output port), respectively. Ability of solar cell to absorb incoming EM radiations, determine how much power the solar cell is gaining. On the other hands, high reflection and transmission coefficients decrease the power gained by the cell as it can be seen from relation (4.5).

$$\mathrm{S}_{11}(\omega) = \frac{\sqrt{\text{power reflected from port1}}}{\sqrt{\text{power incident on port1}}} \tag{4.3}$$

$$\mathrm{S}_{12}(\omega) = \frac{\sqrt{\text{power delivered to port2}}}{\sqrt{\text{power incident on port1}}} \tag{4.4}$$

$$\mathrm{A}\ (\omega)\ = 1 - |\mathrm{S}_{11}\ (\omega)|^2 - |\mathrm{S}_{12}\ (\omega)|^2 \tag{4.5}$$

where $A(\omega)$ is power gain by cell (absorption rate), $S_{11}(\omega)$ and $S_{12}(\omega)$ are scattering parameters expressed in function of power flow from reflected and transmitted radiations. Thus, in order to optimize the power gain (absorption) by the cells; reflected and transmitted radiations need to be minimized as much as possible. Fortunately; in the present study transmission losses have been eliminated by employing metallic substrate at the back of the proposed MPA unit cell. As a result relation (4.5) is replaced by the following relation (4.6) in this study.

$$A(\omega) = 1 - |S_{11}(\omega)|^2 \tag{4.6}$$

4.1.2. Design and Simulation

The proposed design consists of a solid structure as it is shown in Figure 4-1. The bottom layer of the structure taken to be two gold loss metal “Au” (yellow color) holding between them a dielectric material which is chosen to be gallium arsenide “GaAs” (blue color).On the top of the bottom substrates, there is a cylindrical metal (gold) layer filled with GaAs which is responsible for generation of circular surface currents to produce magnetic resonance. Finally, a glass Pyrex lossy layer (grey color) is placed on the top. A glass Pyrex layer on the top is chosen due to its ability to transmit higher visible light and to stand against heat expansion, employing it on the top facilitate enhancement of transmitted radiations that reaching the absorber part (resonator) of MPA structure. All metallic layers (resonators and ground substrate) is taken to be gold lossy and it is selected based on its excellent absorption and reflection capability in the presence of electromagnetic wave. It is also chosen because it has ability to resist against excessive heat [85]. The electric conductivity and thermal conductivity of gold are 4.561×10^{7} Sm^{-1}, and 314 WK^{-1} m^{-1}, correspondingly. Glass Pyrex lossy on the top layer has tangent delta electric constant and thermal conductivity of 0.0054 and 1.1 $WK^{-1}m^{-1}$, separately. In Figure 4-1 the unit cell of the proposed MPA is portrayed.

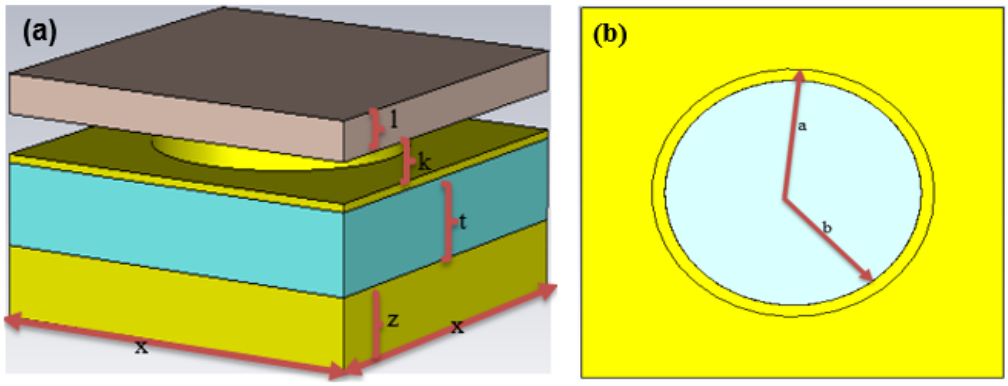

Figure 4-1. (a) A unit cell of the proposed perfect MTM absorber; (b) top view of the proposed design without glass on the top.

The structure geometric parameters are: x=520 nm, z=70 nm, t=80 nm, n (the thickness of Au layer on the top of GaAs spacer) =8.33 nm and l=70 nm. The geometry parametric of the resonator are: inner radius (for a dielectric) a=173.3 nm, outer radius (metal cylindrical strip) b= 157.4 nm and the height k=39 nm.

The simulation is performed by using full wave simulation package based on Finite Integration Technique (FIT) with frequency domain solver. The structure intended to work at frequency ranging from 450 THz to 700 THz and electromagnetic radiations are polarized in a manner that the electric (*E*) and magnetic (*H*) fields are parallel with the design plane while wave vector (*k*) is perpendicular to the structure's geometric plane. The boundary conditions are chosen to be electric and magnetic along x and y directions, respectively. While the simulations environment (z- plane) selected to be open free space.

4.1.3. Results and Discussion

The simulation results shows two peak bands in visible frequency range of solar spectrum. In Figure 4-2, the simulated results in visible frequency range (450 THz - 700 THz) are represented. As it can be observed, dual - bands with perfect absorption (absorption near a unit) are obtained at 543.75 THz and 663.75 THz frequencies with absorption rate of 99.99% and 99.90%, respectively.

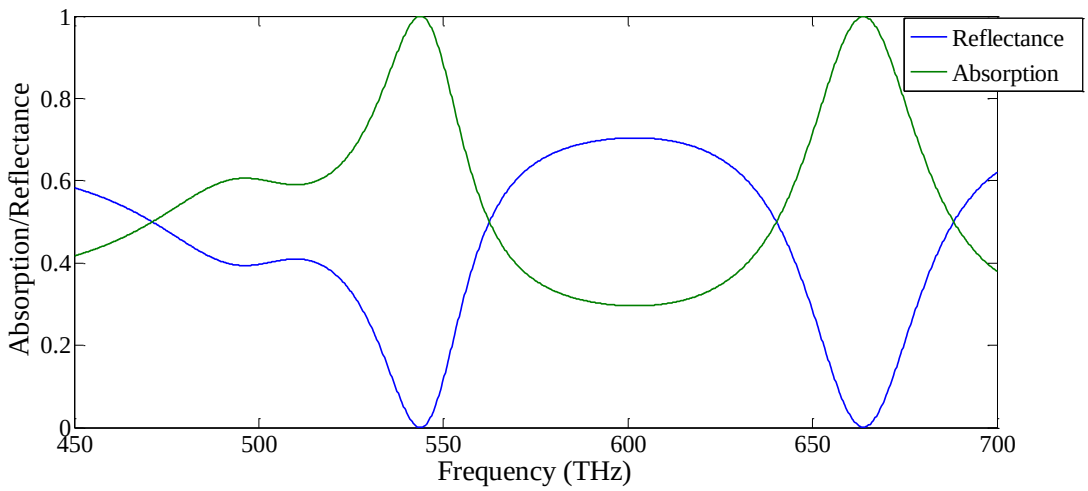

Figure 4-2. The Simulated absorption and reflection coefficients of the proposed MTM in visible spectrum (450 THz-700 THz).

Normally, the perfect absorption is a result of impedance matching and requires more than one or more resonant absorption [60]. This happens by carefully toiling a metamaterial structure geometric parameters which leads to alteration of both electric permittivity ($\varepsilon(\omega)$) and magnetic permeability ($\mu(\omega)$) of the MTM design. By doing this, electromagnetic properties of MTM structure can be adjusted to match the electromagnetic properties of free space and for certain values of dielectric thickness, the impedance of free space (air) matches the impedance of the MTM structure $Z_0\ (\omega)\ = Z\ (\omega)$ at resonance frequency with a very minimum reflection coefficient.

$$Z(w) = \sqrt{\frac{\mu(\omega)}{\varepsilon(\omega)}} \tag{4.8}$$

$$\mathrm{Z_0(w)} = \sqrt{\frac{\mu_0}{\varepsilon_0}} \tag{4.9}$$

where, $Z_0\ (\omega)$ and Z (ω) represent impedance of free space and the structure, in order. μ_0 and ε_0 are magnetic permeability and electric permittivity of free space, respectively.

In this structure, first resonant arose from the resonator (cylindrical substrate), while the second resonant is given by the impedance matching on dielectric embedded between the two bottom metallic strips as a result of strong coupling between resonator and ground metallic plane. For verification of the above explanation, a proposed

metamaterial unit cell is simulated without the bottom dielectric-metallic layers. Figure 4-3 (a) and (b) is showing the geometry of the structure and simulation results without taking into account the ground metallic layer and its embedded dielectric spacer. The simulation results in this case show a single band with absorption rate of 98.95% at 619.25 THz.

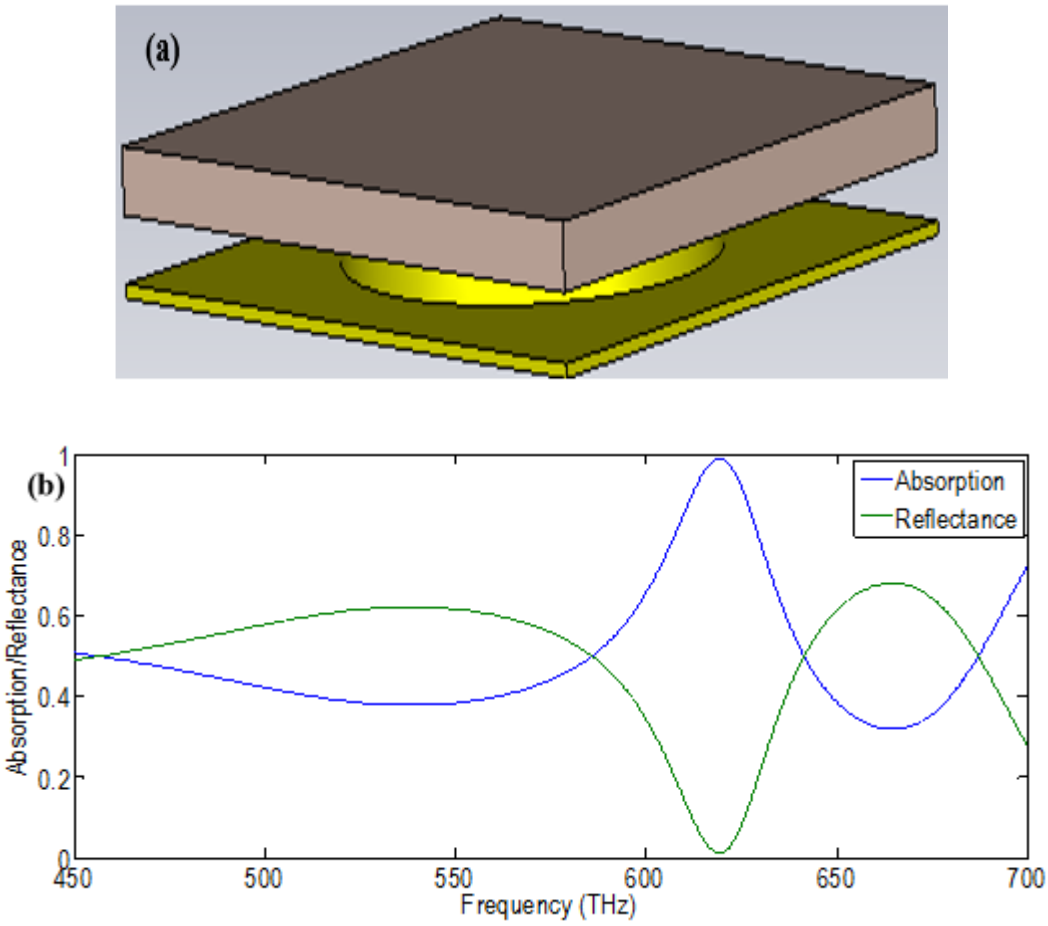

Figure 4-3. (a) A unit cell of the proposed design without ground metallic sheet and intermediate dielectric spacer (b) simulation results of a modified structure.

The selection of the thickness of metallic sheet is an important step in the process to design MTM perfect absorbers. This is due to the fact that for some thicknesses the metal sheet prevent propagation of EM radiations as a result of skin depth effect on the metallic sheet [43-44, 86]. When electromagnetic wave propagate in a medium of finite electric conductivity, its amplitude decays exponentially over a specific distance 'δ' known to the name of "optical skin depth" which is in order of 50 nm for visible frequency range.

$$\delta = \frac{c}{\omega \times \tilde{k}(\omega)} \tag{4.7}$$

where c is the velocity of light, ω is the frequency of EM wave and $\tilde{k}$ is the extinction coefficient. For the proposed MTM structure, its optical skin depth is calculated for both two resonant frequencies (543.75 THz and 663.75 THz). Using data for $\tilde{k}$ from [87]; the calculated value of δ are 36.5 nm and 38.3 nm at 543.75 THz and 663.75 THz, respectively. Ordinarily, for a wave to be able to propagate in a metal layer, its skin depth must be of the same order or greater than its thickness. That is the reason why in the present design in order to prevent propagation (transmitted power losses) in the bottom substrate, gold sheet of thickness much greater than its optical skin depth (z = 70 nm much greater than δ = 38.3 nm) is chosen.

In order to investigate the behavior of the designed MTM structure at other frequency ranges the simulation is performed within ultraviolet EM spectrum (UV) and infrared EM spectrum (IR). The results are shown in Figure 4-4 and Figure 4-5.

For UV frequency range, the simulation is carried out for the range between 800 THz and 1500 THz. In Figure 4-4, the simulation results show triple bands absorptions (94% at 926.4 THz, 99.14% at 1299.8 THz and 92.08% at 1379.6 THz). Even though the absorption values are not perfect within this range compared to the results for visible frequency range; through adjustment of the structure's geometrical parameters it is possible that perfect absorption can be achieved. For infrared spectrum, frequency range set from 3 THz to 450 THz. As it can be seen in Figure 4-5, the simulation results offer a single band at 197 THz with absorption rate of 98.52% accompanied by other two medium peak absorptions of 65.30% and 83.27% at 240.36 THz and 382.06 THz, respectively.

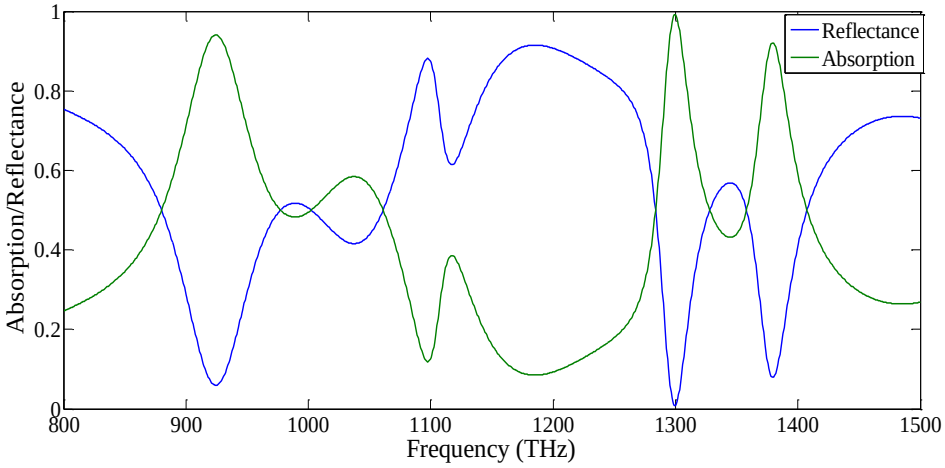

Figure 4. 4. Simulated absorption and reflectance characteristics of the proposed MTM unit cell in Ultraviolet (UV) spectrum range (800 THz-1500 THz).

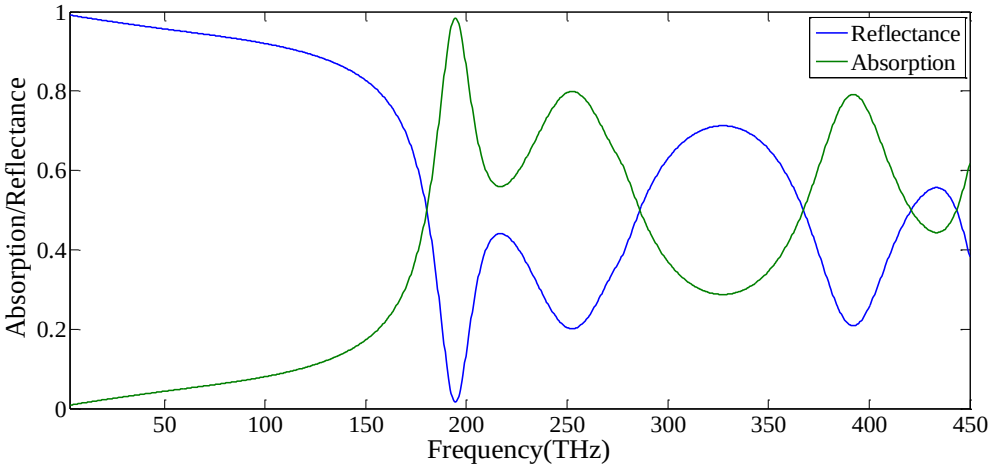

Figure 4-5. Simulated absorption and reflectance characteristics of the proposed MTM unit cell in Infrared (IR) spectrum range (3 THz-450 THz).

The geometrical parameters of the designed MTM absorber is investigated in order to understand their effect on its absorption characteristics. As it is described in Figure 4-6 (a); the structure's periodicity 'x' has been increased from 520 nm to 535 nm and also reduced from 520 nm to 505 nm with step width of 5 nm. Even though the absorption rate remains constant for all values of x, one can observe that for x values greater than 520 nm, the resonant absorption shift towards left (lower frequency range) while for all x values below 520 nm, the peak absorption shift to the right(higher frequency regime). This is an added value for MTM structure in the present study since it is flexible and can keep giving good absorption rate under different values of the

structure geometry , and this is one of the reason we keep getting good absorption rate in a wide range frequency (in visible, IR and UV frequencies).

Afterward, simulations are performed for different values of resonator's radius. As it is labelled in Figure 4-6 (b); the radius 'a' and 'b' of the resonator are changed where a slight enhancement in absorption rate (tending to become wide band perfect absorption for the values of 'a' and 'b' beyond 173.5 nm and 157.4 nm, respectively) is observed for high values of the resonators' radius. This is because, the absorption characteristics of the proposed MTM unit cell depend on coupling between a resonator and its embedded dielectric material. Therefore, at a certain value of 'a' and 'b' strong coupling between cylindrical resonator and its embedded dielectric substrate causes electromagnetic field resonance which leads to the change in absorption rate of the MTM structure at the resonant frequencies.

Likewise, absorption capability of this design strongly depends on the thickness 'k' of the resonator. As it is shown in Figure 4-6 (c), the resonator's thickness is increased from 38.8 nm to 49.8 nm and decreased down to 27.8 nm at the step width of 5.5 nm. The observation is that the absorption rate of MTM design understudy hugely depends on the thickness of the resonator, where for the shorter thickness, absorption rate decrease and shift toward right while for the longer thickness, the absorption coefficient shift and decrease toward the left of the central absorption (absorption for t=38.8 nm).

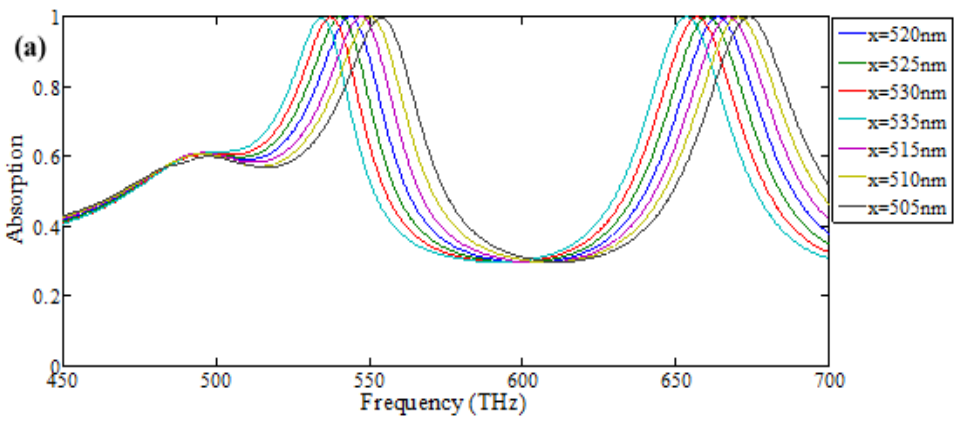

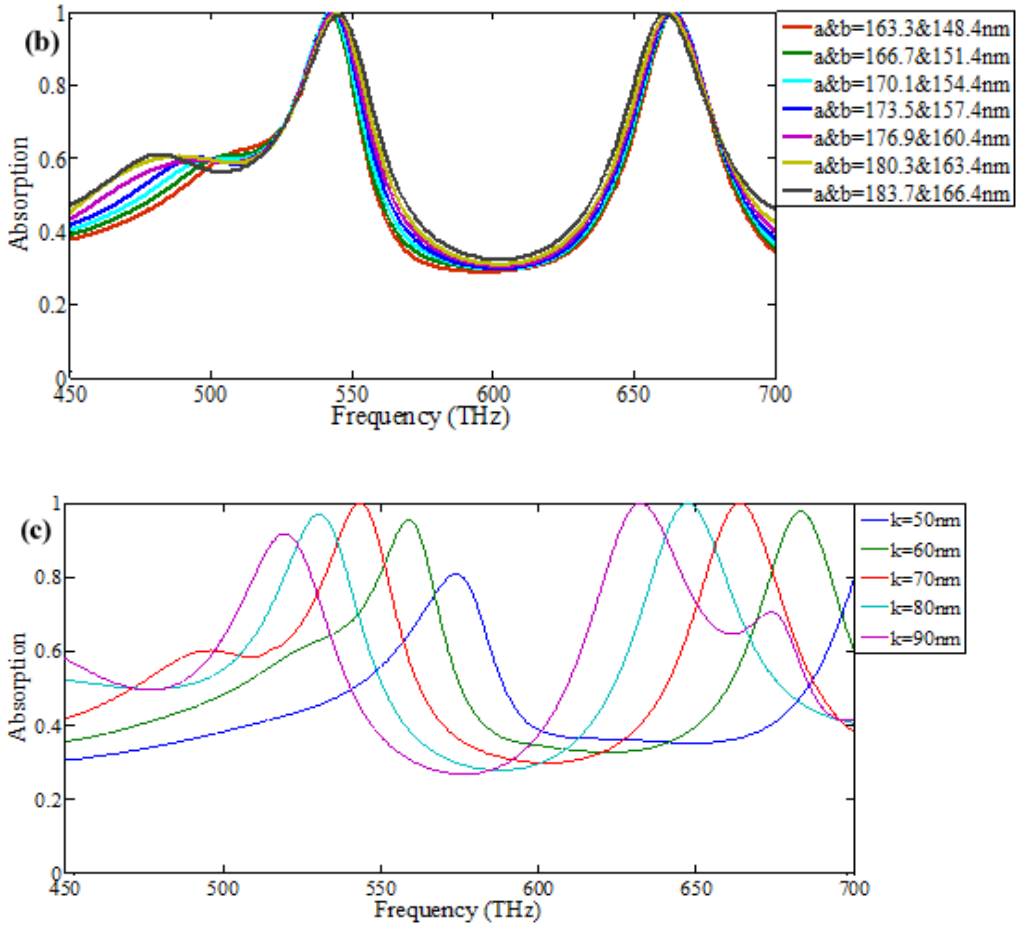

Figure 4-6. Simulated absorption rate of a designed MTM unit cell in visible spectrum range (450 THz-700 THz) for different geometrical parameters: (a). the structure's periodicity 'x', (b) radius of resonator 'a' and ' b' and (c) thickness "k" of the resonator.

Afterward, the absorption characteristic for the proposed structure at different angles of incidence EM radiations is evaluated. In Figure 4-7 simulation results of the proposed dual-bands perfect metamaterial absorber structure under different angles of incident is depicted. The incident angle is changed from 0° to 90° with the step width of 15°. By changing the incident angle, absorption rates of the proposed MTM design remain the same (high), which shows that the absorption response of the proposed MPA unit cell is independent of incident angles of EM radiation. As it is depicted in Figure 4-7 (a) and (b), the absorption rate of a proposed MTM absorber structure also remains constant for a wide range of polarization angles for a polarized wave. Where simulated absorption rate remains higher and unchanged for both transverse electromagnetic (TE) wave and transverse magnetic (TM) wave.

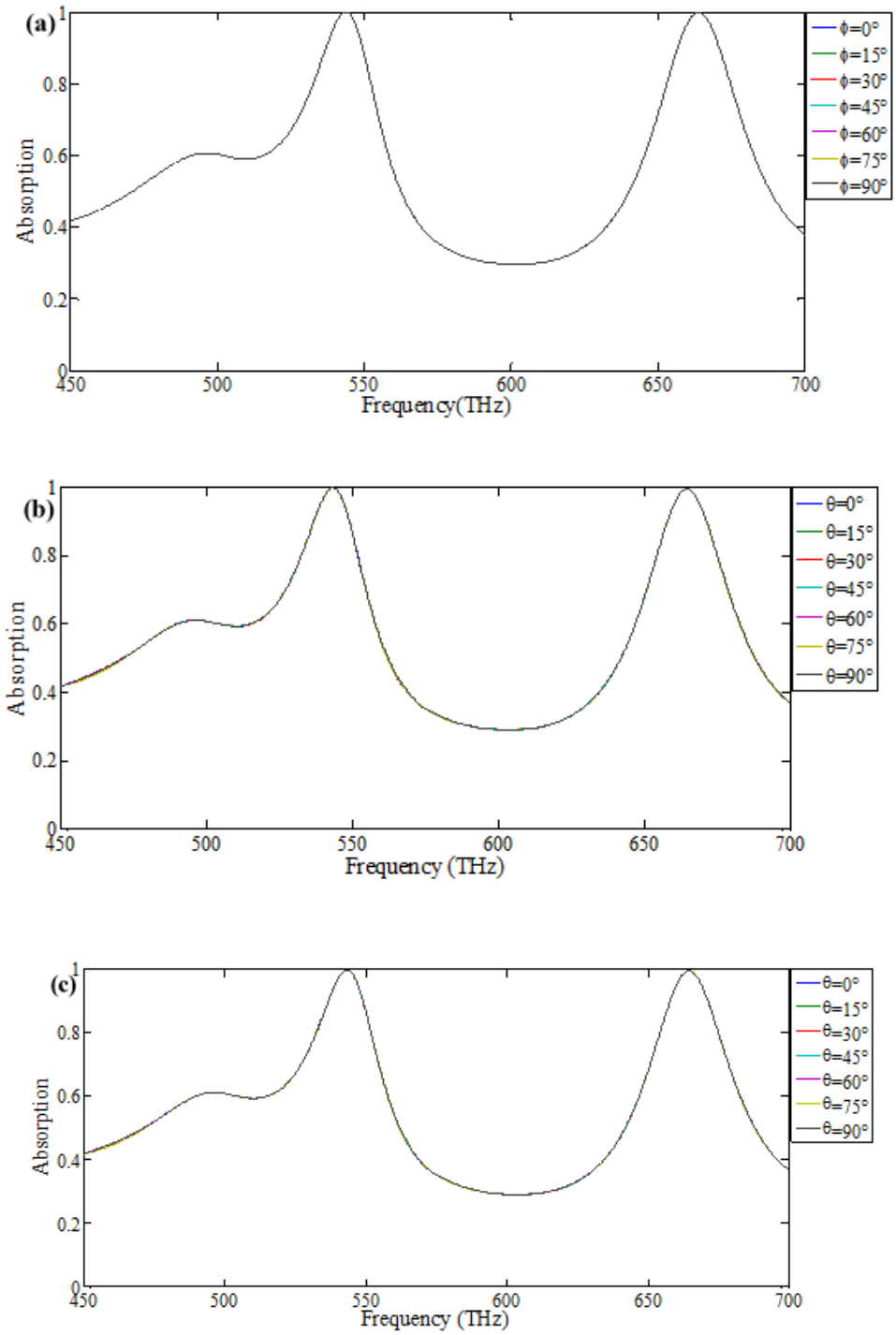

Figure 4-7. Simulated absorption coefficient of the proposed structure in visible spectrum range (450 THz-700 THz) for: (a) different polarization angles (b) TM incident wave, (c) TE incident wave.

In order to understand the physics behind the absorption characteristics of the proposed MTM at resonance frequency, electric field (E-field) and surface current distributions of the proposed MTM structure are examined. In Figure 4-8 and Figure 4-9, electric field and surface current distributions are presented for the resonant frequencies of

543.75 THz and 665.75 THz. As it can be observed in Figure 4-8 (a) and (b), E-fields are strongly located at the surface of the resonator for both two resonant frequencies (543.75 THz and 663.75 THz) and much stronger at the surface of embedded dielectric slab. One also can observe that the arrangement of electric field form symmetric shape around the surface of the resonator for the first resonant frequency of 543.75 THz (see Figure 4-8a) which behaves like an electrical dipole.

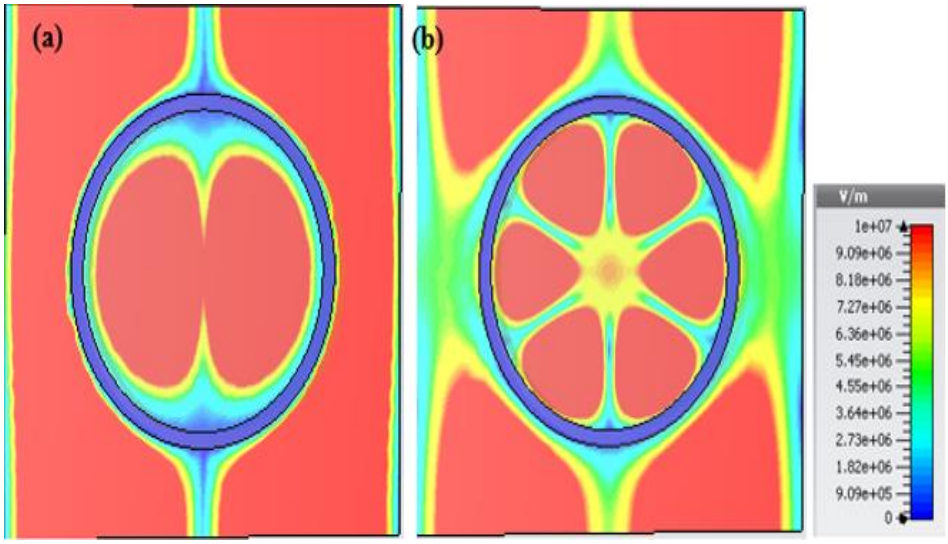

Figure 4-8. Simulated Electric fields distribution for a designed MTM at the resonant frequencies, (a) 543.75.5 THz and (b) 663.5 THz.

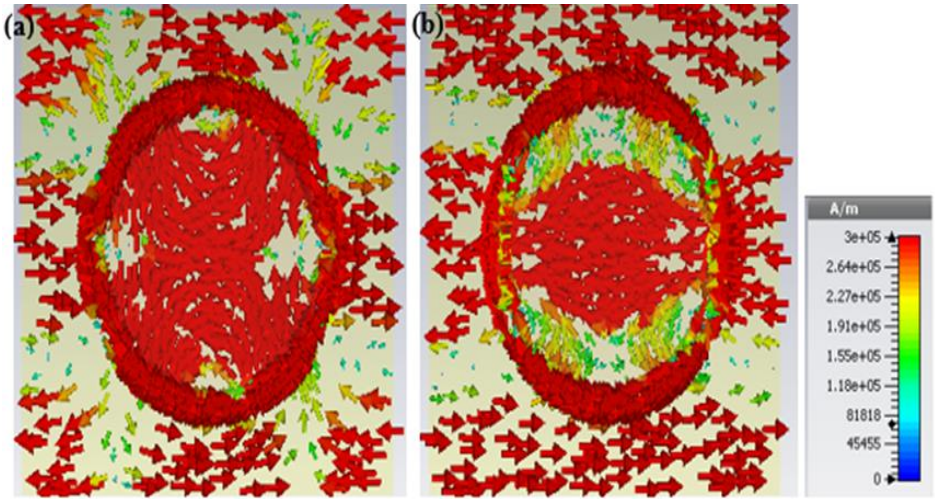

Figure 4-9. Simulated surface currents distribution of a designed MTM at the resonant frequencies, (a). 543.75 THz and (b). 663.75 THz, respectively.

Another observation is that for a second resonant frequency (see Figure 4-8.b) electric field distribution shows six symmetric patterns inside the resonator (at the surface of embedded dielectric) which act as hexapoles electric fields and the four symmetric patterns around resonator at the surface of gold metallic sheet (originated from strong coupling of resonator, intermediate metallic layer, ground metallic plane and dielectric spacer) which behaves as electrical quadripoles. Thus, the strong coupling of electric field with the resonator and coupling of resonator with ground metallic plane create independent electric resonance which produce surface charges to oscillate together with electric fields and cause magnetic polarization. Subsequently, magnetic polarization creates magnetic response that produces resonant absorption. In Figure 4-9 (a) and (b) surface currents distribution are shown for two resonance absorptions of 543.75 THz and 663.75 THz, respectively. One can observe from Figure 4-9 (a) and (b) high concentration of circulating surface currents at the circumference of the cylindrical resonator and at the surface of embedded dielectric bar. One can also observe parallel and antiparallel currents moving around the surface of a metallic sheet. The parallel and anti-parallel currents are responsible for electric resonance while the circulating currents are accountable for magnetic resonance. At resonance frequencies, electric and magnetic responses of the resonator match with electric and magnetic responses of the incident electromagnetic wave. As a result total absorption of all incident EM radiations is obtained at incident matching condition. At this moment (incident matching condition) all incident EM radiations are confined within the MTM structure, and this happens at a very minimum reflection while absorption rate reaches its maximum value.

4.1.4. Conclusions

In this section, a MTM design has been numerically proposed and evaluated for perfect absorption at resonant frequencies. Objective of this study was to examine dual- band PA in visible spectrum range of electromagnetic wave. The designed MTM gives two peaks absorptions nearly 100% insensitive to both TE and TM polarization angles. Similarly, the absorption capability of a proposed MTM structure found to be independent of incident angle for incidence electromagnetic wave. A proposed MTM structure was examined for its performance in the presence of UV and IR EM spectrum

range and outstanding triple bands absorption was observed for both UV and IR frequencies. Moreover, the designed MTM was assessed for the effect of geometric parameters on its absorption characteristics where the proposed MTM design showed high flexibility. Fabrication of the proposed MTM absorber structure will lead to realization of higher efficiency solar cells and other devices working in high EM frequencies range with wide incident angle and polarization angle independencies.

4.2. A Novel Patches Based Dual-Band Perfect Metamaterial Absorber for Solar Cell Applications

4.2.1 Introduction

In the previous section a ring resonator based dual band perfect metamaterial absorber has been designed and characterized for its absorption characteristics. It was found that the perfect absorption is a results of strong electric and magnetic response generated by the resonator which caused the absorption of all radiation incident on metamaterial structure's surface (perfect absorption). Though resonator based MPA displays the best results, however there is still some challenges linked with them such as complication (complex structure) in their fabrication processes. On the other hands, periodically arrangement of patches on the top of a dielectric spacer is another way used for absorption enhancement in MPA structures and it has been used by some researchers [71] to design metamaterial absorbers. Even though it is not easy to gain perfect absorption with patches based MPA structure, by carefully employing them in metamaterial unit cell perfect absorption can be obtained. Additionally, patches based MPA designs are easy to fabricate compared to resonators based MPA designs.

In this section, patches based dual–bands polarization insensitive MTM absorber is proposed to operate in visible frequency range for effectively harvest solar radiations. According to the results, two distinct absorption bands with almost unity absorption in visible frequency range are obtained. Additionally, the polarization angles dependency of the designed structure is analyzed and the results show that the proposed MPA is polarization insensitive for wide angles of incident waves.

4.2.2 Designing, Simulations and Discussion

The proposed design consists of three basic layers as shown in Figure 4-10. The bottom plate is a metallic layer (ground plane), the intermediate layer is a dielectric host material, and the top layer consist of three patches which are responsible for the EM resonances [88]. All metallic layers are made of gold (yellow color) with electric conductivity $\sigma = 4.5 \times 10^7 S/m$, whereas a dielectric spacer is selected to be gallium arsenide (grey color) with the relative electric permittivity $\varepsilon = 12.94$ and the tangent loss of 0.006 at room temperature. The dimensions of the proposed structure are: a = 600 nm, b = 120 nm, t = 50 nm, z = 93.5 nm, c = 150 nm, d = 66.7 nm and, x (thickness of the patches) = 1.28 nm.

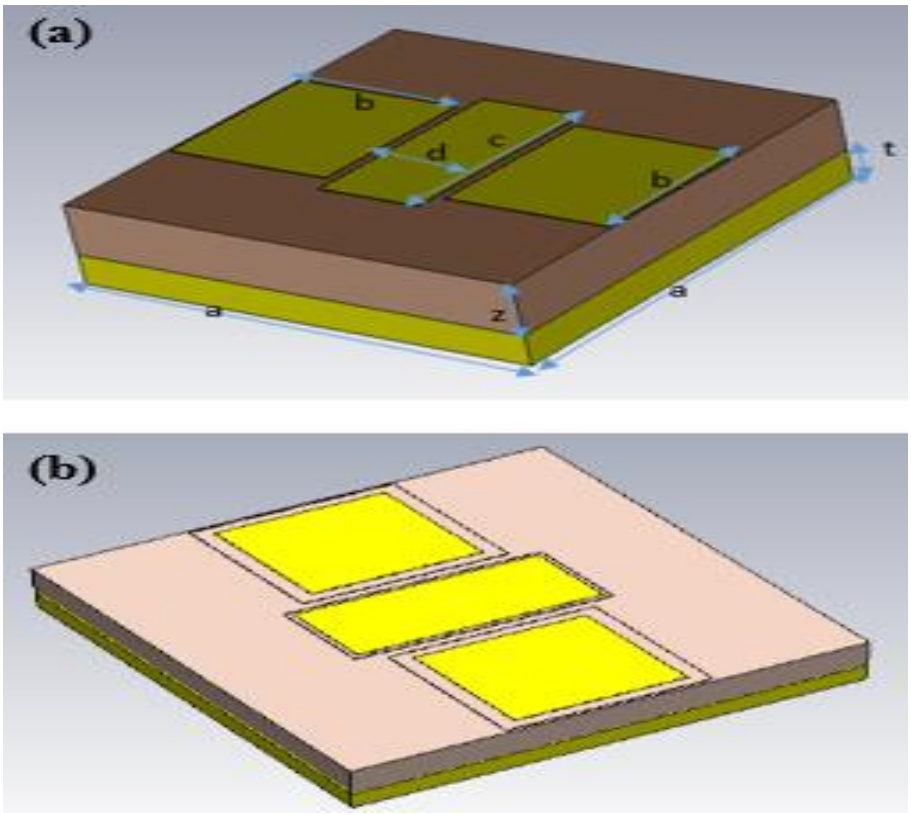

Figure 4-10. (a) Perspective view of the proposed MTM structure unit cell with its geometric parameters, (b). Top view of the proposed design with additional patches on the top of each other.

The numerical simulations is performed using a full wave electromagnetic simulation based on finite integration technique (FIT). FIT method is chosen because it offers high accurate results and is suitable for the study of high frequency and 3-dimensions

EM structures [78, 89]. In the simulations, EM radiations are polarized in a manner that the electric (*E*) and magnetic (*H*) fields are parallel to the plane of incident while propagation wave vector (*k*) is perpendicular to the structure's geometric plane. The boundary conditions was chosen to be periodic while the simulation environment is designated to be free space.

The absorption characteristics of MTM absorber strongly depend on both its transmittance $T(\omega)$ and reflectance $R(\omega)$ as it is described in this relation: $A(\omega) = 1 - R(\omega) - T(\omega)$. Therefore, by adjusting the metallic ground plane much thicker than the skin depth at resonant frequency [19], the transmission can be eliminated for the proposed design. By careful tuning MTM geometric parameters and by selecting a suitable dielectric material (lossy enough), the MTM absorber's constitutive parameters can be manipulated to match to free space parameters at resonant frequency. The outcome from this process is a very minimum (negligible) reflection which leads to the realization of a perfect absorption (near a unit absorption rate).

Absorption and reflection versus frequency for the proposed dual-bands metamaterial absorber are shown in Figure 4-11. As it can be observed from Figure 4-11 (a), two different maximum absorptions obtained at 613.4 THz and 700.1 THz, with the absorption rates of 99.96% and 99.37%, respectively. Furthermore, additional patches (combination of dielectric and metallic layers, see Figure 4-11 (b)) on the top of each other lead to enhancement of both bandwidth and absorption rates of the MPA structure. In Figure 4-11 (b) the results for the additional patches are shown. One can observe that for the additional single layer of patches (1P), the absorption and bandwidth are small compared to the ones with more additional patches (from 2P to 5P). This is because the additional patches make the electric resonance stronger which yields an enhancement in the resonance character.

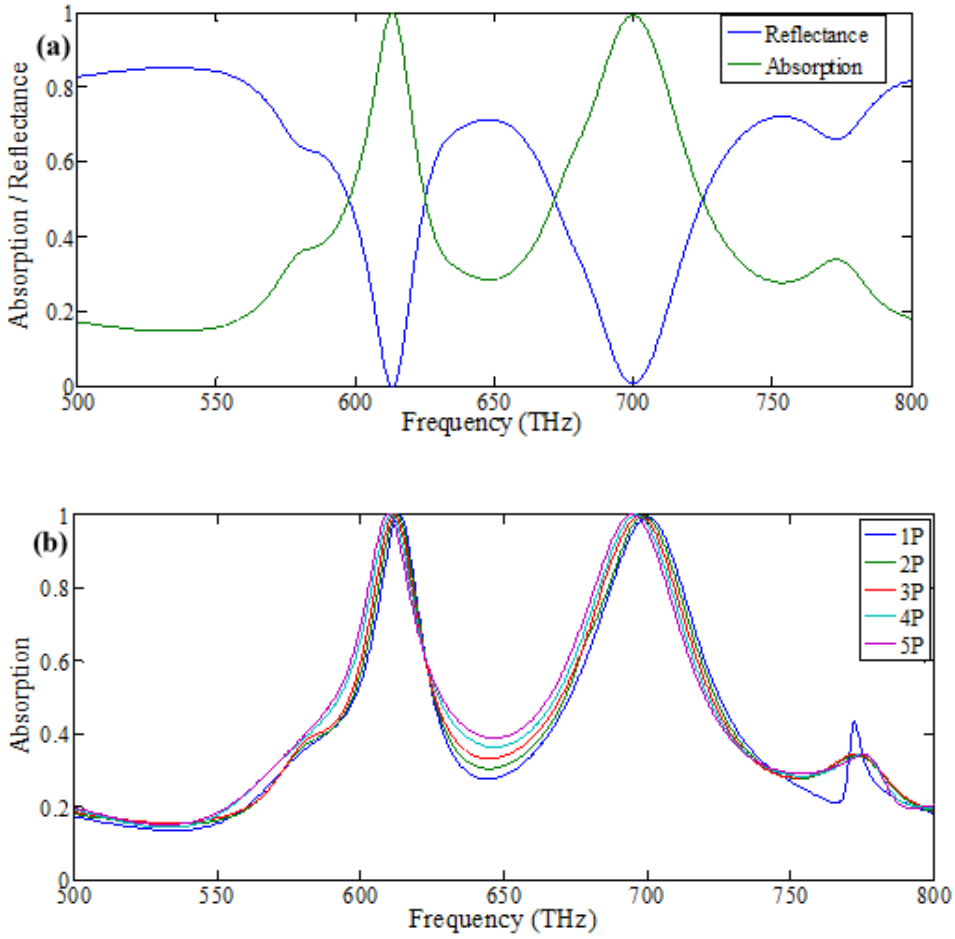

Figure 4-11. (a) Absorption and reflection coefficient of the proposed MPA structure, (b) Absorption rates for the design with additional patches (P) at the top layer (1P-5P).

For validation of the absorption characteristics (absorption resonance) reported in Figure 4-11(a) from FIT based solver with other numerical method, a finite element method based software is used for simulation of the same design and simulation results are given in Figure 4-12.

Similar to FIT based simulation, the periodic boundary conditions (PBC) and Floquet port are employed to simulate the infinite periodic cell. FEM based simulation rely much on the mesh setting and in this simulation tetrahedral mesh is used with 10^4 elements. As it can be observed in Figure 4-12, both solvers (FIT based solver and FEM based solver) offer the same absorption behavior in the frequency range of interest where dual-bands absorption resonance with absorption rate of about 99% at resonance frequency of 613.4 THz and 700.1 THz obtained for both solvers.

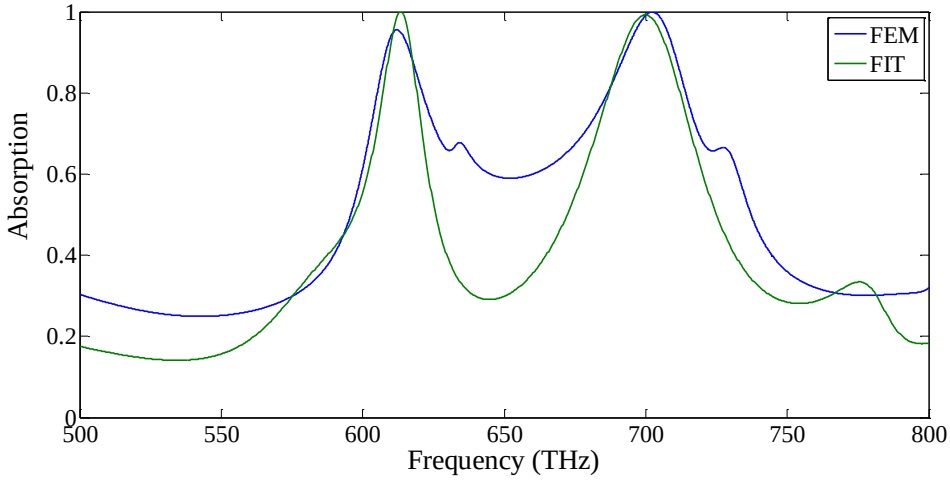

Figure 4-12. A validation of absorption characteristics of the proposed MPA structure using two different software (FIT and FEM based Software) the resonant frequency of 613.4 THz and 700.1 THz.

As the properties of MTM structures enormously rely on the effective electric permittivity and magnetic permeability and these parameters also affected by MTM structure's geometry; thus, a study on the effect of geometrical parameters on absorption capability of the proposed MTM absorber was conducted. First of all, analysis about influence of the structure's periodicity 'a' is investigated. In Figure 4-13 (a), absorption for different values of 'a' is shown where the periodicity is increased and decreased from 600 nm with 5 nm step width. In both cases, the absorption remains almost the same as in the 600 nm case. The only difference is the frequency shift of resonance: red-shift and blued-shift observed for a>600 nm and a<600 nm, respectively. This is due to the symmetry character of MPA design understudy. This is an added value to the proposed design, because it will keep the absorption rate as almost unity for different value of the periodicity 'a'. Secondly, the impact of the thickness of the dielectric spacer 'z' to the absorption mechanism is examined. Figure 4-13 (b), shows the absorption rate for different thicknesses of the dielectric spacer. As one can see from Figure 4-13 (b), the proposed structure is sensitive to the change of dielectric layer's thickness where dual-bands and unity absorption is observed for the thicknesses of 55 nm and 60 nm. The absorption decreases for dielectric thicknesses of 50 nm and 65 nm, but the structure still provides single-band and unity absorption. The unity and dual-bands absorption rates are the results of the impedance matching condition occurs at resonance frequencies, where the electric permittivity

and magnetic permeability of the proposed design matches that of a free space parameters. This corresponds to a very low reflection rate and maximum absorption rate (approximately 100 % absorption) [42, 90].

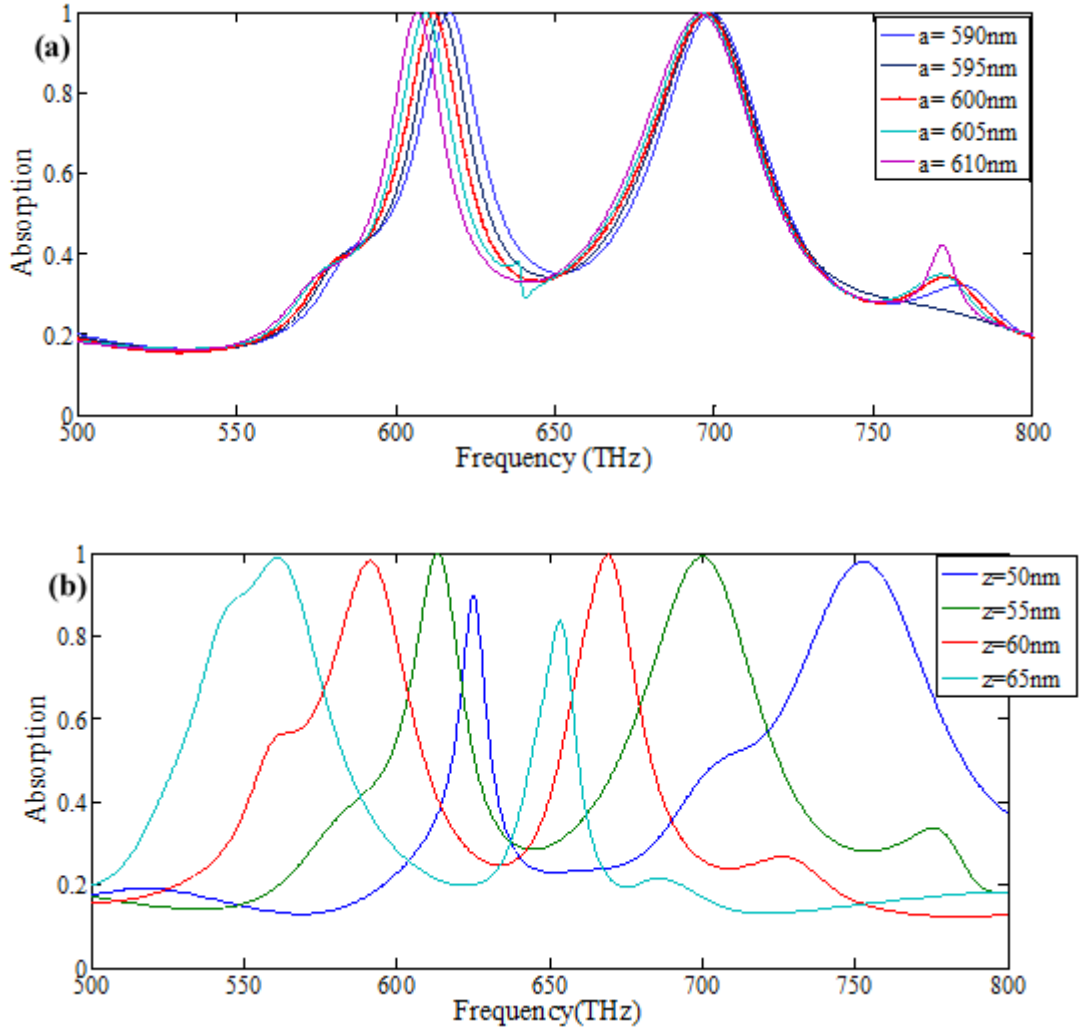

Figure 4-13. (a) Absorption result for different periodicity 'a' for the proposed MPA. (b) Absorption result for different values of thickness of the dielectric spacer 'z'.

In order to understand the physics behind the absorption mechanism of the proposed MPA structure, a study on the electric field and surface current distributions is conducted for two resonant frequencies (613.4 THz and 701.1 THz). The results for electric field and surface current distributions are shown in Figure 4-14 and Figure 4-15, respectively. As it can be seen from Figure 4-14 (a) and (b), the electric fields concentrate between and at the edges of the patches and it is strongly confined in the dielectric spacer where they formed a symmetric shape with respect to the patches.

The symmetric distribution of the electric field can also be observed from back side of the structure (see Figure 4-14 (c-d)). As one can notice from Figure 4-14 (c-d), the electric fields are symmetrically disposed. Thus, high concentration of the electric fields between and at the edges of patches and in the dielectric substrate is an evidence of strong electric resonance resulting from strong coupling of patches-dielectric spacer and the ground metal plane. This is one of the reasons of absorption rate enhancement (see Figure 4-11 (b)) observed when more patches are added at the top of one another. Electric polarization on the other hand produces surface charges which induce magnetic field accountable for magnetic resonance and resonant absorption.

In Figure 4-15 (a) and (b), the surface current distributions for both resonant frequencies is shown. As one can observe that parallel and anti-parallel surface currents are distributed at the surface of patches for both resonant frequencies (613.4 THz and 701.1 THz) and they are strong at the edges of the patches. Parallel surface current distributions control the electric response whereas antiparallel surface currents are accountable for magnetic response. The origin of surface currents is a strong magnetic and electric coupling. These currents produce magnetic and electric resonance to be coupled with external applied EM fields. At resonant frequencies, local electromagnetic fields are generated and produce perfect absorption of incident EM radiation when impedance match condition is fulfilled. At this situation, the incident EM radiation are trapped within absorber and the reflection rate reaches its very minimum value while absorption coefficient gets to its peak (perfect absorber).

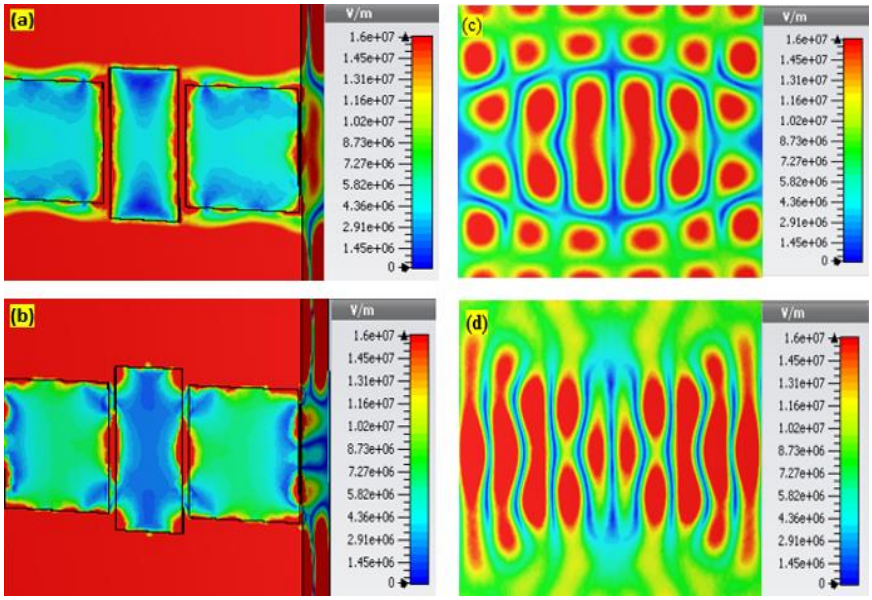

Figure 4-14. Electric fields distribution for the proposed MPA structure at 613.4 THz and 701.1 THz, respectively. (a) & (b) Perspective view, (c) and (d) back side view.

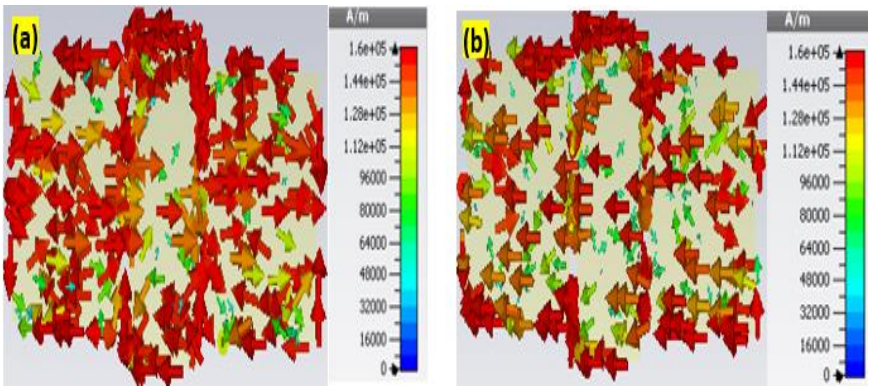

Figure 4-15. Surface currents distribution of the proposed MPA structure at (a) 613.4 THz and (b) 701.1 THz.

Due to the fact that the performance of MPA design over different polarization and incident angles for EM radiations play a great importance in the studies of MTM structures for solar cells applications. Absorption characteristics of MPA structure understudy is inspected for its performance at different angles of incident for EM radiation. As the main aim in designing solar cell is to capture as much solar energy as it can, one remark to keep in mind is that some radiations contain random polarized components. Besides, the incident angle of EM radiation changes over the time (which is not always normal to the cells surface). In Figure 4-16 (a)-(c), the absorption rate under different polarizations (transverse electromagnetic: TE and transverse magnetic: TM) and different angles of incident (normal and oblique incident) for EM radiation

are depicted. The simulation was performed under different angles from 0° to 90° with a step width of 15°. As it can be observed in Figure 4-16 (a) and (b), two high absorption peaks are always obtained for both TE and TM waves for all angles except for 45°. In this case (for 45°), the absorption rate tends to drop down and produces wide band with outstanding absorption rate of around 90 %. Another observation is a slight shift of the resonant frequencies (shift to the left side of the spectrum) detected for all angles below 45° for TE polarization and all angles above 45° for TM polarization. On the other hands, as one can see from Figure 4-16 (c), the absorption rates remain higher and insensitive of normal and oblique incident angles for EM radiation resulting from strong symmetry of the proposed MPA structure. MTM designs of this kind offer potential applications in production of efficient absorber solar cells, where their absorption capability remains unchanged regardless of the position of the sun and direction of its radiations.

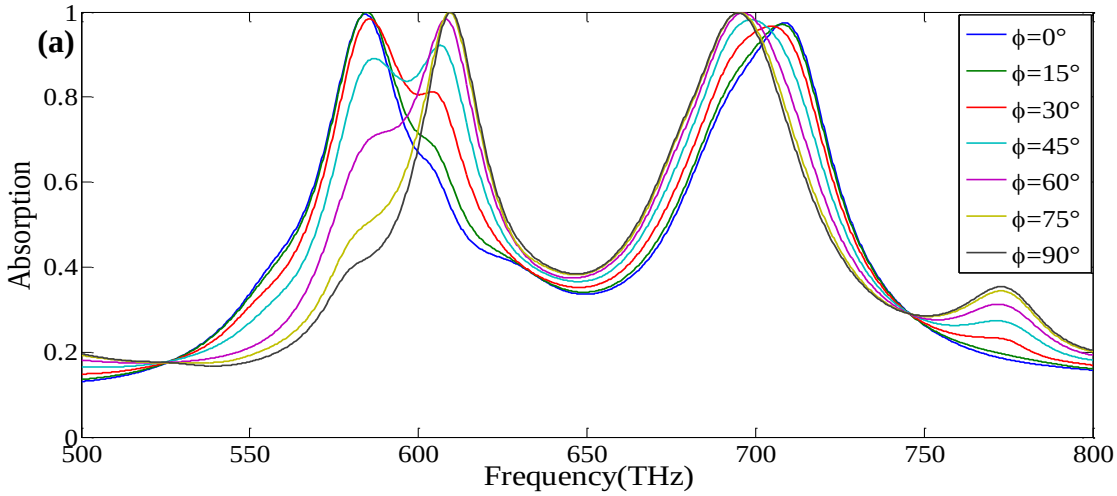

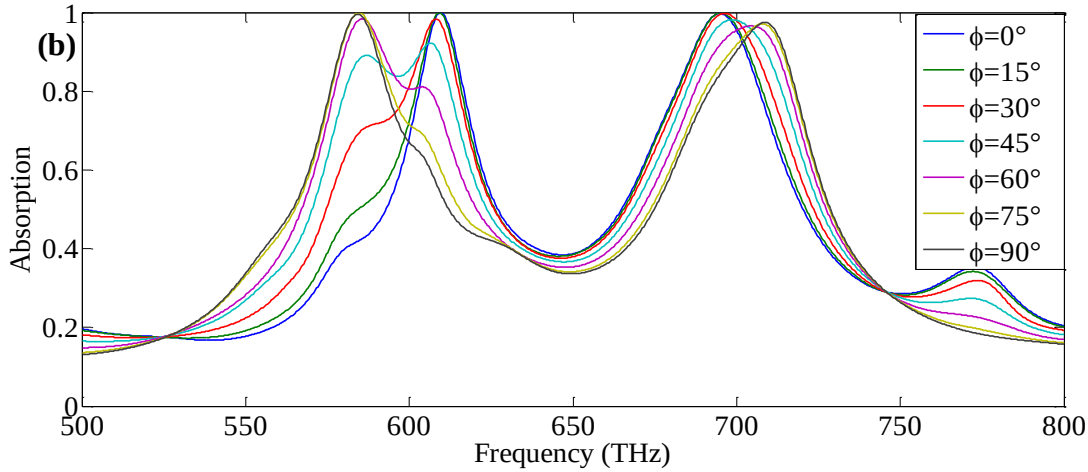

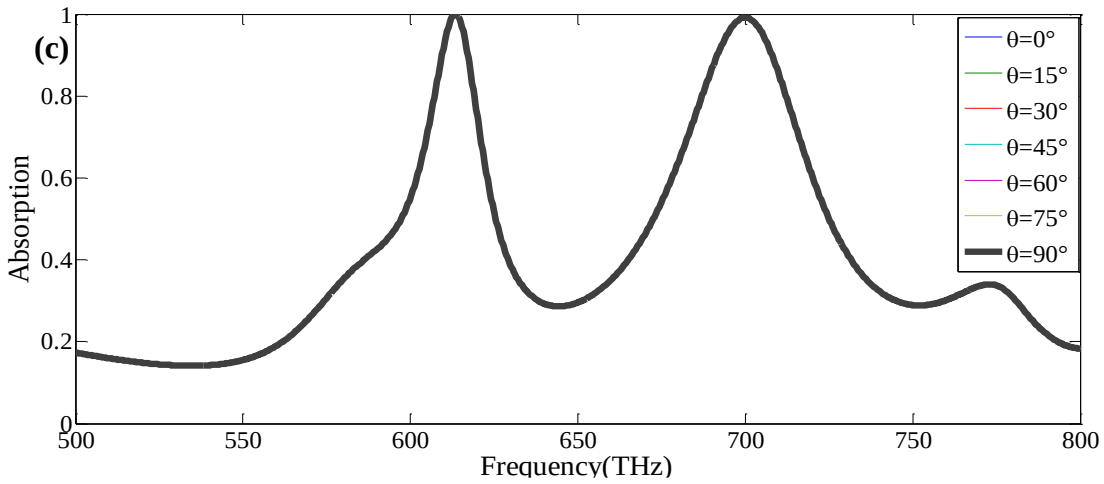

Figure 4-16. (a) Simulated absorption rated for different TE polarization angle (ϕ). (b) Simulated absorption rate for different TM polarization angle (ϕ). (c) Simulated absorption results for different incident angle (θ) of EM wave (oblique incident radiation).

4.2.3. Conclusions

Perfect metamaterial absorber based on metallic patch resonators has been proposed and discussed in this section. The frequency response of the structure provided two perfect (nearly 100 %) absorption peaks. Furthermore, the geometric parameters of the proposed design has been characterized and discussed for their effect on absorption behavior of the proposed MPA where the design understudy dısplays high flexibility and ability to maintain higher dual-band absorption rate. Finally, analysis of absorption characteristics of a proposed MPA structure at different incident angles (normal and oblique incident) of EM radiation was performed and was shown incident angle and polarization angle insensitive for both TM and TE radiations.

CHAPTER 5

POLARIZATION INSENSITIVE TUNABLE PERFECT METAMATERIAL ABSORBER FOR SOLAR CELLS APPLICATIONS

The main objective of this thesis is to realize a wide band perfect metamaterial absorber and as a step further toward realization of this objective in this chapter a novel wide-band tunable polarization and incident angle insensitive perfect metamaterial absorber is proposed in order to harness solar energy resource in visible frequency realm. One of the advantages of the proposed design is that it offers a high symmetric flexibility which enables it to give a resonant absorption of near a unit with very good absorption bandwidth of more than 15% with respect to the resonant (central) frequency and additionally, this design is simple for fabrication process.

5.1. Structure Design and Geometric Parameters

The proposed perfect metamaterial absorber unit cell consists of three basic layers: ground metallic plane, dielectric spacer, and patches (two metallic layers with a sandwiched dielectric material) on the top of a dielectric spacer as it is shown in Figure 5-1. The ground layer is made of a metallic material which is selected to be gold lossy with a much higher thickness than its surface roughness in the frequency of interest and its electric conductivity $\sigma = 4.561 \times 10^{7}\ S\ m^{-1}$. Gold is chosen because it has some good properties such as its ability to stand against excessive heat and it has high reflectance in the presence of high frequency radiations. This makes gold a good candidate in designing MPA structure for visible frequency radiations, however, depending on the intended applications for any proposed MPA structure, other metals such as aluminum, copper and silver can be used in the place of gold while the absorption characteristics of the MPA unit cell remain unchanged [37-39]. The reason is because the absorption behavior of a MTM structure has no huge dependency on the material composition, instead it is governed by the selection of its unit cell geometrical parameters such as its shape, orientation and size. Another fact is that in high frequencies (visible) range, several metals behave like lossy materials.

On top of the ground metallic plane there is a dielectric spacer which is chosen to be gallium arsenide lossy (grey color) with electric permittivity $\varepsilon = 12.9$ and tangent delta of 0.006. The top most layer is made of periodic arrangement of two patches (metals) made of gold (yellow color) holding between them gallium arsenide. The geometric parameters of the proposed MPA are: a=550 nm, z=80 nm, t=100 nm, b=342.9 nm, c =240 nm, d=100.9 nm, and k (thickness of the top patches) =5 nm.

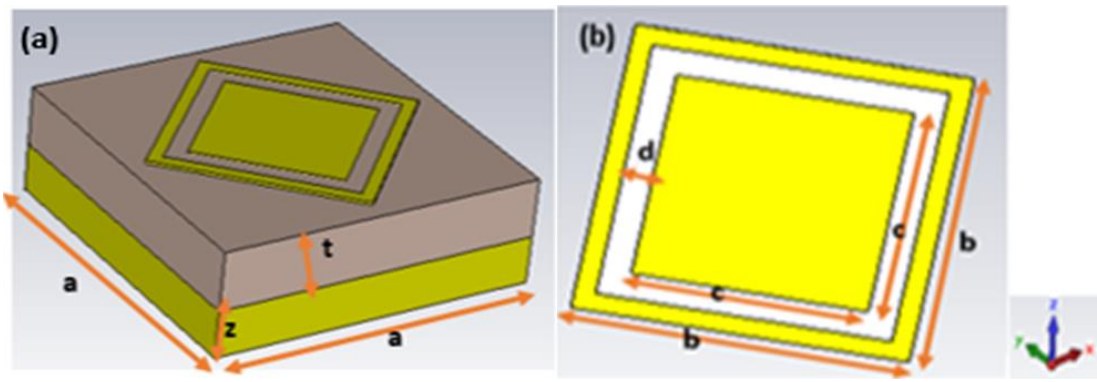

Figure 5-1.The proposed MPA unit cell. (a) Isometric view and (b) top view (Patches)

5.2. Simulation and Discussion of Results

The simulation is performed by using a full wave electromagnetic simulator which uses finite integrate technique (FIT) with high frequency solver. The radiations are polarized in a way that both electric field (*E*) and magnetic field (*H*) are in phase with the plane of incident whereas a wave vector (*k*) is perpendicular to the geometric plane of the MPA unit cell. Here, the periodic boundary conditions are selected along x-axis and y-axis, whereas open free space is selected to be the simulation environment (z-axis) in order to get a better accurate results the user need to selection of mesh need to be made. As a results in this study tetrahedral mesh is used. The minimum number of steps per wavelength and minimum number of steps employed are 4 and 20, respectively, and this corresponds to 49 641 tetrahedrons. The intended structure is to work in visible frequencies ranging from 450 THz to 750 THz.

Since the coupled model system is being used in this study (ground metallic with thickness much greater than the skin depth of gold in visible frequencies), then the transmission losses are eliminated ($T(\omega) \cong 0$). As a result, the only parameter involving in simulation results is reflection coefficient $R(\omega)$. In Figure 5-2, the

simulation results for both reflection and absorption rates are reported. As it can be seen from Figure 5-2, nearly a unit (0.997) absorption rate is gained at 614.4 THz which corresponds to a very minimum reflection coefficient (0.054) at this frequency.

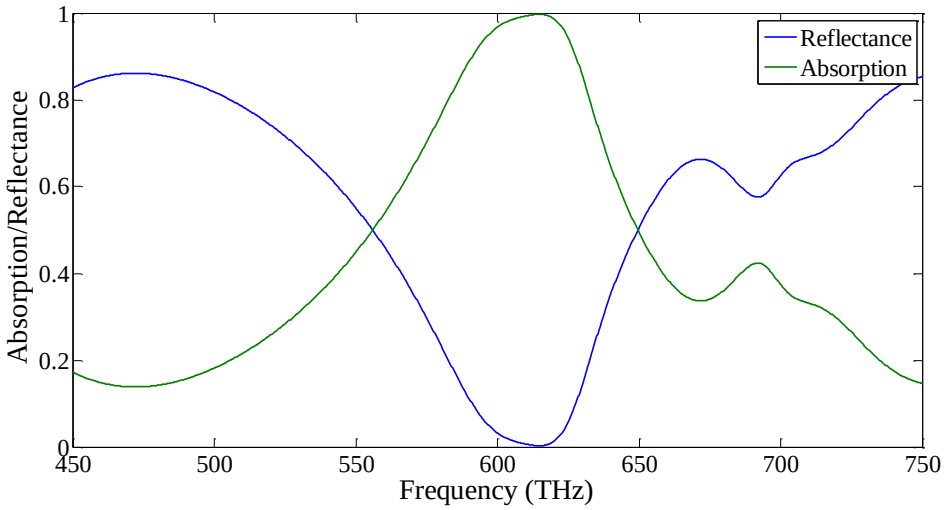

Figure 5-2. Simulated absorption and reflection rates at resonance frequency of 614.4 THz.

The source of this perfect absorption is the strong coupling of incident electric and magnetic fields with the top patches (combination of both metallic and dielectric layers) and a dielectric spacer and the ground metallic plane which produces electric and magnetic resonance and this lead to the perfect absorption at the resonant frequency. As one can observe, the single-band metamaterial absorber for the proposed design has an outstanding bandwidth of 15.5 % (which covers 87.25 THz frequency ranges with absorption rate higher than 90%) with respect to the resonant frequency .The origin of this absorption resonance is a high surface plasmon resonance resulted from the coupling of the two top metallic layers (top patches) and the sandwiched dielectric layer.

In order to understand the absorption performance of the proposed MPA structure, a study of electric and surface current distribution is performed for resonant frequency of 614.4 THz. In Figure 5-3, electric field and surface current distributions are shown. As one can notice from Figure 5-3 (a), the strong electric fields are distributed at the surface of a dielectric spacer and also it is stronger at the surface of the dielectric inserted between the top patches. The strong E-fields also forms a symmetric shape (electric multi-poles) around the metallic patches at the top layer. The same

mechanism is observed for the bottom view of a sandwiched dielectric spacer, as it is labelled in Figure 5-3 (b). This is a strong evidence of electric resonance (absorption resonance) which results from the strong coupling of the top patches and their sandwiched dielectric slab and the strong coupling of the top layer – intermediate dielectric spacer and ground metallic plate. The observed electric multipoles (electric polarization) produces surface charges which generate induced magnetic fields and this magnetic field are responsible for both magnetic resonance and resonant absorption at the peak frequency. In Figure 5-3 (c) surface current distributions are reported. As it can be seen, high parallel and antiparallel surface currents are concentrating around the patch's surface.

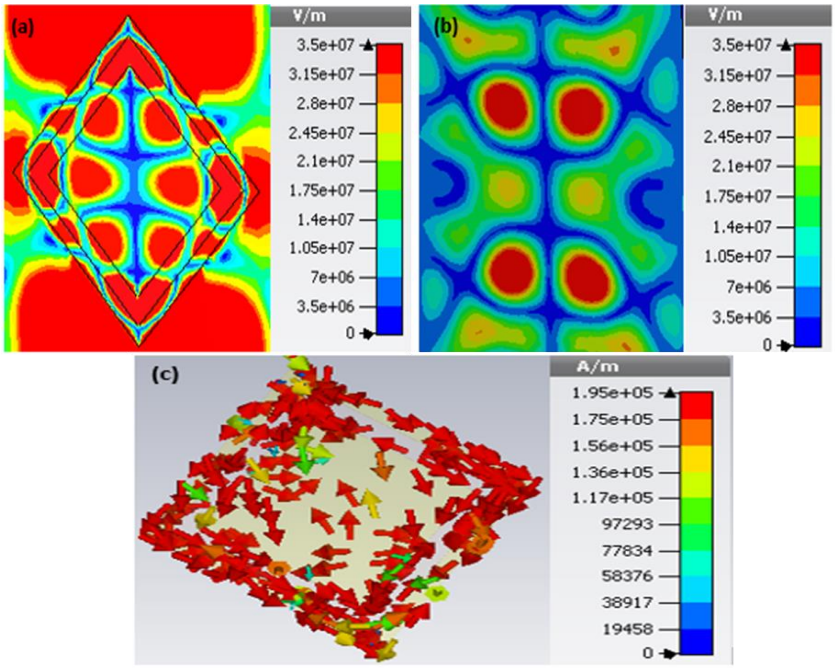

Figure 5-3. (a) Front of view of electric field distribution, (b) back view of electric field distribution, and (c) surface current distributions of the proposed MPA design at the resonance frequency of 614.4 THz.

The presence of high parallel surface current proves the existence of electric response (parallel surface currents are accountable for electric resonance) while the presence of high anti-parallel (control magnetic resonance) confirm magnetic response. Therefore, the generated electric and magnetic resonant coupled with external electromagnetic fields and at the resonance frequency local fields are produced and cause perfect absorption of all incidence EM radiations (this happens when the impedance matches

conditions are accomplished). In that moment, EM radiations are trapped within absorber parts of MTM structure and the reflection coefficient declines to a very minimum value (near zero) while absorption rate climbs to its maximum (nearly 100% absorption).

One of the fascinating parts of metamaterial absorber structures is their electromagnetic properties which strongly rely on their unit cell geometry. Due to this fact, in order to investigate the absorption characteristics of the proposed MPA structure, its geometrical parameters are examined to get their effect on absorption rates of its unit cell. First, the structure is simulated for different thicknesses of an intermediate dielectric spacer, where its thickness 't' is changed from 90 nm to 130 nm with step width of 10 nm. The simulated absorption results under different dielectric's thicknesses are labelled in Figure 5-4. As reported in Figure 5-4, a shift toward left (lower frequencies) of peak frequency is noticed, but, in all cases the absorption rate remains high (perfect).

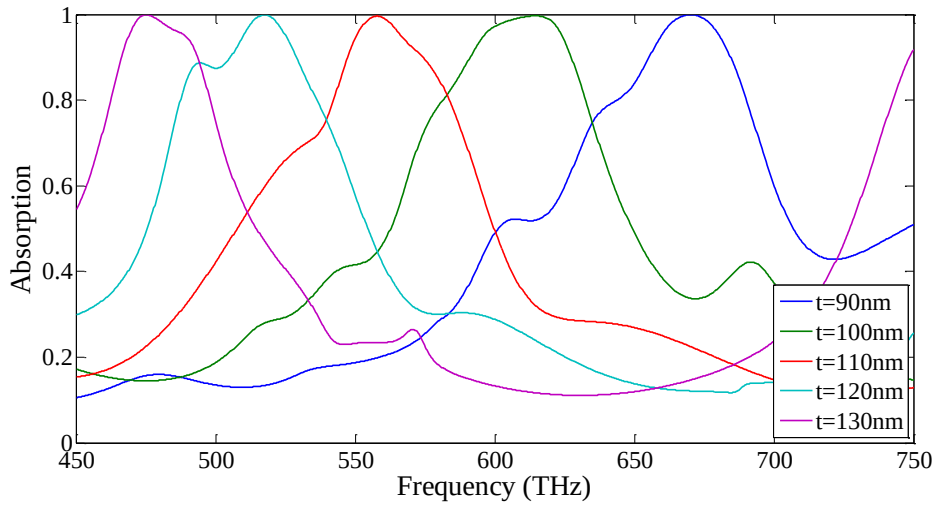

Figure 5-4. Absorption characteristics of a proposed MPA unit cell for different dielectric thicknesses't' of dielectric spacer.

These results show that the dielectric spacer has a crucial role in absorption resonance of the MPA unit cell through the coupling mechanism discussed in the previous paragraphs, and it is an added value to the MPA design in the present study.

Secondly, the simulation is carried out by changing top patch's periodicity 'b' to different length and different patch thickness 'k'. It can be seen from Figure 5-5 (a),

that by changing ‘b’ from 314.4 nm to 348.6 nm with step width of 5.7 nm, the absorption characteristic of the proposed MPA does not change much, however, enhancement on the resonant absorption bandwidth is noticed for shorter values of b. besides, the simulation results for different value of patch’s thicknesses are reported in Figure 5-5 (b), and it is clearly seen that the smaller the patches thickness is, the more the absorption resonance is enhanced. One can also observe that the best absorption rate is obtained for the smallest k= 5 nm.

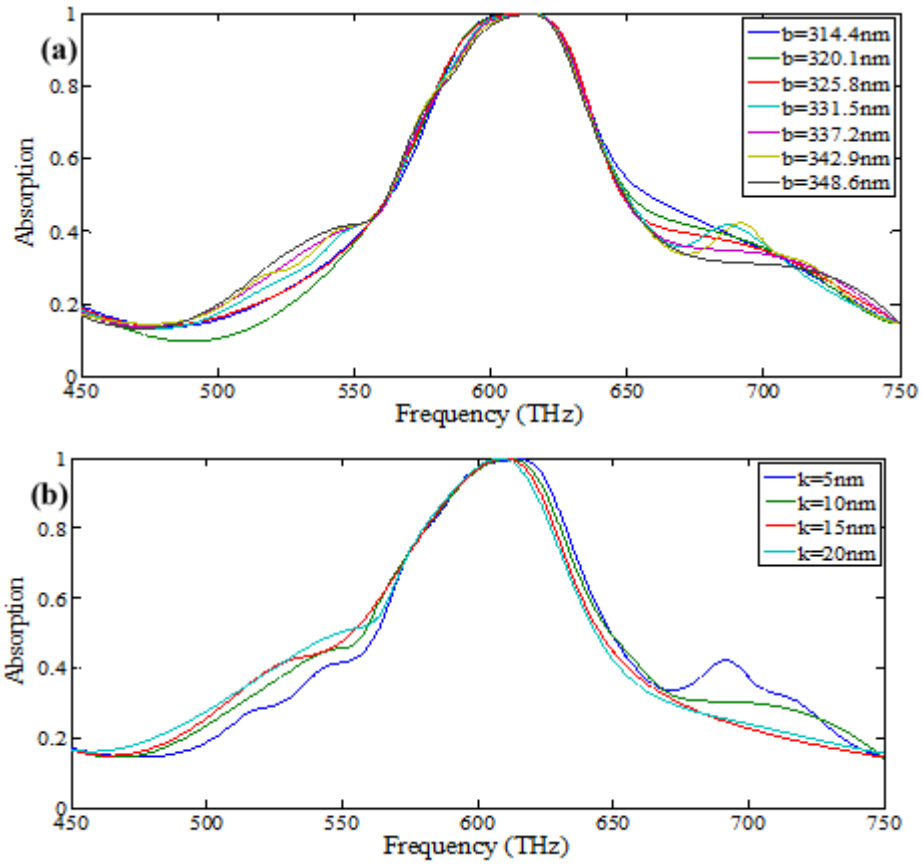

Figure 5-5. Simulated absorption characteristics of the proposed MPA structure with different patches’ geometric parameters: (a) different values of patches’ periodicity ‘b’, (b) different patches thickness ‘k’.

The direction of solar radiations changes at every time of day in the sky and also some of them hit the unit cell in unpolarized form. Thus in order to optimize absorption coefficient of a MTM unit cell for all incidence EM radiations at the operating frequency, the metamaterial structure must be independent of both incident angles and polarization angles for EM (TE and TM) radiations. Therefore, the absorption capability of MPA unit cell in the present study is inspected for both TE and TM

polarization and for different incident angles of EM radiations. In Figure 5-6 (a) & (b), simulated absorption results for the proposed MPA structure at different polarization (TE and TM wave) are shown.

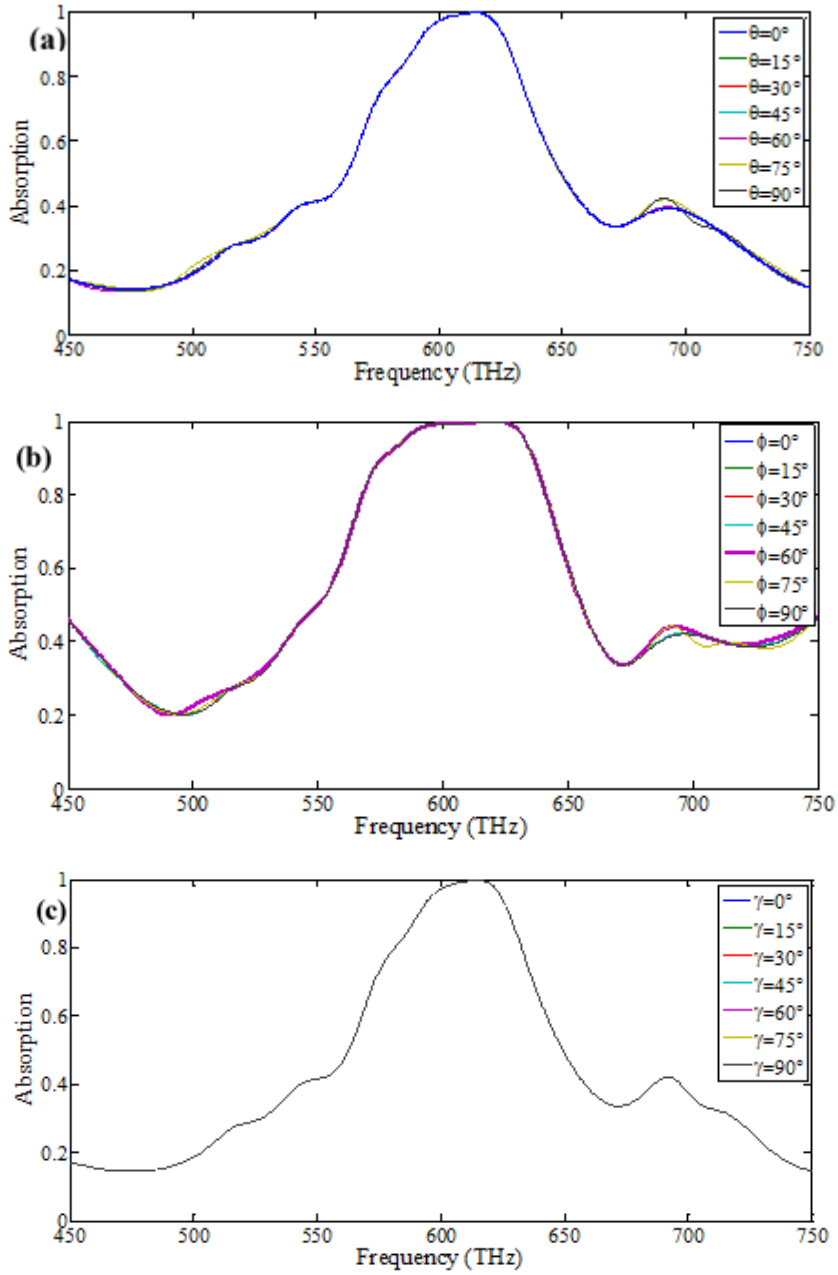

Figure 5-6. Simulated absorption characteristics of a proposed MPA for different incident angles: (a) TE incident wave (θ), TM incident wave (ϕ), and (c) simulated absorption characteristics of the proposed MPA for different polarization angles (γ) of EM wave.

By changing the polarization angles of a polarized EM wave from 0° to 90° with a step width of 15°, it is realized that the absorption rate remains constant over a wide range

of angles for both TE and TM polarized wave. In addition to that, as one can observe from Figure 5-6 (b), for TM incident wave, the absorption bandwidth becomes much wider than in the case of TE. As it can also be noticed from Figure 5-6 (c), due to the high symmetry of the suggested MPA unit cell, its absorption rate remains unchanged for over wide range of angles of incidence EM radiations, where by changing incident angle of EM radiations from 0° to 90°, the absorption results remain high and constant in all cases. Therefore the proposed MPA structure is a very good candidate for fabrication of outstanding solar cells without issues of polarized waves with the advantage that the absorption will be independent to azimuthal angle or the position and direction of solar radiations.

5.3. Conclusions

In this chapter, a single band metamaterial perfect absorber has been proposed, simulated and characterized for its absorption capability by using coupling model system (impedance matching condition). Firstly, an outstanding single band of 99.7% absorption with an outstanding bandwidth of 15.5% with respect to the central frequency has been obtained. Secondly, the parametric studies has confirmed the high flexibility character of a proposed MPA, and tunability for a dielectric thickness has been observed. Thirdly, in order to understand the absorption mechanism of a proposed MPAs, electric field, and surface current distributions were analyzed. At last, the high symmetry and flexibility of a proposed structure has been examined by testing its absorption characteristic under different incident angles and polarization angles, and for both cases, the proposed MPA unit cell proved to be insensitive to incidence EM radiations for a wide range of incident angles and also insensitive to polarization angles for TE and TM radiations. The proposed design is an outstanding candidate towards high quality solar cell in a visible frequency regime.

CHAPTER 6

THE PROPOSED WIDE-BAND PERFECT METAMATERIAL ABSORBERS FOR SOLAR CELL APPLICATIONS

6.1. Introduction

In a previous chapters perfect metamaterial absorber designs which display dual-bands and tunable wide band response in visible frequencies have been discussed and characterized. It has been found that even though the proposed dual-band designs produce two perfect absorptions response in visible frequency range, however, their bandwidth with respect to the resonant frequency is not wide enough which affects the overall power gain (total absorption rate) by a unit cell. Although a MPA design proposed in Chapter 5 gave a wide band absorption response, its absorption bandwidth of 15% is not enough. Thus, designing a metamaterial absorber to operate over a wide range of frequencies will enhance the cells overall absorption as well as its overall efficiency. In this chapter a wide-band MPA structure is proposed, discussed and characterized using numerical simulation and theoretical analysis for their absorption performance in visible frequency realm. Furthermore, a thermal analysis of the proposed wide-band metamaterial absorber is conducted in order to verify its absorption behavior under different temperature. In the last section of this chapter a validation of the simulation results from Finite Integrate Technique (FIT) with the simulation results from Finite Element Method (FEM) is reported. The advantage of the proposed wide-band MPA design is that it offers both perfect absorption coefficient within a wide range of frequency which makes it a better candidate in the fabrication of solar cell with high overall power gain.

6.2. Wide Band Perfect Metamaterial Absorber for Solar Cell Application

6.2.1. Structure Design and Simulation

In this section, a metamaterial absorber with perfect and wide band absorption resonance is designed. The proposed MPA unit cell consists of three basic components: the top ring resonator, ground metallic plane, glass Pyrex lossy (grey color) and intermediate dielectric spacer. In Figure 6-1, the geometrical representation

of intended wide band MPA unit cell is shown. All metallic layers are carefully chosen to be gold lossy metal (yellow color) whose electric conductivity is $4.561 \times 10^7 \frac{S}{m}$. Gold is chosen due to its ability to resist to excessive heat, however, changing the metal type does not affect much the absorption coefficient of metamaterial absorber designs working at high frequencies as discussed in the previous chapter. Thus, gold layers can be replaced by any other noble metal while absorption rate remains the same. Glass properties are electric permittivity $\varepsilon = 4.82$ and tangent delta electric constant of 0.0054. Dielectrics layer are chosen to be gallium arsenide lossy (GaAs) (green color) whose electric permittivity and loss tangent delta are 12.94 and 0.006, respectively. GaAs is chosen mainly because of its high electron mobility and saturated electron velocity, it is also insensitive to heat due to its wide band gap and it has direct band gap which makes it a better absorber and emitter of light.

The simulation for the intended MPA design is executed with full wave electromagnetic software of Finite Integration Technique (FIT), with frequency domain solver. The proposed structure intended to work at visible frequency ranging from 450 THz to 800 THz. The incidence EM radiations polarize in a way that the electric (*E*) field and magnetic (*H*) field propagate in direction parallel to the MPA structure plane, while wave vector (k) is perpendicular to the geometric plane of the unit cell structure. In simulation of electromagnetic wave problems, mesh density setting plays important role. This is because the structure to simulate need to be divided into mesh cells. The mesh density can be generated automatically by setting correctly minimum number of steps per wavelength and minimum number of steps. In this study, tetrahedral mesh is used, the minimum number of steps per wavelength and minimum number of steps taken by default to be 4 and 10, respectively and this generate 113170 tetrahedrons enough to give accurate simulation results. The periodic boundary conditions are selected whereas the open and add space is chosen as simulation environment (Z plane). The geometric parameters of the intended metamaterial perfect absorber are: a = 17 nm, b=102 nm, c = .2 nm, d = 57.8 nm, e = 27.2 nm, f = 40.8 nm, t = 103.4 nm, z = 103.4 nm, x = 530 nm, n = 16 nm, and k (thickness of resonator) = 6.8 nm.

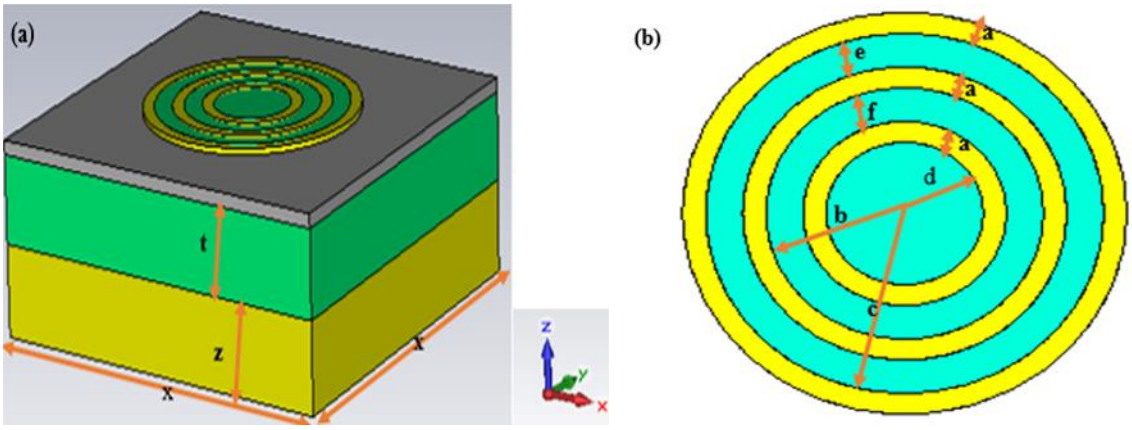

Figure 6-1. (a) A unit cell of the proposed perfect metamaterial absorber, (b) Top view of the proposed MPA unit cell (showing resonators).

6.2.2. Results and Discussion

The simulation results for the proposed metamaterial unit cell are given in Figure 6-2. As one can observe in Figure 6-2 (a), a wide-band is obtained which is a result of the combination of triple-bands resonant absorptions combined together to form a wide band with perfect absorption. The triple-bands absorption response is believed to be resulting from individual electromagnetic resonance produced by strong coupling of each one of the three ring resonators with the substrate and also from the strong coupling between the resonators and the ground plane.

In order to understand the origin of wide band absorption characteristics of the MPA structure understudy; separate numerical simulations for each individual resonator are performed. The absorption rate for each one of three ring resonators are presented in Figure 6-2 (b). As one can observe, from Figure 6-2 (b), each resonator produces a single band absorption resonance with absorption rate of about 90%. However, the combination of all three resonators bring about a strong electric and magnetic field resonance which lead to the enhancement of total absorption (near prefect absorption rate) and creation of a wide-band absorption resonance. In Figure 6-2, the results for the simulated absorbance are reported where the nearly unit (99.99%) absorptions is obtained at 565.15 THZ, 582.5 THz and 598.75 THz, respectively.

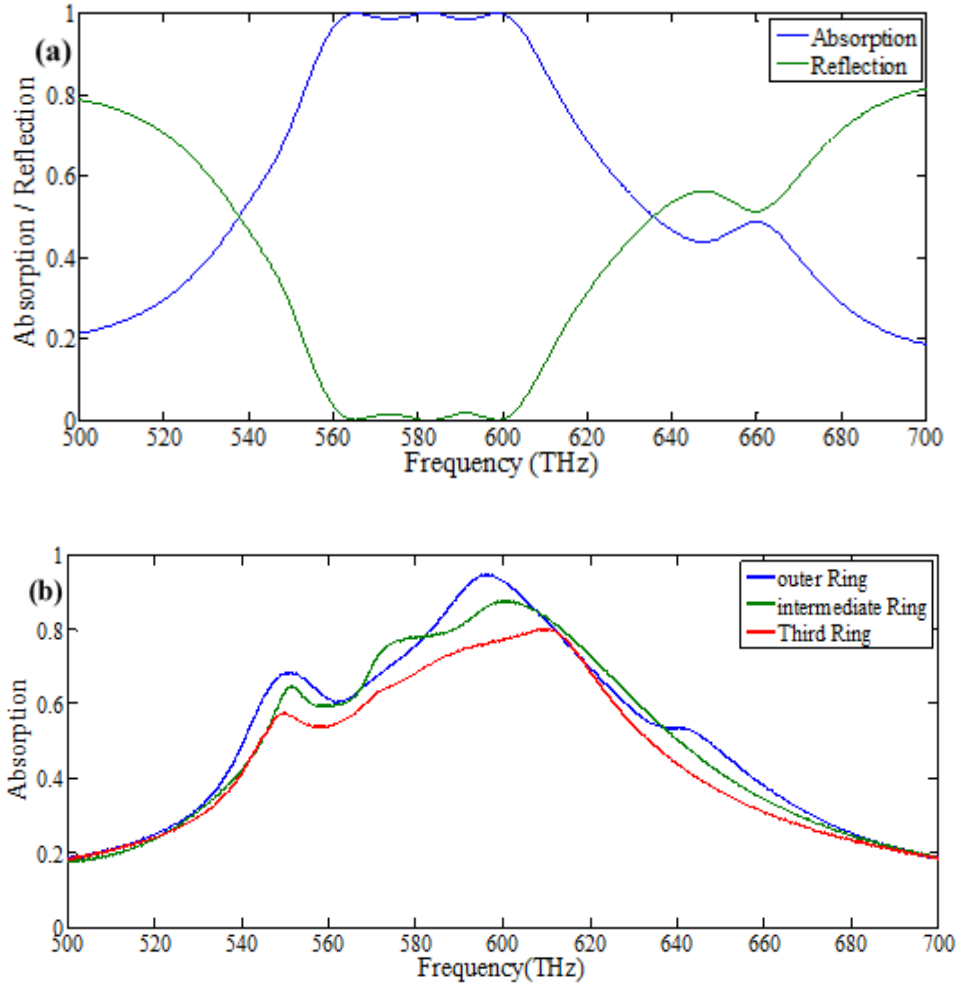

Figure 6-2. Simulated absorption rate of the proposed wide band MPA unit cell. (a) Wide band perfect absorption, (b) simulated absorption rate for each ring.

6.2.3. Geometry Parametric Study

In order to understand the impact of the structure geometrical parameters on absorption response of the suggested MPA design, the parametric study is conducted. In Figure 6-3, the simulation results for geometrical parametric study are reported. Firstly, numerical simulation is conducted under different thickness‘t’ of the dielectric spacer for the proposed MPA unit cell. The dielectric thickness is changed around its reference value (98.7 nm) by increasing it with 4.2 nm step up and decreasing it by 4.2 nm step down, see Figure 6-3 (a). The absorption rate of the proposed MPA unit cell remains almost high and wide for all dielectric’s thicknesses that are closer to 94.5 nm and 102.9 nm. However, as one can notice from Figure 6-3 (a), at the case of thickness smaller than the reference dielectric spacer thickness ($t < 98.7$ nm) blue shift of the

resonant frequencies occurs while for all thicknesses greater than the dielectric's reference thickness($t > 98.7\ nm$) a redshift of resonant frequency is noticed. Additionally, for the shorter dielectric thickness the band width of the proposed design can be enhanced though at that instant its absorption rate drops (see blue line in Figure 6-3 (a)). This results is an evidence that the proposed MPA is a good candidate for the realization of broadband absorbers for a wide range in visible frequency regime, where by adjusting the thickness of a dielectric spacer the absorption bandwidth can be improved while the absorption coefficient also get enhanced.

Secondly, it is found that the absorption coefficient of the proposed metamaterial absorber unit cell strongly rely on the thickness 'k' of the resonator. The simulation is performed by changing the thickness from 3.4 nm to 17 nm with a step width of 3.4 nm. As it can been seen from Figure 6-3 (b), the results from numerical simulation shows a highest absorption rate at $k = 6.8\ nm$ and start to decline for all $k > 6.8\ nm$. As a result, in order to keep high absorption rate, the thickness of the resonator for the proposed MPA unit cell must be in the range of 6.8 nm.

Thirdly, the analysis on the structure periodicity 'x' is performed and the simulation results are reported in Figure 6-3 (c). The simulation is carried out by decreasing the periodicity of the unit cell from 530 nm to 515 nm and increasing it from 530 nm to 545 nm with a step width of 7.5 nm at all the two cases and the observation is that changing the structure periodicity 'x' does not affect much its absorption characteristic, the only observation is the shift toward left and shift toward right of resonant frequencies noticed for all $x > 530$ nm and $x < 530$ nm , respectively.

Finally, it is observed that the thickness of glass Pyrex lossy does a great job in the achievement of perfect absorption where some radiations transmitted by the top resonator are consume in this layer while the rest non absorbed radiations transmitted to the dielectric spacer (lossy layer) to be absorbed there (glass Pyrex lossy plays a role of an intermediate absorber). Therefore, as it can be observed in Figure 6-3 (d), by varying the thickness 'n' of glass layer enhancement of absorption rate and bandwidth is gained without any variation in resonant frequencies.

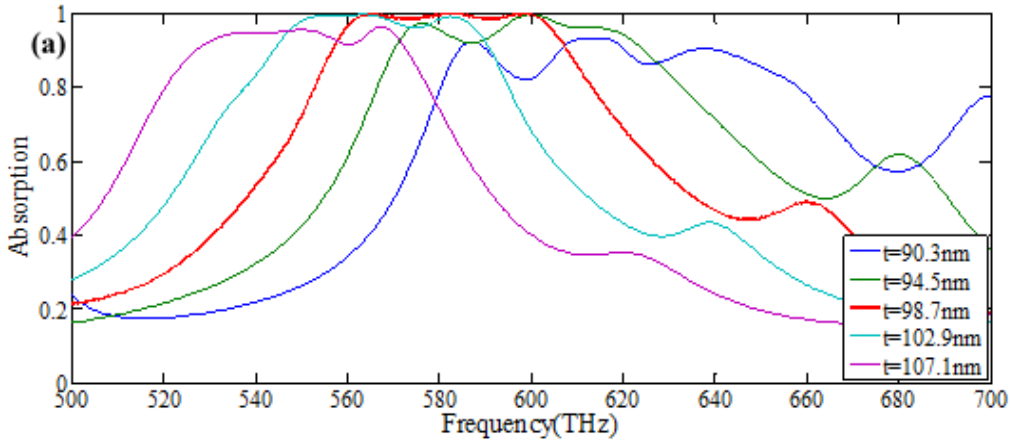
(a)
Absorption
Frequency(THz)
t=90.3nm
t=94.5nm
t=98.7nm
t=102.9nm
t=107.1nm

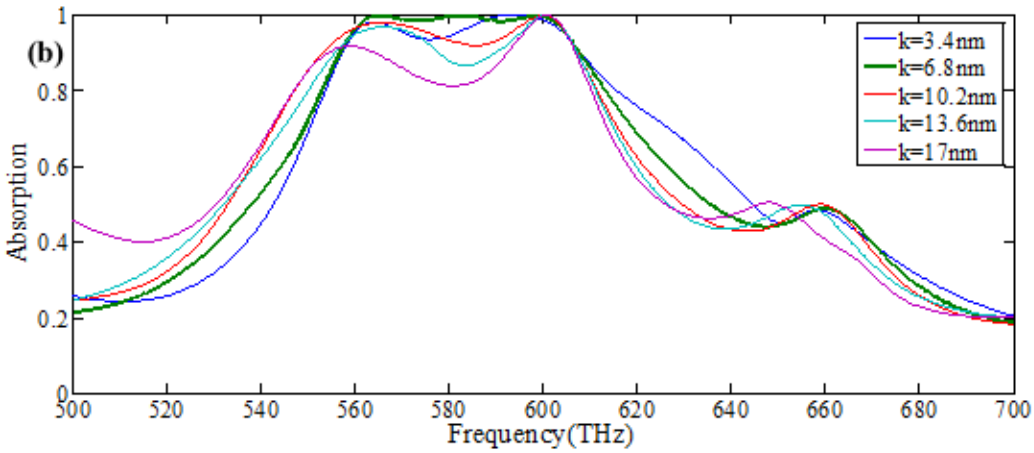
(b)
Absorption
Frequency(THz)
k=3.4nm
k=6.8nm
k=10.2nm
k=13.6nm
k=17nm

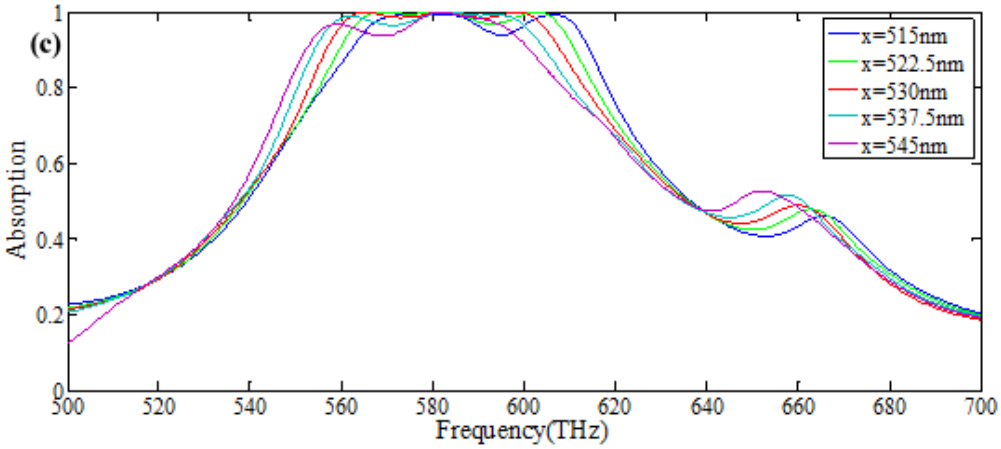
(c)
Absorption
Frequency(THz)
x=515nm
x=522.5nm
x=530nm
x=537.5nm
x=545nm

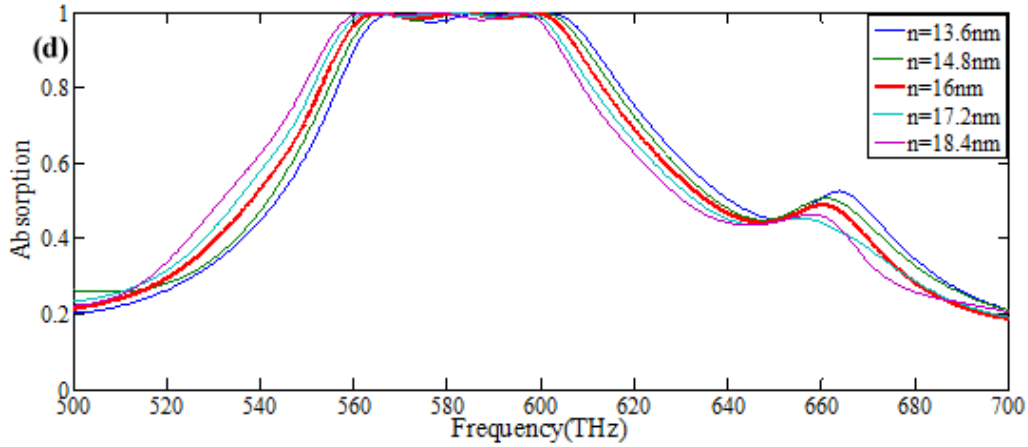

Figure 6-3. Simulated absorption results for the proposed wide-band MPA unit cell under different dimension of geometric parameter: (a) different dielectric thickness 't', (b) different thicknesses of resonator 'k', (c) different length of structure periodicity 'x' and (d) different thickness 'n' of a glass layer.

6.2.4. Polarization Angles, Fields and Surface Currents Distributions Analysis

To further understand the absorption characteristics of the proposed MPA structure with respect to the source of radiations, the numerical simulation has been conducted under different polarization angles for TE and TM radiations and under different angles of incidence electromagnetic radiation. In Figure 6-4, numerical simulation results for different polarization angles (TM and TE waves) and different angles of incident EM radiations are depicted. As one can observe in Figure 6-4 (a) and (b), the absorption response of the MPA design under study is polarization independent for a wide range of angles (from 0° to 90°) for both TE and TM radiations. Besides, as one can also observe in Figure 6-4 (c), the proposed MPA design offers constant and perfect absorption for all angles (normal and oblique angles) of incidence EM radiations. This is obtained by conducting simulation of the proposed MPA unit cell at different angles of incident radiations where by changing incident angles from 0° to 90° with step width of 15°, the absorption rate found to be the same for all incident angles. This behavior is a result of high symmetry character of the structure understudy. The absorbers of this type have huge potential applications in fabrication of advanced absorber devices operating in visible frequency range and can be utilized for fabrication of more efficiency solar cells, where the absorbance of the cells can be

retained high regardless of the polarization angle for both TE and TM waves and also for different angles of incidence for electromagnetic radiation.

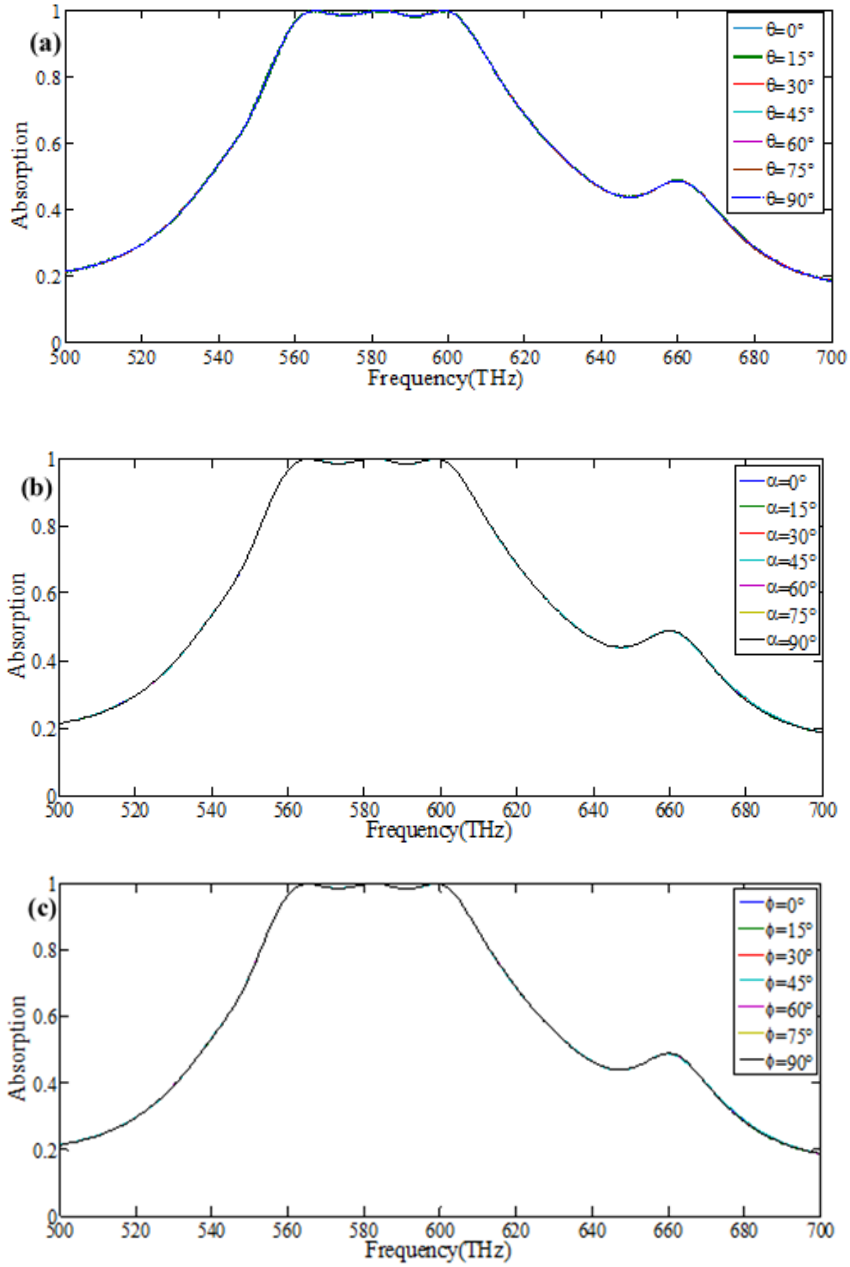

Figure 6-4. Simulated absorption characteristics of the proposed MPA structure under different polarization angles and angles of incident EM radiations. (a) TE polarization (θ), (b) TM polarization (α), and (c) different incident angles (∅) of incidence electromagnetic radiations.

Finally, in order to understand the physics behind absorption mechanism of the proposed MPA design, the electric fields and surface currents distributions of the proposed structure is discussed for the three resonant frequencies of 565.15 THz, 582.5

THz and 598.75 THz, respectively. In Figure 6-5 and, E-fields, and surface currents distributions are depicted. As one can observe at all resonant frequencies the strong electric fields distribute at the surface of a glass lossy layer and the inserted dielectric layer surrounded by resonators which produce electric polarization. The strong electric fields around the resonator induce surface charges which produce the surface currents resonant responsible for magnetic resonance and the resonant absorption [22].

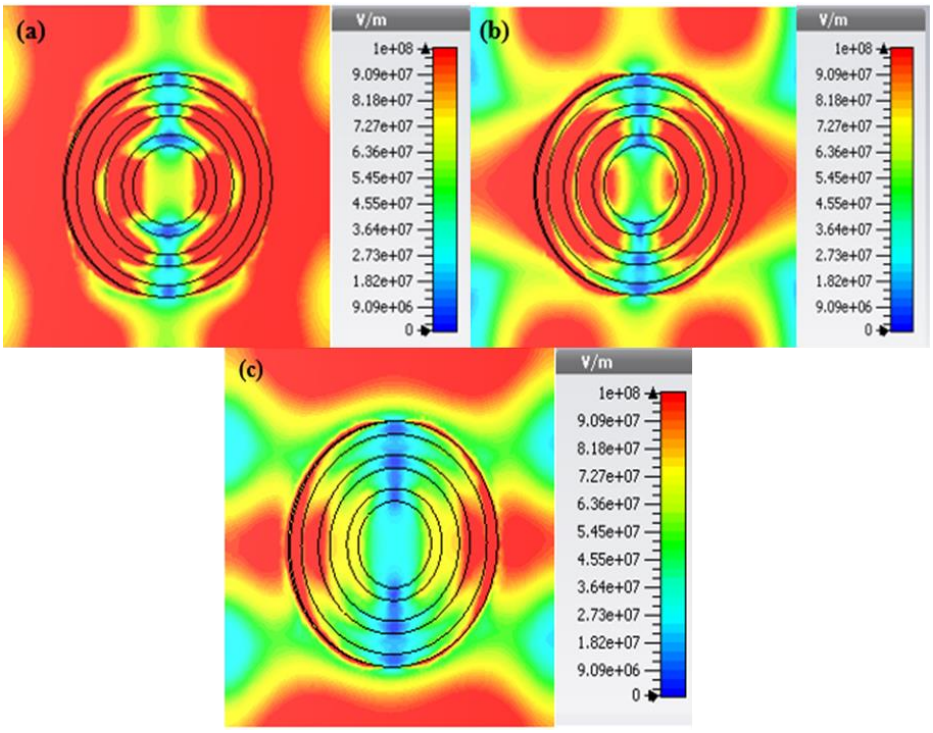

Figure 6-5. Electric fields distribution for the proposed MPA unit cell at the resonant frequencies of: (a) 565.15 THz, (b) 582.5 THz and (c) 598.75 THz.

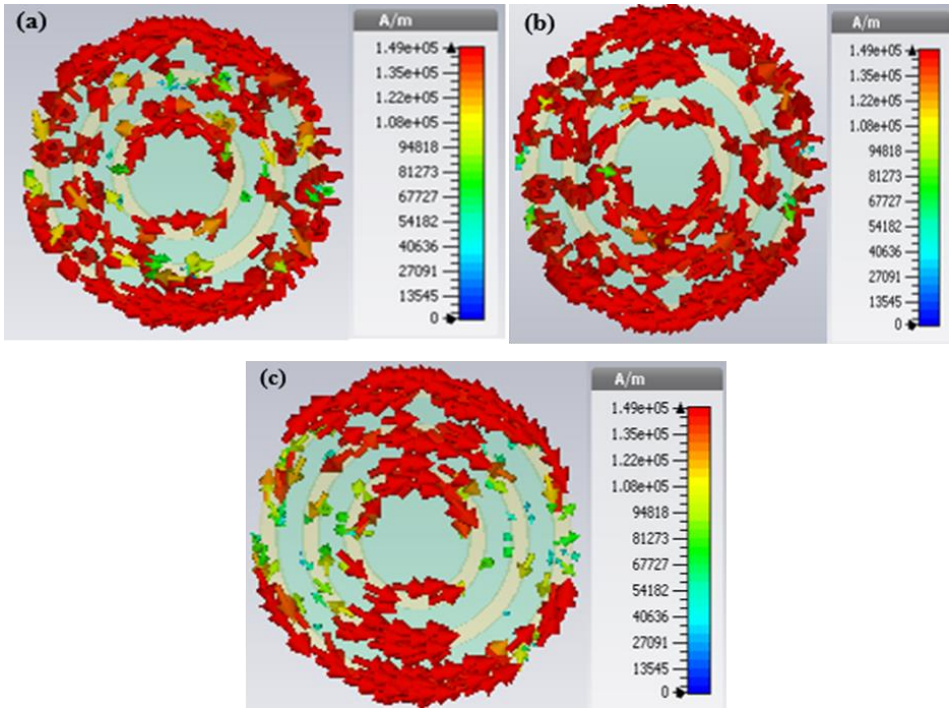

Figure 6-6. Surface current distributions for the proposed MPA unit cell at the resonant frequencies of: (a) 565.15 THz, (b) 582.5 THz and (c) 598.75 THz

The strong symmetric, antisymmetric and circular surface currents distributions observed from Figure 6-6 arose from the coupling of resonators layer with dielectric spacer and the ground plane. These surface currents are accountable for the three perfect (near a unit) absorptions obtained at the frequencies of 565.15 THz, 582.5 THz and 598.75 THz, respectively. Even though, for all three resonant frequencies a near a unit absorption rate is attained, the highest absorption observed at 582.5 THz can be confirmed by the strong surface currents distributions around the ring resonators detected at this frequency see Figure 6-6 (b). This means that at this frequency the impedance of the structure understudy matches well the one for a free space ($Z(\omega) = Z_0(\omega)$) leading to high absorption of all electromagnetic radiations which struck the resonator's surface.

6.3. Theoretical Characterization of the Proposed Wide Band Metamaterial Absorber Using Interference Theory

6.3.1. Introduction

The study of metamaterial absorbers attracted interest of many scientists and engineers; various techniques had also been developed to characterize and analyze metamaterial absorber designs and their interaction with electromagnetic radiations. The most famous method in the study of MPA is the coupling model system (conventional method to analyze metamaterial absorber structures) which uses impedance matching theory [21], and this method has been discussed in the previous sections.

The theory of impedance matching condition describe a MPA as homogenous medium made up by periodic arrangement of metallic resonator and dielectric material. The metallic resonator supply electric resonance to couple with electric permittivity and the strong coupling of the resonator and ground metal generate magnetic resonance to tune the magnetic permeability of the MPA structure. This theory state that at the impedance match condition, the value of electric permittivity and magnetic permeability are the same ($\mu(\omega) = \varepsilon(\omega)$) which causes the impedance of the whole MPA structure to match the one for a free space ($Z_0(\omega)$) at a very minimum refection coefficient.$Z(\omega) = Z_0(\omega) = 1$.

Impedance matching theory continue stating that, by employing a dielectric substrate which is high loss enough, this is to say that it will not allow the transmission of EM radiation through the ground metal surface, perfect absorption happens at resonance frequency. Nonetheless, the drawback with this technique is that it treats MPA structure as a homogeneous medium, as a result this theory is not an appropriate theory for the study of the interaction between the ground plane and resonator layer.

In the recent years, different theories have been developed for the study of metamaterial absorbers and to explain the concept of electromagnetic resonance in metamaterial absorbers. Wen et al. [91] in 2009 conducted a study of metamaterial absorber by using Transmission Line (TL) model. From TL model they calculated

scattering parameters(S-parameters), energy consumption and the power loss density of the absorber. In their model, the absorption rate strongly depends on the capacitance and inductance (LC) resonance of the resonator layer which contribute to the electromagnetic resonance. Subsequently, Zhou et al [92] in 2011 using transfer matrix method analyzed single and multilayers metamaterials, where they modeled each individually layer as a metasurface having effective surface electric and magnetic susceptibility derived through a thin film approximation. Their finding is that their model can be employed as an alternative interpretation of metamaterial perfect absorbers, where it works as a modified Fabry-Perot resonance. In article [49] Zhou et al. design an extremely broad band metamaterial absorber using destructive interference model. In this method, they used a metamaterial unit cell which consisted of multilayer SSRs structure. Their SRRs structure produce an appropriate refractive index dispersion spectrum which in turn produce successive antireflection waves in a wide frequency range. In their study Zhou et al. managed to achieve a perfect absorption which generated by the destructive interference of the two waves reflected from the surfaces of MTM structure. Other method which used for analysis and study of metamaterial perfect absorber is interference theory. This method to analyze MPA was first introduced by Cheng [54, 93] in 2012, where he used a multiple reflections interference model to prove a negligible near field along the two nearest metal layers in a typical metamaterial absorber. In his model, he suggested that if the two layers of metal structures is decoupled the only observation from a MTM structure is a multiple reflection between the layers. Thus by combining numerical simulations and mathematical calculations he was able to prove that the perfect absorption of a metamaterial can be a result of interference and superposition of EM radiations in a MTM structures instead of excitation of magnetic resonance. After publication of this first interference theory for analysis of metamaterial perfect absorber, other researchers had drawn their attentions to this theory [94 - 96], but still the problem was that their studies was limited to normal incident angle of EM radiations. In 2013 Huang et al. [97] proposed an extended interference theory to investigated metamaterial perfect absorption for both normal and oblique incident angle EM radiations.

In this thesis, the interference model and extended interference model from [54] and [97] are combined in order to theoretically validate the numerical simulation results of the wide-band MPA structures proposed in this thesis.

6.3.2. Extended Interference Theory Model

Typically, the perfect absorption of metamaterials absorbers structure are verified through the process of impedance matching condition which resulting from tuning individually electric permittivity and magnetic permeability of a metamaterial absorber structures. This process in known to the name of "coupled model", where a metal sheet of the thickness much bigger than the structure skin depth is placed at the ground plane of the structure unit cell in order to prevent transmission of EM radiations back to the space and also this metallic plane reflect back the radiations to the dielectric spacer to be consumed there and facilitate the process of achieving perfect absorption of EM radiation. The extended interference theory model which is the model used for theoretical investigation of the perfect absorption of MPA structures for both normal incidence and oblique incidence radiation on the other hands, it uses the process called "decoupled model." In this model, the ground metallic layer of a MPA design is removed and the scattering parameter which extracted from the numerical simulation are used in superposition and interference relations for the calculation of absorption coefficient.

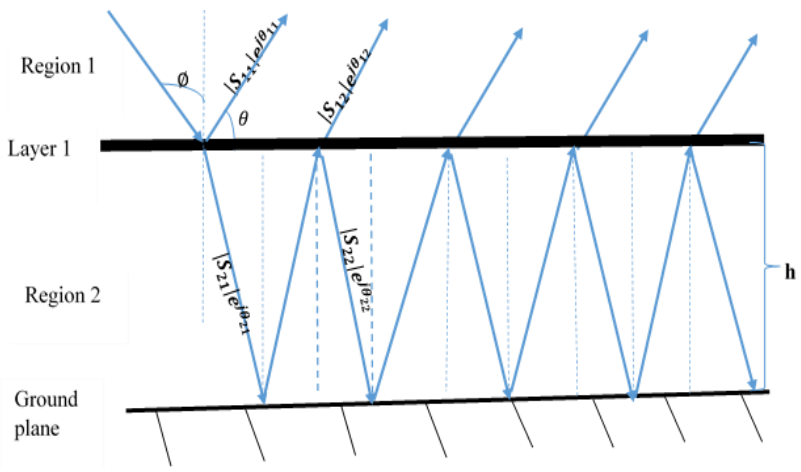

Figure 6-7. Multiple reflection and interference theory model

In the interference theory model, the thickness of layer 1 is assumed to be roughly equal to zero. The S-parameters are defined as: $S_{11} = |S_{11}|e^{j\theta_{11}}$ which represents the reflection coefficient of layer 1 from region 1 to region 1, $S_{12} = |S_{12}|e^{j\theta_{12}}$ is the transmission rate of layer 1 from region 2 to region 1, $S_{21} = |S_{21}|e^{j\theta_{21}}$ is the transmission rate of layer 1 from region 1 to region 2 and $S_{22} = |S_{22}|e^{j\theta_{22}}$ is the reflection rate of layer 1 from region 2 to region 2. The total electromagnetic radiation of layer 1 reflected from the region 1 back to the region 1 can be calculated using interference model (6.1) which used by [54, 93-96] for the studies of metamaterial absorber structures.

$$S_{11total} = S_{11}+S_{12}e^{-j(2\beta+\pi)}S_{21} + S_{12}e^{-j(2\beta+\pi)}\left(S_{22}e^{-j(2\beta+\pi)}\right)^{1}S_{21} + S_{12}e^{-j(2\beta+\pi)}\left(S_{22}e^{-j(2\beta+\pi)}\right)^{2}S_{21} + S_{12}e^{-j(2\beta+\pi)}\left(S_{22}e^{-j(2\beta+\pi)}\right)^{3}S_{21} + S_{12}e^{-j(2\beta+\pi)}\left(S_{22}e^{-j(2\beta+\pi)}\right)^{4}S_{21} + \ldots\ldots + S_{12}e^{-j(2\beta+\pi)}\left(S_{22}e^{-j(2\beta+\pi)}\right)^{n}S_{21} \quad (6.1)$$

By simplifying equation (6.1), the total reflected electromagnetic radiations in layer 1 which result from the reflected radiations from the region 1 back to the region 1 can be described by relation (6.2):

$$S_{11total}=S_{11}+S_{12}e^{-j(2\beta+\pi)}\left(\sum_{n=0}^{\infty}\left(S_{22}e^{-j(2\beta+\pi)}\right)^{n}\right)S_{21} \quad (6.2)$$

Through superposition principle equation (6.2) can be rearranged to become (6.3).

$$S_{11total} = S_{11} + \frac{S_{12}S_{21}e^{-j(2\beta+\pi)}}{1-S_{22}e^{-j(2\beta+\pi)}} \quad (6.3)$$

By combining together the scattering parameters with their phase angle, the total electromagnetic radiation of layer 1 reflected from the region 1 back to the region 1 can be given by the relation (6.4).

$$S_{11total} = S_{11total} = |S_{11}|e^{\theta_{11}} + \frac{|S_{12}||S_{21}|e^{-j(2\beta+\pi-\theta_{12}-\theta_{21})}}{1-|S_{22}|e^{-j(2\beta+\pi-\theta_{22})}} \quad (6.4)$$

In passive metamaterial absorber structure model, $S_{12} = S_{21}$ and the equation (6.4) can be simply reported as:

$$S_{11total} = |S_{11}|e^{\theta_{11}} + \frac{|S_{12}|e^{-j(2\beta+\pi-2\theta_{12})}}{1-|S_{22}|e^{-j(2\beta+\pi-\theta_{22})}} \quad (6.5)$$

β Is the complex propagation phase and is given by $\beta = kd$,where k represents wave number for region 2 and d symbolizes the distance between layer 1 and the ground plane. The transmitting distance can be calculated from (6.6) and by using Snell's law of refraction (6.7);

$$d = h\, cos\, (\emptyset_2) \quad (6.6)$$

$$n_1 sin\emptyset_1 = n_2 sin\emptyset_2 \quad (6.7)$$

$$\emptyset_2 = \arcsin(\frac{n_1}{n_2} sin\emptyset_1) \quad (6.8)$$

where n_1 and $n_1$represent the indexes of refraction of region 1 and region 2, respectively, while $\emptyset$ symbolizes the angle between the normal at the interface and the angle of incidence radiations.

$$n = \sqrt{\varepsilon\mu} \quad (6.9)$$

By using relation (6.9), equation (6.8) can be revised into the following (6.10);

$$\emptyset_2 = \arcsin(\sqrt{\frac{\varepsilon_1\mu_1}{\varepsilon_2\mu_2}} sin\emptyset_1) \quad (6.10)$$

Assuming that magnetic permeability (μ_1) of region 1 is equal to magnetic permeability (μ_2) of region 2, thus equation (10) will be transformed to become (6.11);

$$\emptyset_2 = \arcsin(\sqrt{\frac{\varepsilon_1}{\varepsilon_2}} sin\emptyset_1) \quad (6.11)$$

From the relation (6.11) equation (6.6) can deduced to give the final expression for the transmitting distance as:

$$d = h\cos(\arcsin(\sqrt{\frac{\varepsilon_1}{\varepsilon_2}} sin\emptyset_1)) \quad (6.12)$$

where h is the thickness of the region 2 (thickness of a dielectric spacer) while ε_1 and ε_2 are electric permittivity of region 1 and region 2, respectively.

If all the parameters are available, then model in (6.5) can be employed to calculate the total absorption by using equation (6.13).

$$A(\omega) = 1 - S_{11total} \tag{6.13}$$

This model (6.13) is used in this thesis in order to compare the simulation results from a coupled model (of the proposed wide-band perfect metamaterial absorber with one ring resonator only). In order to obtain the total reflection coefficient $\boldsymbol{S_{11total}}$ ground metallic plane of the proposed wide-band MPA design is removed before performing simulation "decoupling system". In Figure 6-8, the proposed structure unit cell for coupled and decoupled model are shown. The S-parameters obtained from the numerical simulation and by using relation (6.5) and (6.13) the absorption rate for the decoupled model is calculated. In Figure 6-9 and Figure 6-10, the results for coupled model (conventional metamaterial) and decoupled model (interference theory) for normal incident EM radiations are reported.

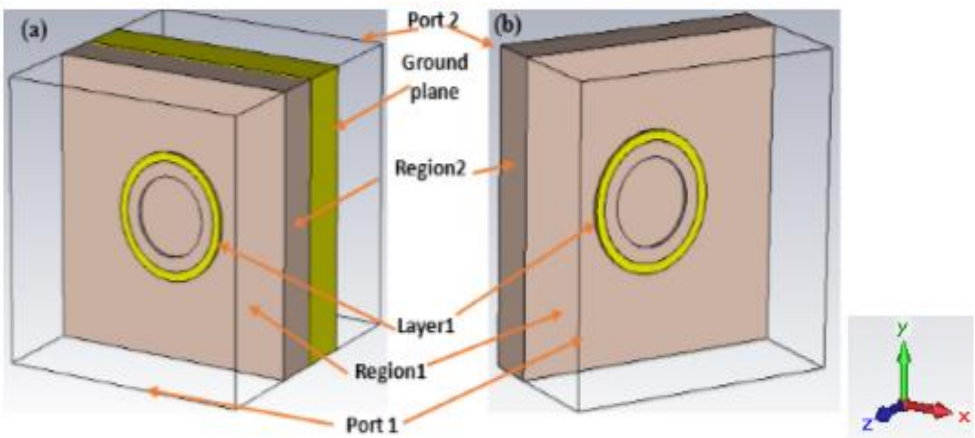

Figure 6-8. A unit cell of the proposed MPA structure. (a) Coupled model (for numerical simulation) , (b) Decoupled model (for interference theory).

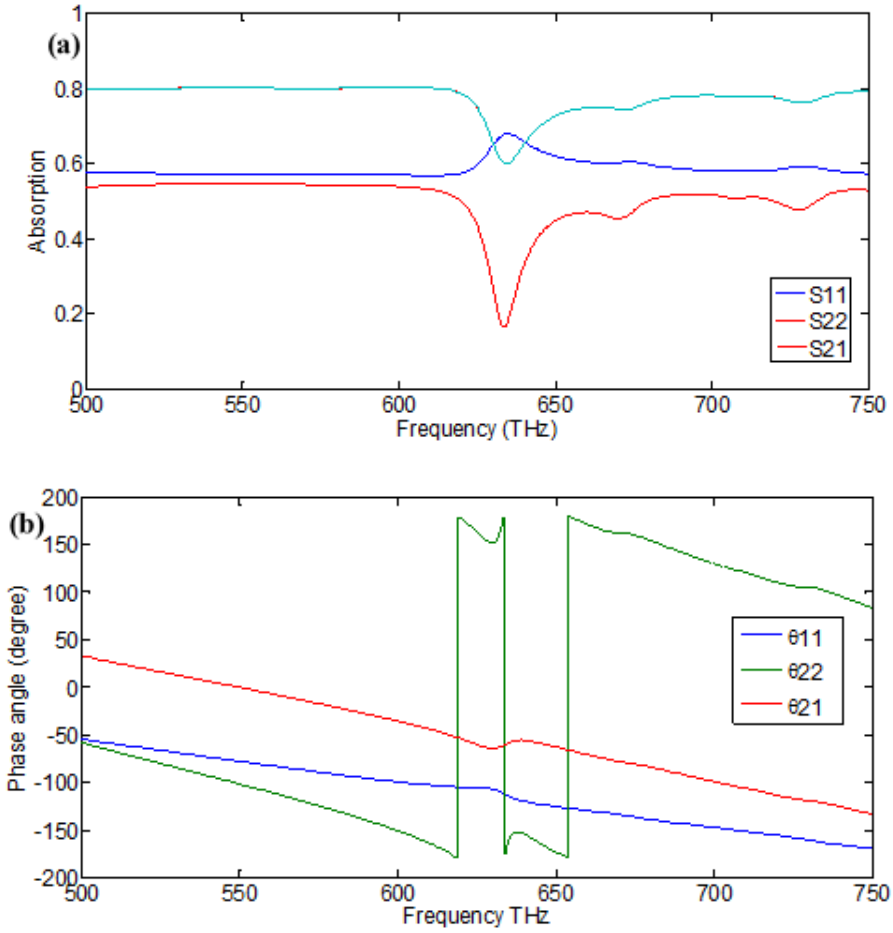

Figure 6-9. (a) S-parameters for the decoupled model, (b) Phase angle for S- parameters

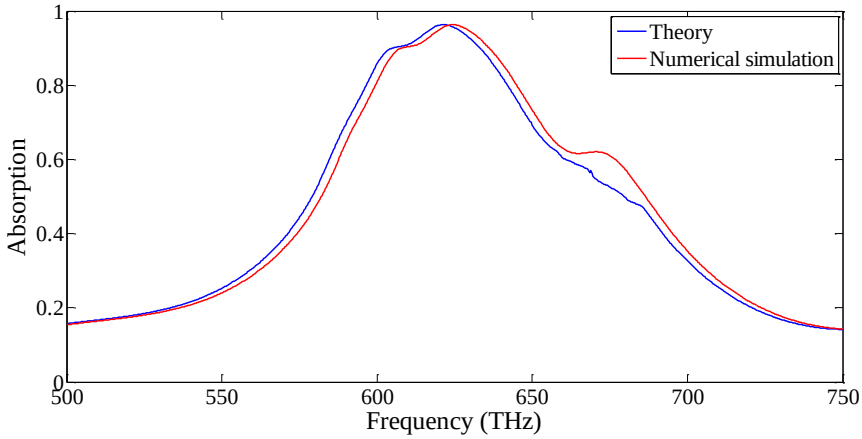

Figure 6-10. Absorption results for coupled (conventional metamaterial) and decoupled (interference theory) model.

The dimensions of the coupled model design and decoupled are similar to the one in the previous section with only outer ring resonator, where its periodicity is 530 nm, the thickness of the ground metallic layer is 103.4 nm and the thickness of the dielectric spacer is 121 nm. Unlike to the design in section 6.1 of this chapter (see Figure 6-1 (a)), the design in this section does not contains glass lossy layer and the comparison was made based on the results from the present coupled model (Figure 6-8) without a glass layer.

As one can observe from Figure 6-10, both two models, the coupled model and decoupled model offer the same magnitude of absorption rate of approximately 96.3% at the resonance frequency of 622.9 THz. However, one can also notice difference in the bandwidth and a little shift of resonance frequency. The interpretation of this is that in the coupled model, the ground metallic plane brings together all radiations which transmitted from a dielectric spacer and it reflects them back to be consumed in the dielectric spacer which leading to the enhancement of absorption band width while in decoupled model, the ground metallic layer is not applied [94-97].

6.4. Thermal Characterization of the Proposed Wide-Band Perfect Metamaterial Absorber

Generally, absorption characteristics of a metamaterial absorber is a fixed value for any given design and the geometrical parameters of the structure unit cell are the factors which affect much its absorption behavior where by changing the size or shape of the structure unit cell, the absorption response changes accordingly. Nevertheless, it had also be found that the absorption characteristic of a metamaterial absorber can be influenced by some external factors, such as temperature, applied external voltage, and so on. Metamaterial unit cell consists of combination of metals and dielectric materials whose properties (dielectric constant, electric conductivity) depend on external temperature. There are some studies about external factors which affect absorption characteristics of metamaterials which developed in order to create controllable metamaterials. One of those works is a switchable metamaterial that proposed by Chen et al. [98] in 2006 and it was realized by controlling external applied voltage of their metamaterial unit cell. Other works discussing about tunability of

metamaterial absorber such as electric and thermal tunability were published in [99-104].

In this thesis, the influence of external temperature on the absorption characteristic of the proposed wide-band perfect metamaterial absorber is investigated. This is done by examining the behavior of the electric permittivity of a dielectric material and resistivity of a metal under different temperature. The mathematical equation (6.14) from reference [8] is used to calculate the values of electric permittivity of dielectric material under different temperature.

$$\varepsilon_{s,\infty}(T) = \varepsilon_{s,\infty}(0) + \left(\frac{\alpha T^2}{\beta + T}\right) \tag{6.14}$$

where $\varepsilon_s\,(0)\ and\ \varepsilon_\infty(0)$ represent static and high frequency dielectric constant of material at temperature of zero Kelvin, α is a constant symbolizing inverse of Kelvin and β represents a quantity proportional to Debye temperature in Kelvin where T characterize absolute temperature. In order to investigate the behavior of a metallic layer of the proposed metamaterial absorber structure at different temperature, relation (6.15) and temperature dependent electric resistivity data from [105] are used to calculate its electric conductivity under different values of temperature.

$$\sigma = \frac{1}{\rho(T)} \tag{6.15}$$

with σ representing electric conductivity while ρ characterize electric resistivity.

From equation (6.14), it is clear that for any given dielectric material, the values of electric permittivity ε at any temperature can be determined. In this thesis, the dielectric material used is gallium arsenide and its characteristics at room temperature is $\varepsilon(300) = 12.96$ while α and β equal to $4.84 \times 10^{-3} K^{-1}$ and 550K, respectively [106]. In this thesis temperature is changed from 100 K to 400 K where for each value of temperature, electric permittivity is calculated and used in the simulation model together with the calculated electric conductivity. Afterward, the absorption response of the proposed metamaterial absorber design under different external temperature is investigated and the simulated absorption characteristics of the proposed wide-band perfect metamaterial absorber is shown in Figure 6-11.

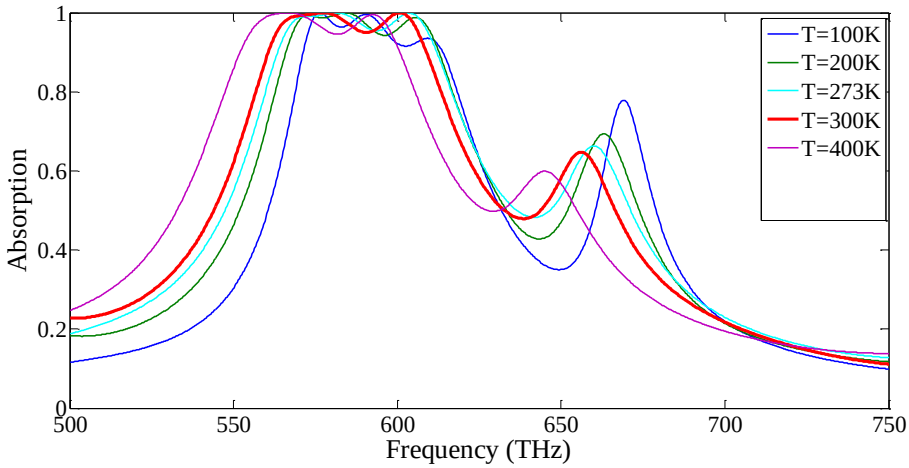

Figure 6-11. Absorption characteristics of the proposed wide-band MPA structure at difference value of temperature (100 K-400 K).

As it can be observed from Figure 6-11, for all temperature below room temperature (red color curve "300K"), the absorption band tends to shift to the right (high frequency regime) for all temperature above 300K the absorption band shift to the left (lower frequency). However, at both cases, the absorption rate remains nearly perfect (100% absorption rate) and starts to decline at higher temperature which is in agreement with what reported in [99- 100] and the physics behind this is the dipolar contributions which turn to be active at high temperature and also the rising in the temperature increase carrier density and plasma frequency of a dielectric material (semiconductor) which lead to the creation of thermal tunability of the metamaterial absorbers.

6.5. Finite Integration Technique versus Finite Element Method

Finite Integration Technique has been used throughout this thesis for all numerical simulations and as it has been described in Chapter 4, FIT method uses integral form of Maxell's equations to a set of staggered grids and is one of the most popular method to solve electromagnetic problems. On the other hands, Finite Element Method is a method which utilized to solve partial and differential equations and it gives solution based on completely removal of time derivatives terms or by transforming partial differential equations into equivalent ordinary differential equations which can easily be solved using finite differences technique. In order to validate the accuracy of the results presented in this thesis, the proposed wide band perfect metamaterial absorber

design is tested by comparing the simulations results from FIT and FEM method. Similar to FIT based solver, when a FEM based solver is utilized to solve electromagnetic wave problems, there are some important parameters that need to be considered carefully in order to acquire an accurate simulation results. Some of these parameters are: boundary conditions, wave excitation and mesh setting. Herein impedance boundary conditions are used along x-axis and y-axis while the wave port is utilized for source of electromagnetic radiation in z-axis. Tetrahedral mesh are utilized with the following parameters: aspect ratio is 5, maximum length of element and maximum number of elements are equal to $106\ nm$ and 1×10^5, respectively. In Figure 6-12, the proposed wide-band metamaterial absorber design is presented along with the simulations results from both two numerical methods (FEM and FIT solvers). The structure geometrical parameters are the same as the ones in Figure 6-1.

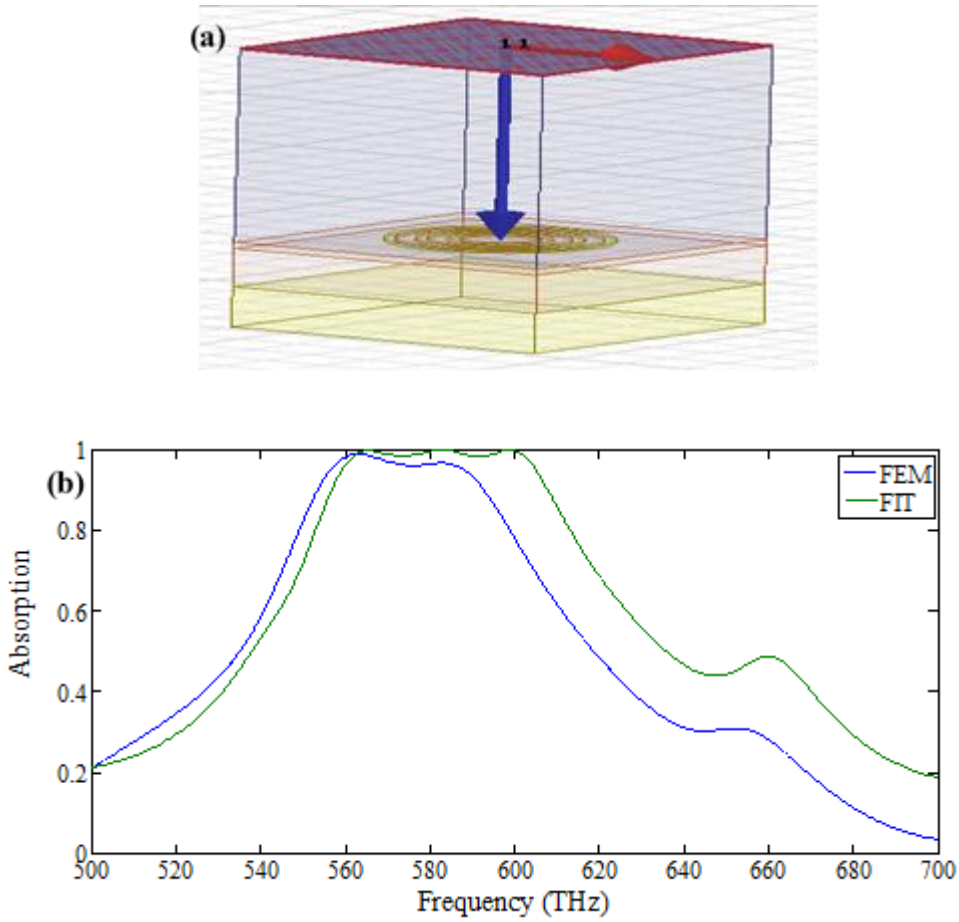

Figure 6-12. (a) The proposed wide-band metamaterial unit cell in FEM simulator, (b) the absorption characteristics of the proposed structure from FIT and FEM.

As one can observe, both two methods give a wide-band absorption response in the frequency range of interest (from 560 THz to 620 THz) and the results are quite similar despite a slight shift in the resonant frequency observed. This is a confirmation for the correctness of the simulations results in this thesis. It is believed that the slight difference in absorption band noticed in Figure 6-12 (b), can be a result of the materials composition in the library of the simulators package. In FIT simulation gold and gallium arsenide lossy materials were used, but in FEM simulation the material gold and gallium materials used there were not lossy and it has been noticed that the electric conductivity of gold in FEM simulation package is different to the one from FIT simulation package (the conductivity of gold for FIT and FEM library are $4.561 \times 10^7 \frac{S}{m}$ and $4.1 \times 10^7 \frac{S}{m}$, respectively).

6.6. Conclusions

In the first section of this chapter a wide-band metamaterial perfect absorber to effectively harvest solar radiations has been proposed characterized and numerically analyzed. In the second section theoretical analysis of the proposed MPA design were conducted using interference theory. Furthermore, in the section three, thermal characterization of the proposed MPA design has been discussed and in the last section the numerical simulation results were validated for two different method (FIT and FEM).

CHAPTER 7

GRAPHENE BASED WIDE BAND PERFECT METAMATERIAL ABSORBER FOR SOLAR CELLS APPLICATIONS

7.1. Introduction

Graphene is a single atomic layer of graphite an allotrope of carbon which is abundantly available in nature and is made up by tight bonds of carbon atoms which are arranged into hexagonal lattice structure. Even though the studies about graphene was broadly conducted for several years as a building block of graphite, it was only in 2004 that Novoselov et al. [107] was able to isolate a monolayer graphene from graphite. Before the discovery of graphene, it was believed that there was no ways to the existence of two dimensional carbon compound due to thermal disturbance when it is separated. It is only after experimental work on graphene that they came to conclude that two dimensional compound (graphene) exist thanks to the very small and strong covalent bonds between carbon atoms in graphene which prevents it from thermal disturbance and keeps the compound stable. As a result the isolation of graphene became possible and caused many scientists to turn their research attention in this research field.

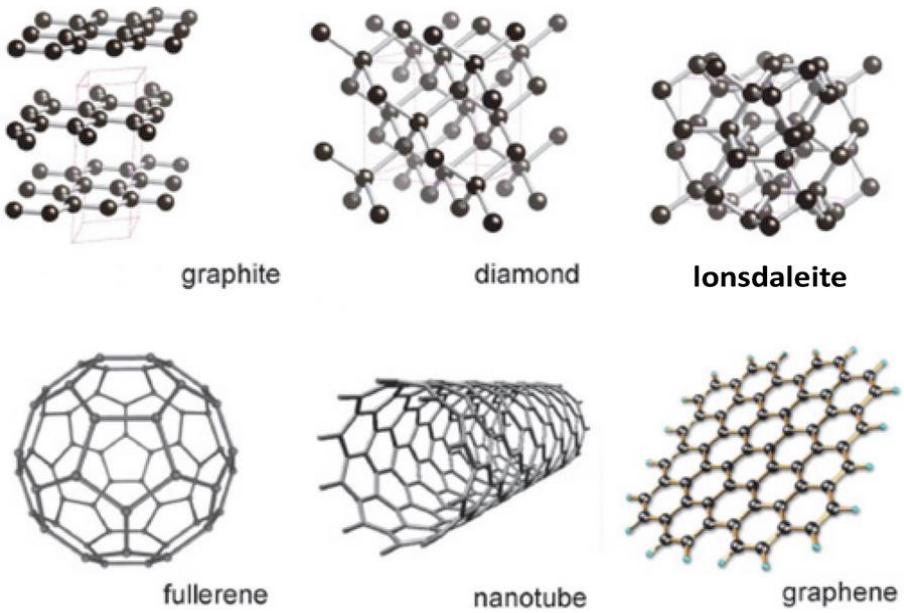

Figure 7-1. Structures representation of some carbon's allotropes including graphene [108].

But what attracted the researchers most are extraordinary electronic, mechanical and optical properties graphene found to hold which served as an open door to the numerous potential applications in the field of nanotechnology. Having a zero band gap graphene has been considered as a next generation conducting material tending to replace silicon (graphene is considered as the 21st century silicon). In the following section exotic properties of graphene are discussed.

7.2. Evolution of Graphene Material

The studies of allotropes elements of carbon has been conducted for several years, however the break point have been reached when the scientists from University of Manchester [108] experimentally discovered a single layer graphene through mechanical exfoliation of graphite [107]. Since then lots of studies about graphene and its extraordinary properties were conducted where from 2004 to 2013 thousands of graphene related papers were published and many investigations are still being conducted to these days [109-110].

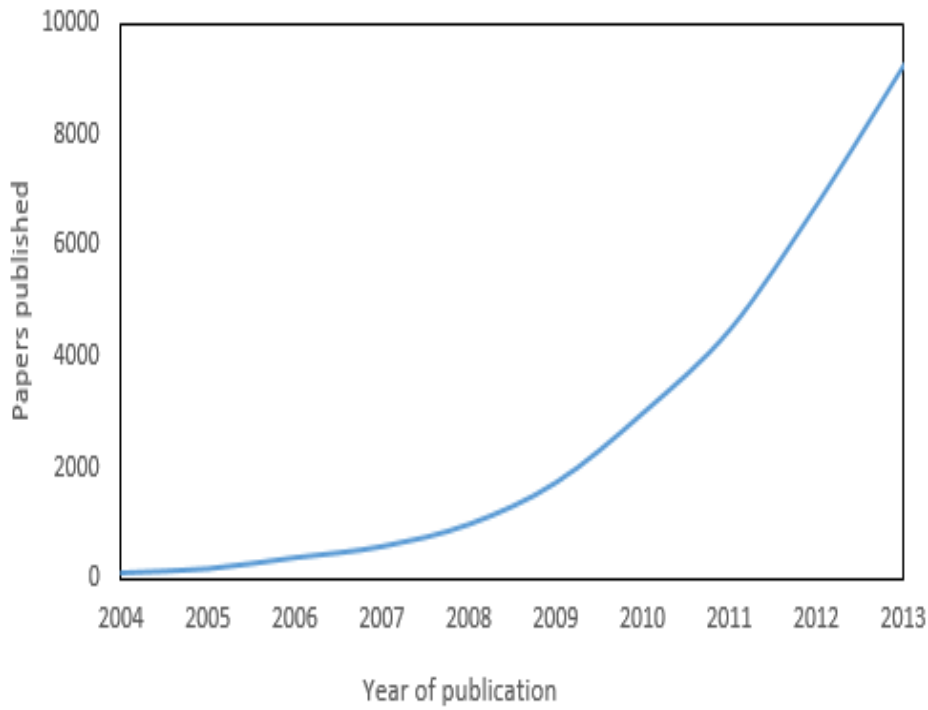

Figure 7-1. Growth in graphene related researches for a decade (2004-2013) after its discovery [110].

Both scientists and engineers are working hard on graphene material because of its superior properties. It is believed that many new research topics related with graphene

will continue to grow due to the fact that it has many applications and different scholars are working on its development.

7.3. Properties of Graphene

7.3.1. Electronic and Optical Properties of Graphene

It is scientifically known that sp^2 C to C bonds is the strongest bonding in chemistry, thus, owing such bonding characteristic makes graphene to be the strongest material ever exist. Besides, the conduction band and valance band in graphene overlap to each other and this is the reason why it is considered as a semi-metal with a zero band gap. Ordinarily, carbon atom has four electrons at its outer most shell which participate in bonding process, but in graphene only three electrons contribute in bonding process (giving graphene a shape and mechanical properties similar to those of diamond) which causes graphene to have one free electron (p_z electron) which moves in Z-direction and is responsible for electronic conduction. Carbon atoms in graphene organize themselves in a hexagonal lattice in 2D-plane with a nearest distance separating its atoms $a_0 = 1.42$ Å .Each of these three atoms shares a σ- bond, while the fourth bond in Z- direction is a π -bond. Thus every atom contains π -bond which hybridize together to produce π -band and π^* -bands and these bands are accountable for the astonishing electronic properties of graphene material. In addition to its extraordinary conductivity, graphene displays other special electronic and optical properties such as excellent fractional quantum hall effect and outstanding ambipolar electric effect where its charge carriers (electrons and holes) concentration reaches 10^{13} cm^{-2} while its mobility at room temperature can reach about $10^4 cm^2 V^{-1} s^{-1}$. Graphene is one of the materials with high thermal conductivity where thermal conductivity of its single layer sheet at room temperature is nearly 5000 $Wm^{-1}K^{-1}$ [112-116]. Another important optical properties of graphene which plays a very big role in the processes of designing perfect metamaterial absorber, is its high optical transparency. Although it is a one atom thick, graphene had revealed the ability to increase absorption of a structure up to 2.3% for every addition layer of graphene on an absorber structure(graphene's opacity $\pi\alpha = 2.3\%$ which matches with universal dynamic conductivity given by $\sigma(\omega) = \frac{e^4}{4\hbar}$ where e represents the charge of electron

and $\hbar = \frac{h}{2\pi}$, h is Plank's constant $= 6.62606957 \times 10^{-34} m^2 kg\ s^{-1}$) in visible light. This is because of the electrons in graphene behave like the massless charge carries with a very high mobility [117].

7.3.2. Mechanical Properties of Graphene

Due to its strong C-C bonds, graphene displays an exceptional mechanical strength where its tensile strength is reported to be 130 GPa [118-120]. This is the highest ever measured strength for all existing material, 325 times stronger than A36 structural steel and 346 stronger than Aramid. The second important mechanical property of graphene is its very light weight where 1 m^2 of graphene sheet weight 0.77 mg, almost one thousand times lighter than one square meter of a sheet of paper. Another amazing mechanical properties of graphene is its special elasticity and ability to regain its initial form and shape when it is being stretched. Even though it is one atom thick, the studies claims that a single sheet of graphene with a weight of 1g can be stretched to cover the whole football pitch.

7.4. Applications of Graphene

The advancement in research for graphene material has brought numerous applications in different fields due to its interesting chemical and physical properties. As of present, lots of potential applications about graphene technology have been revealed such as nanoelectronic devices, biosensors, chemical sensors, energy storage, and clean energy devices and there are still many to come with the continual spreading research in this field.

7.4.1. Application in Nanoelectronic Devices

Owing high electric conductivity and high mechanical flexibility, graphene won potential applications in the fabrication of excellent light emitting diode (LED), memory, field effect transistor (FET). The unusual electronic band structure of graphene causes it carries to be bipolar and they can always be controlled by applied gate electric field [121-122]. Graphene based transistors showed a very useful band

gap with high switching speed and outstanding carrier mobility (graphene has field effect mobility much higher than silicon) at room temperature [123-124].

7.4.2. Application in Transparent Conductive Films

High carrier mobility, high electrical conductivity together with high optical transparency in the visible frequency range permit graphene to be a great candidate for the production of transparent conductive films (TCFs) such touchscreens, liquid crystal displays (LCDs) [125-126], organic light emitting diode (OLEDs) [127-128] and organic photovoltaic cell [129-130]. Indium tin oxide (ITO) is a material normally used in the transparent conductive films, but graphene based TCFs has proved to be the best in comparison with ITO based TCFs. This is mainly because of graphene material has higher mechanical strength and higher flexibility than its opponents.

7.4.3. Applications in Sensors

Sensors industry is another sector which benefited from the discovery of graphene. Due to its mysterious optical and electronic properties [131-132], lots of studies showed monolayer graphene to be a best candidate for fabrication of numerous novel molecules detectors such as gases detector, biomolecules detectors, electrochemical sensors and biosensors [132-138], as a result of interaction in movement of charge in graphene layer and adsorbed molecules that produce chemical response.

7.4.4. Applications in Energy Storage Devices and Solar Cells and Fuel Cells

The optical transparent and high electric conductivity properties of graphene make it to be a useful material for fabrication of novel solar cells. A single layer of graphene behaves like a semiconductor with zero bandgap and its charge carries are delocalized within a wide surface area which help in preventing scattering of charge carries. The excellent high charge mobility of graphene endorse it to be used as a good charge collector and transport of charge carries in photovoltaic cells [129-130, 139]. In addition, by carefully perforating graphene sheet together with hexagonal boron nitride; protons can be allowed to travel through it which enables monolayer graphene to be useful for extraction of hydrogen gas in atmosphere where its layer allows protons to pass through while blocking motion of H_2 molecule and the extracted

hydrogen can be used for power generation [140-141]. One of the fascinating properties of graphene is its theoretical surface density of 2630 m^2 g-1 and its ability to allow free motion of charges carries (electrons and holes) along its 2D- surface area [121]. Having these abilities make graphene to be a good material for production of electrode, where due to its excellent electrical conductivity and outstanding surface area, rechargeable lithium ion batteries whose anode ordinarily made from graphite can be replaced by graphene based anode to enhance their performance [121, 142-144]. Outstanding surface density of graphene also permit it to be a potential material in manufacturing of high energy storage supercapacitors [145-146].

7.5. The Current State of Art in Graphene Application: Graphene Based Metamaterial Absorbers

Metamaterial research field is another sector that profited from discovery of graphene where numerous works on graphene based metamaterial absorbers have been developed to display exotic properties and different potential applications. The interesting electronic transport properties (electrons in graphene act like massless particles) of graphene are far better than those of metals and semiconductors. Its high conductivity and excellent mechanical properties made it to be a good candidate in metamaterial industry where graphene sheets are used in metamaterial absorber designs in order to manipulate the propagating path of electromagnetic wave and enhancement of absorption characteristics of MTM structures [147]. In 2012 Raoul et al. [148] proposed a metamaterial perfect absorber based on graphene micro-ribbon (considered as a meta-surface) where they used graphene flakes as cornerstone to achieve perfect absorption. Sailing et al. [149] also designed a broad band terahertz absorber with graphene based anisotropic metamaterial films. In their design, a multiple layers combination of graphene sheet -dielectric were deposited to a metallic plane in a pyramid shape. Their proposed multiple-layers comprised graphene-dielectric which behaved like an effectively homogeneous metamaterial with a hyperbolic dispersion and anisotropic permittivity. Surface plasmonic waves were excited on the graphene sheet and different incidence radiations were absorbed. Subsequently, Renxia and his research group [150] theoretically investigated a wide angle broadband absorption in the graphene based hyperbolic metamaterial. In their

study a monolayer graphene sheet along with a dielectric spacer were utilized where by using the chemical potential (bias voltage) the refractive index of their structure were transformed, and by varying the thickness of a dielectric spacer they gained absorption rate of nearly 70% with a bandwidth of 45% in THz frequency range. Moreover, based on its tunability of sheet conductivity, graphene monolayer had been integrated in metamaterial structures to enable creation of tunable and switchable graphene based metamaterials [151-154].

7.6. Wide-Band Graphene Based Perfect Metamaterial Absorber

In this thesis, a graphene monolayer sheet is being integrated in the wide-band MPA design proposed in Chapter 5 in order to enhance the structure's absorption characteristics and enhancing absorption bandwidth, where a glass Pyrex lossy on the top of a dielectric spacer is replaced by the graphene sheet. Graphene layer is also used to cover the top face of the resonators surface. The simulation of graphene is made possible by using its surface conductivity which can be controlled by chemical potential or bias electrostatic voltage and regulate graphene transport properties. The Kubo-formula (7.1), which is normally used for modelling of conductivity (σ_g) of graphene [148, 155-157], is utilized in this study and the values of conductivity are used to determine the permittivity of graphene by using equation (7.2).

$$\sigma_g = \frac{ie^2}{4\pi\hbar} ln\left[\frac{2|\mu_c|-(\omega+i2\Gamma)\hbar}{2|\mu_c|+(\omega+i2\Gamma)\hbar}\right] + \frac{ie^2}{\pi\hbar^2(\omega+i2\Gamma)}\left[\frac{\mu_c}{k_B T} + 2ln\left(e^{-\mu_c/k_B T}+1\right)\right] \quad (7.1)$$

where e, k_B, and $\hbar$ are universal constants which symbolizing the charge of electron ($1.6 \times 10^{-19}\ C$), Boltzmann's constant ($1.3806 \times 10^{-23}\ m^2 kg\ s^{-2} K^{-1}$) and Plank's constant ($1.0545 \times 10^{-34} m^2 kg s^{-1}$), respectively. T represents temperature and is taken to be room temperature (300K) in the present study; μ_c and Γ denote physical parameters of graphene monolayer sheet and are responsible for chemical potential (Fermi energy) and intrinsic losses/phonological scattering rate , in order. $\Gamma = \frac{\hbar}{\tau}$, τ represent electron relaxation time.

$$\varepsilon_g = \frac{\sigma_g}{(\mathrm{n}\omega)} + \varepsilon_0 \quad (7.2)$$

where ε_g and ε_0 represent permittivity of graphene and free space, respectively, while n and ω symbolize the thickness of graphene sheet and working frequency, in that order. The input value for phonological scattering rate is fixed to $\Gamma = 1 \times 10^{-2}$eV referring to the estimated maximum value of electron mobility in graphene [155]. In this thesis, the operational frequency ω is visible spectrum range (450 THz - 800 THz) and the thickness (n) of graphene has been chosen to be 1nm. By using the model in (7.1) conductivity was calculated at different chemical potential (μ_c) (bias electrostatic voltage) and by using (7.2) the permittivity of graphene were determined. The calculated permittivity is integrated in the computer simulator (FIT) in order to numerically analyze the contribution of graphene on the absorption characteristics of the proposed wide band MPA structure. In Figure 7-3, enhanced wide-band absorption results for the proposed MPA structure are reported. In Figure 7-3 (c) comparison for the simulation results of the proposed wide-band graphene based MPA absorber with FIT and FEM based solvers is reported and the results from both two method are close to each other at the resonant frequencies varying from 560 THz to 640 THz.

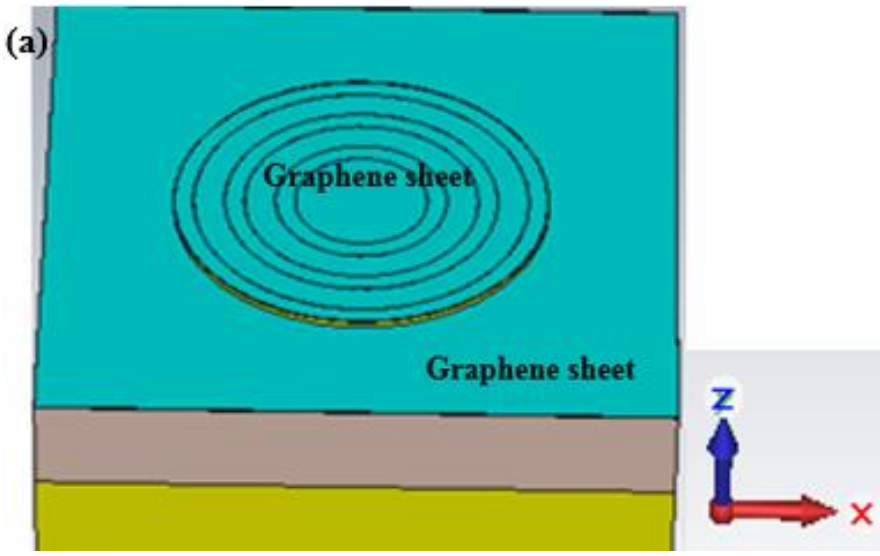

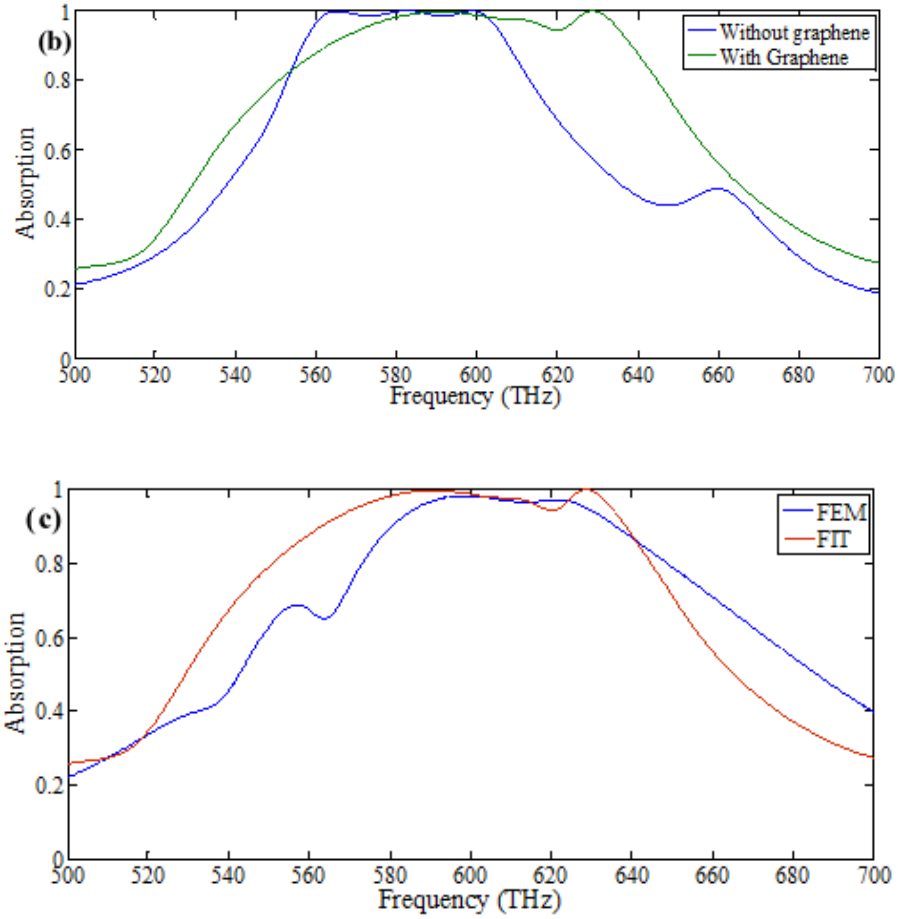

Figure 7-3. (a) A unit cell of the proposed metamaterial structure with graphene integrated, (b) comparison between enhanced absorption bandwidth using graphene and the results without graphene, (c) comparison between simulation results of the proposed wide-band MTM absorber with graphene using FIT and FM based solvers.

An improved absorption bandwidth can be noticed from Figure 7-3, as a result of replacing glass layer with graphene monolayer sheet and also by covering the resonators' face with the sheet of graphene which causes excitation of surface plasmonic waves and lead to enhancement of the absorption band width. Adding graphene sheet on the proposed structure increases absorption bandwidth the up to 26% of the initial bandwidth without graphene monolayer where absorption rate of more than 90% covers a wide frequency range of 137 THz.

The geometrical parameters of the graphene sheet is also investigated in order to understand their impact on enhancement of the absorption bandwidth. In Figure 7-4, the results from parametric study are reported.

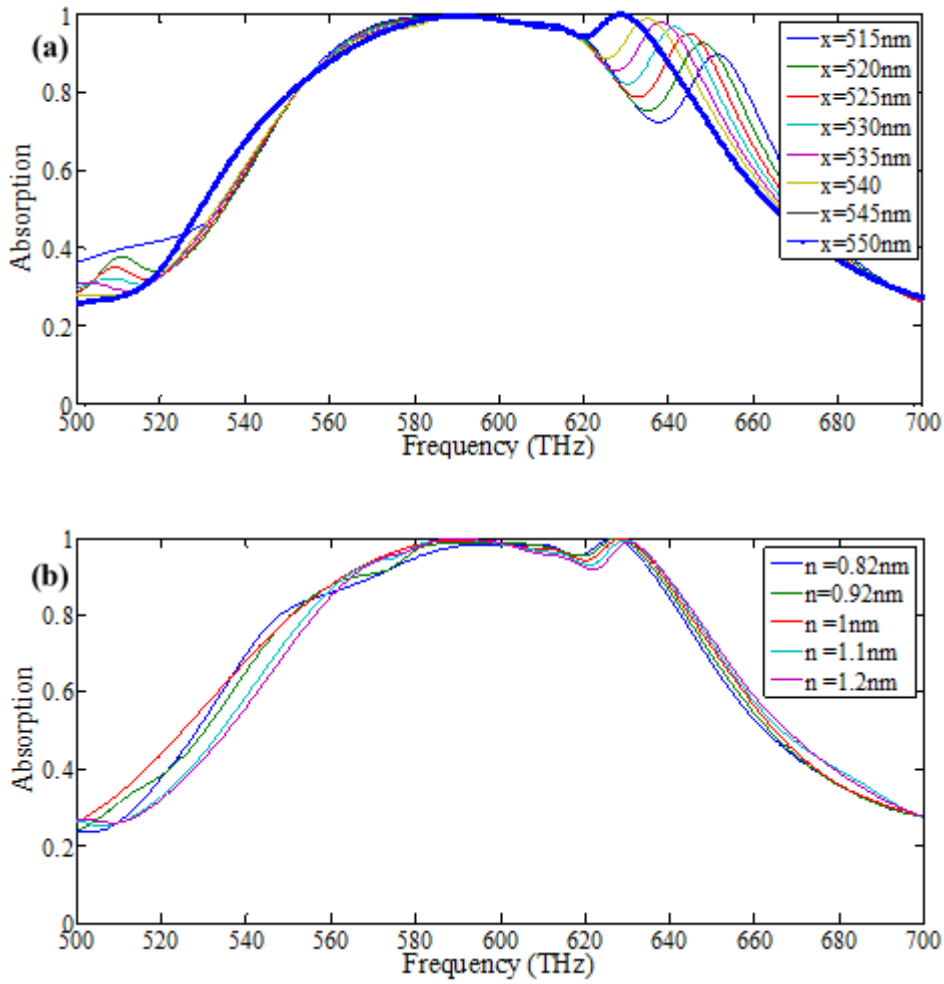

Figure 7-4. Absorption characteristics of the proposed graphene based wide-band MPA structure under different geometric parameters. (a) Different value of graphene periodicity 'x', (b) Different thickness 'n' of graphene sheet.

The first observation is noticed from the effect of structure periodicity 'x', where by changing the values of x from 515 nm to 550 nm with a step width of 5 nm, the absorption rate is found to improve and the ripples start to decline up to a slight ripple obtained at x = 550 nm. Another important geometrical parameter is graphene's thickness 'n'. Typically, the thickness of graphene must be small enough and in this study the value is set as n = 1 nm, referring to the thickness of graphene based metamaterial absorber found in literature [148]; and this corresponds roughly to three layers of graphene. By performing simulations of the proposed structure at different thicknesses of graphene sheet, it is realized that the absorption rate is get enhanced for smaller value of n and begin to decrease for all thickness greater than 1 nm.

7.7. Conclusion

In this chapter, background, history, properties and applications of graphene have been reported. Afterward, the graphene monolayer sheet has been integrated in the proposed wide-band metamaterial perfect absorber structure to enhance its absorption capability and 26% increase in absorption bandwidth has been detected for the proposed MPA design after integration of graphene.

CHAPTER 8

CONCLUSIONS

8.1. The conclusions of the thesis

Solar PV is ranked among the best technologies to effectively harvest solar energy resource, however the limited efficiency of these devices prevent their fast growth. As it was outlined in Chapter one, improving absorption capability of the solar cell will lead to enhancement of their efficient. In this thesis, various novel metamaterial perfect absorber (absorption more than 99%) designs were described, simulated and numerically characterized. The extraordinary properties of metamaterial were discussed in this thesis and it was supported by numerous applications which were discovered, thanks to metamaterial development. Several research on metamaterial absorbers have been done in almost all the ranges of solar spectrum, but little work has been done in visible frequency range. Most of the existing MPA designs display single and narrow band absorption response which causes limitation in their application. Thus, it is obvious that designing a metamaterial absorbers with dual, triple, multiple and wide-band response will bring huge potential application in the process for increasing efficiency of solar PV cells. Hence, the first two metamaterial absorber structure proposed in this thesis offered dual-bands absorption response at the resonant frequencies in visible regime of solar spectrum. The symmetric nature of the proposed MPA designs caused them to be polarization angle insensitive.

In order to improve the absorption flexibility of the solar cell, a tunable metamaterial perfect absorber structure for solar cell application was also proposed in this thesis which offered an absorption of more than 99% with a frequency bandwidth of 15.5% in visible spectrum. The tunability character of this MPA structure was achieved through adjustment of its dielectric spacer's thickness.

The main objective of this thesis was to design a wide-band perfect metamaterial absorber operating in visible range of solar spectrum, which was discussed in Chapter 6. The proposed wide-band MPA comprised of three resonators which generated electromagnetic resonance and produced single band absorption resonance for each

resonator and the combination of those resonances produce a wide – band absorption response with near perfect absorption resonance (absorption rate of more than 90% retained over 97 THz frequency difference) in visible frequency regime. Besides, the wide-band resonance characteristic which the proposed MPA displayed, it also showed a high geometric flexibility which was confirmed by its polarization angle independency.

Furthermore, the simulation results for the proposed wide band metamaterial absorber design was theoretically validated by the use of interference theory model (decoupled model) and a match between the two methods was obtained.

De facto, the external factor such as: temperature and external applied voltage altered the absorption characteristics of a MTM absorber. The proposed wide-band MPA design was thermally characterized which showed a tunability character in the presence of high temperature which is an added value to the proposed structure due to its absorptivity retained in the presence of high temperature.

Graphene technology has been discussed in Chapter 7. In order to enhance absorption bandwidth of the proposed MPA design, graphene monolayer sheet was employed on the proposed structure and it was observed that an addition of graphene monolayer sheet on the proposed MPA unit cell caused improvement of its absorption bandwidth up to 26%.

Based on the findings from metamaterial absorber designs proposed in this thesis, it is believed that implementation of them in solar cells will lead to enhancement of the efficiency of these devices.

Some of the results reported in this thesis have been presented in international conferences such as Science & Application of Thin Films (SATF2014) and Third Turkish Solar Electricity Conference and Exhibition (Solar TR-3). One journal paper from this thesis was published in Vacuum journal with two more journals still under-review for publication.

8.2. Future work

In this thesis numerical and theoretical analysis of metamaterial perfect absorber designs were successfully conducted. However, future work should be based on the experimental characterization of the proposed metamaterial perfect absorber structures.

BIBLIOGRAPHY

[1] C. de Boer and I. Catsburg. The impact of nuclear accidents on attitudes toward nuclear energy" .Oxf. Univ. Press, the public opinion Quarterly, 2(1988)254-261.

[2] J E Ten Hoeve and M Z Jacobson, "Worldwide health effects of the Fukushima Daiichi nuclear accident". Energy. Environ. Science, 5(2012)8743-8757.

[3] K H Solangi, M R Islamb, R Saidura, N A Rahimb, H Fayaz. A review on global solar energy policy. Renew. Sust. Energy Rev., 15(2011)2149–2163.

[4] G.R. Timilsina, L.Kurdgelashvili, P.A. Narbel. A Review of Solar Energy Markets, Economics and Policies. the World Bank Development Research Group Environment and Energy Team, Policy Research Working paper 5845, 2011.

[5] A.shah, P.Torres, R.Tscharner, N.Wyrsch, and H.Keppner. Photovoltaic Technology: The Case for Thin-Film Solar Cells. Science, 285(1999)692-698.

[6] M.A. Green. Solar cells: operating principles, technology, and system applications. Prentice-Hall, Englewood Cliffs, NJ (1982).

[7] H.S. Rauschenbach. Solar cell array design handbook - The principles and technology of photovoltaic energy conversion. Van Nostrand Reinhold C, New York (1980)

[8] A.A.Rockett. The future of energy – Photovoltaics. Current Opinion in Solid State and Materials Science, 14 (2010) 117–122.

[9] H.B.Gray. Electrons and chemical bonding. W. A. Benjamin, Inc, New York (1965)

[10] J .C. Bose. On the rotation of plane of polarization of electric waves by a twisted Structure. Proc. Roy. Soc., 63(1898) 146–152.

[11] I. V. Lindell, A. H. Sihvola, J. Kurkijarvi and K. F. Lindman. The last Hertzian, and a Harbinger of electromagnetic chirality. IEEE Ant. Propag. Mag., 34(1992)24–30.

[12] W. E. Kock. Metallic delay lenses. B. Sys. Tech. J., 27(1948) 58–82.

[13] N. Angheta & R. W. Ziolkowski. Metamaterials, physics and engineering explorations .J Wiley & sons, New York, 2006.

[14] V. G. Vesalago, P. N. Labedev. The electrodynamics of substances with simultaneously negative values of ε and μ. Sov. Phy.Usp, 10(4), 01(1968)509-514.

[15] D. R. Smith, W. J. Padilla, D. C. Vier, S. C. Nemat-Nasser and S. Schultz. Composite medium with simultaneously negative permeability and permittivity. Phys. Rev. Let. 18, 84(2000)4184-4187.

[16] J. B. Pendry. Perfect cylindrical lenses. Opt. Exp. 11, 7(2003) 755-760.

[17] J. W. Shirley. An early experimental determination of Snell's law. Americ. J. Phy. 19(1951)507.

[18] V. M. Shalaev and W. Cai. Optical Metamaterials: Fundamentals and Applications: Springer, New York, 2010

[19] P. W. Gilberd. The anomalous skin effect and the optical properties of metals. J. Phys. F: Met. Phys., 12(1982)1845-1860.

[20] R.W.Wood and C.Lukens. Optical properties of the alkali metals. Phys.Rev. 54(1938)332.

[21] S.Roberts. Interpretation of the optical properties of metal surface. Phys.Rev. 100(1955)1667

[22] K.L. Kelly, E. Coronado, L.L.Zhao, and C.Schatz. The optical properties of metal nano particles: The influence of size, shape, and dielectric environment. J. Phys. Chem. B, 107 (2003)668–677.

[23] M. Bass, C. DeCusatis, J.Enoch, V. Lakshminarayanan, G. Li, C.MacDonald, V. Mahajan, and E. W. Van Stryland. Handbook of Optics: Volume 4, Optical Properties of Materials, Nonlinear Optics, Quantum Optics 3rd edition, McGraw-Hill, 2010.

[24] J. B. Pendry, D. Schurig, and D. R. Smith. Controlling electromagnetic fields. Science 312 (2006) 1780-1782.

[25] B. Dodson, Oops! Invisibility cloaks actually make objects easier to see [online image]. Retrieved June 6, 2015 from http://www.gizmag.com/invisibility-cloaks-make-objects-easier-to-see/29722/

[26] Y. Lai, H. Chen, Z.Q. Zhang, and C. T. Chan. A complementary media invisibility cloak that can cloak objects at a distance outside the cloaking shell. Phys. Rev. Lett. 102(2009) 093901.

[27] F. Zolla, S. Guenneau, A. Nicolet, J.B. Pendry. Electromagnetic analysis of cylindrical invisibility cloaks and the mirage effect. Opt. Lett., 32(2007)1069-1071.

[28] A. Alu and N. Angheta. Multifrequency optical invisibility cloak with layered plasmonic shells. Phys. Rev. Lett., 100(2008)113901-4.

[29] A. Ishimaru, S. Jaruwatanadilok, andY. Kuga.Generalized surface plasmon resonance sensors using metamaterials and negative index materials. Prog. Electromagn. Res., 51(2005)139–152.

[30] Z. Jaksic, O.Jakic, Z.Djuric, and C.Kment. A consideration of the use of metamaterials for sensing appliactions: field fluctuations and ultimate performance. J. Opt. A: Pure Appl. Opt., 9 (2007) S377–S384.

[31] J. Zhu and G. V. Eleftheriades. Dual-band metamaterial inspired small monopole antenna for WiFi applications. Electron Lett.45 (2009)1104–1106.

[32] A.V. Kabashin, P.Evans, S. Pastkovsky, W.Hendren, G.A. Wurtz, R. Aktinson, R.Pollard, V.A.Podolskiy, and A.V.Zayats. Polasmonic nanorod metamaterials for biosensing. Nature mat., 8(2009)867-871.

[33] H.Chen, B.I. Wu, L. Ran, T. M. Grzegorczyk, and J. Au Kong. Controllable left-handed metamaterial and its application to a steerable antenna. Appl. Phys. Lett., 89(2006) 053509-3.

[34] T.Chen, S.Li, and H.Sun. Metamaterials application in sensing. Sensors, 12(2012)2742-2765.

[35] R. Melik, E. Unal, N. K. Perkgoz, C. Puttlitz, and H. V. Demir. Flexible metamaterials for wireless strain sensing. Appl. Phys. Let. Strain sensing, 95(2006)181105-3.

[36] N. Liu, M. Mesch, T. Weiss, M. Hentschel, and H. Giessen. Infrared perfect absorber and its application as plasmonic sensor. Nano Lett., 10(2010)2342-2348.

[37] S. A. Maier. Plasmonics: fundamentals and applications. Springer, New York, 2007

[38] J.B. Pendry. Negative refraction makes a perfect lens. Phys. Rev. Lett. 85 (2000)
3966-3969.

[39] C. L. Holloway, E. R. Kuester, J. A. Gordon, J. O'Hara, J. C. Booth, and D. R. Smith. An overview of the theory and applications of metasurfaces: the two-dimensional equivalents of metamaterials. IEEE Trans. Antennas Propag., 54, 10 (2012).

[40] M. Lapine, D. Powell, M. Gorkunov, I. Shadrivov, R. Marqués, and Y. Kivshar. Structural tunability in metamaterials. Appl. Phys. Lett., 95(2009) 084105-3.

[41] D.R.Smith, J.B. Pendry,and M.C.K., Wiltshire. Metamaterials and negative refractive index. Science, 305(2004)788-792.

[42] B. Wang, T. Koschny, and C. M. Soukoulis .Wide-angle and polarization-independent chiral metamaterial absorber. Phys. Rev. B, 80(2009)033108-4

[43] S. Kawata and V. M. Shalaev. Tip enhancement. Advances in nano-optics and nano-photonics. Elsevier: New York; 2007.

[44] S. Jahani and Z. Jacob. Photonic skin-depth engineering. J. Opt. Soc. Am. B, 32(2015)1346-1353.

[45] L. Huang and H. Chen. Multiple band and polarization insensitive metamaterial absorber. Prog. Electromagn. Res., 113(2011)103-110.

[46] B. Zhu, Z. Wang, C. Huang, Y. Feng, J. Zhao, and T. Jiang. Polarization insensitive metamaterial absorber with wide incident angle. Prog. Electromagn. Res., 101(2010)231-239.

[47] N. I. Landy, S .S. Sajuyigbe, J. J Mock, D. R. Smith and W. J. Padilla. A perfect metamaterial absorber. Phys. Rev. Lett., 100(2008)207402.

[48] B. Zhu, Y.Feng, J. Zhao, C. Huang, Z. Wang, T.Jiang. Polarization modulation by tunable electromagnetic metamaterial reflector/absorber. Opt. Exp., 18(2010) 23196-23203.

[49] J. Sun, L. Liu, G. Dong, and J. Zhou. An extremely broad band metamaterial absorber based on destructive interference. Opt. Exp., 19(2011) 21155-21162.

[50] L. Li, Y. Yang, and C. Liang. A wide-angle polarization-insensitive ultra-thin metamaterial absorber with three resonant modes. J. Appl. Phys., 110, 063702-5 (2011).

[51] J.W. Park, P. Van Tuong, J.Y. Rhee, K. W. Kim,W. H. Jang,E. H. Choi, L. Yao Chen and Y. Lee. Multi-band metamaterial absorber based on thearrangement of donut-type resonators. Opt. Exp., 21(2013) 9691-9702.

[52] H.Tao, N. I. Landy, C. M. Bingham, X. Zhang, R.D. Averitt, and W. J. Padilla. A metamaterial absorber for the terahertz regime: Design, fabrication and characterization. Opt. Exp., 16(2008) 7181-7188.

[53] H.Tao, C. M. Bingham, A. C. Strikwerda, D. Pilon, D. Shrekenhamer, N. I. Landy, K. Fan, X. Zhang, W. J. Padilla, and R. D. Averitt. Highly flexible wide angle of incidence terahertz metamaterial absorber: Design, fabrication,and characterization. Phys. Rev. B, 78(2008)241103-4.

[54] H.T. Chen. Interference theory of metamaterial perfect absorbers. Opt. Exp., 20(2012)7165-7172.

[55] Q.Y. Wen, H. W. Zhang, Y. S. Xie, Q. H. Yang, and Y.L.Liu. Dual band terahertz metamaterial absorber: Design, fabrication, and characterization. Appl. Phys. Lett. 95(2009) 241111-3.

[56] X. Shen, Y. Yang,Y. Zang, J. Gu, J. Han,W.Zhang, and T. J. Cui1, Triple-band terahertz metamaterial absorber: Design, experiment, and physical interpretation. Appl. Phys. Lett. 101(2012) 154102-4.

[57] G. D. Wang, J.F. Chen, X. W. Hu, Z. Q. Chen, and M.H. Liu. Polarization-insensitive Triple-Band Microwave Metamaterial Absorber Based on Rotated Square Rings. Progr. Electromagn. Res., 145(2014) 175-183.

[58] G. D. Wang, M. H. Liu, X. W. Hu, L. H. Kong, L. L. Cheng, and Z. Q. Chen .Broadband and ultra-thin terahertz metamaterial absorber based on multi-circular patches," Eur. Phys. J. B, 86(2013)304-7.

[59] X. Liu, T. Starr, A. F. Starr, and W. J. Padilla. Infrared Spatial and Frequency Selective Metamaterial with Near-Unity Absorbance. Phys. Rev. Lett., 104(2010)207403-4.

[60] Y. Avitzour, Y.A. Urzhumov, and G. Shvets. Wide-angle infrared absorber based on a negative-index plasmonic metamaterial. Phys. Rev. B, 79(2009)045131-5.

[61] Y. He, H. Deng, X. Jiao, S. He, J.Gao, and X.D. Yang. Infrared perfect absorber based on nanowire metamaterial cavities. Opt. Lett., 38(2013)1179-1181.

[62] D. Cheng, J. Xie, H. Zhang, C. Wang, N. Zhang, and L. Deng. Pantoscopic and polarization-insensitive perfect absorbers in the middle infrared spectrum. J. Opt. Soc. Am. B, 29(2012) 1505-1510.

[63] G. Dayal and S. A. Ramakrishna. Design of highly absorbing Metamaterials for Infrared frequencies. Opt. Exp., 20(2012)17503-17508.

[64] G. Dayal and S. Anantha Ramakrishna. Broadband infrared metamaterial absorber with visible transparency using ITO as ground plane. Opt. Exp., 22(2014)15104-15109.

[65] B. Zhang, Y. Zhao, Q. Hao,B.Kiraly, I.C.Khoo, S.Chen, and T. J. Huang. Polarization-independent dual-band infrared perfect absorber based on a metal-dielectric-metal elliptical nanodisk array. Opt. Exp., 19(2011) 15221-15228.

[66] P. Pitchappa, C. P. Ho, P. Kropelnicki, N. Singh, D. L. Kwong, and C. Lee. Dual band complementary metamaterial absorber in near infrared region. J. Appl. Phys. 115(2014)193109-6.

[67] C. M. Watts, X. Liu, and W. J. Padilla. Metamaterial electromagnetic wave absorbers. Adv. Mater. 24(2012) 98–120.

[68] X. Duan, S.Chen, W.Liu, H. Cheng, Z. Li and J.Tian. Polarization-insensitive and wide-angle broadband nearly perfect absorber by tunable planar metamaterials in the visible regime. J. Opt., 16 (2014) 125107-7

[69] C. Wu, B. Neuner , J. John, A. Milder, B. Zollars, S.Savoy and G. Shvets. Metamaterial-based integrated plasmonic absorber/emitter for solar thermo-photovoltaic systems. J. Opt., 14 (2012) 024005-7.

[70] L.Mo, L. Yang, A.Nadzeyka, S. Bauerdick, and S. He. Enhanced broadband absorption in gold by plasmonic tapered coaxial holes. Opt. Exp., 22(2014)32233-32244.

[71] J. Wang,C. Fan, P. Ding,J.He, Y. Cheng, W. Hu, G. Cai, E.Liang, and Q. Xue. Tunable broad-band perfect absorber by exciting of multiple plasmon resonances at optical frequency. Opt. Exp., 20 (2012) 14872-14878.

[72] M. K. Hedayati , M. Javaherirahim , B. Mozooni , R. Abdelaziz ,A. Tavassolizadeh , V. S. K. Chakravadhanula , V. Zaporojtchenko ,T. Strunkus , F. Faupel , and M. Elbahri. Design of a Perfect Black Absorber at Visible Frequencies Using Plasmonic Metamaterials. Adv. Mater. 23(2011) 5410–5414.

[73] M .Yan, J. Dai and M. Qiu. Lithography-free broadband visible light absorber based on a mono-layer of gold nanoparticles. J. Opt. 16 (2014) 025002-9

[74] G.Y. Zhou, A.W. Lee, J.Y. Chang, C. H. Huang and J.K. Chen. Fabrication of metamaterial absorber using polymer brush – gold nanoassemblies for visualizing the reversible pH-responsiveness. J. Mater. Chem. C, 2(2014)8226–8234.

[75] Z. Rahimi. The Finite Integration Technique (FIT) and the Application in Lithography Simulations. Als Dissertation genehmigt von der Technischen Fakultat der Universitat Erlangen-Nournberg. 10. January, 2011.

[76] K. S. Yee. Numerical solution of initial boundary value problems involving Maxwell's equations in isotropic media," IEEE Transaction Antennas and Propagation, 14(1966)302-307.

[77] S. M. Rao, G. K. Gothard, and D. R. Wilton. Application of finite integration technique to electromagnetic scattering by two-dimensional cavity-backed aperture in a ground plane. IEEE Trans. Ant. Prop., 46(1998) 679-686.

[78] R. Marklein, The finite integration technique as general tool to compute acoustic, electromagnetic, elastodynamic, and coupled wave fields. IEEE Ant. Wireless. Prop. Lett., 1(2002)31-34.

[79] S. Gutschling, H. Krger, and T. Weiland. Time domain simulation of dispersive media with the finite integration technique. Int. J. Num. Modeling, 13(329-348)2000.

[80] T. Koschny, M. Kafesaki, E. N. Economou, and C. M. Soukoulis. Effective medium theory of left-handed materials. Phys. Rev. Lett., 93(2004)107402.

[81] L. Hao, W. Tao, G. R. Zhou, N. Yan, W. Xian. Extending the bandwidth of electric ring resonator metamaterial absorber. Chin. Phys. Lett., 28 (2011) 034204-4.

[82] Y. Cheng, H. Yang, Z. Cheng, N. Wu. Perfect metamaterial absorber based on a split-ring-cross resonator. Appl. Phys. A., 102(2011)99–103.

[83] Y. Q. Xu, P. H. Zhou, H. B. Zhang, L. Chen, and L.J. Deng. A wide-angle planar metamaterial absorber based on split ring resonator coupling. J. Appl. Phys.110 (2011) 044102-5.

[84] Y. Liu, Y. Chen, J. Li, T. C. Hung & L. Jianping. Study of energy absorption on solar cell using metamaterials. Solar energy; 86(2012)1586-1599.

[85] O. Loebich. The optical properties of gold: A review of their technical utilization. http:/www.springer.com/content/pdf/10.1007/BF03215148.pdf. [Accessed 02 September 2014].

[86] M. S. Dresselhaus. Solid state physics II: Optical Properties of Solids. http:/www.mit.edu/course/6/6.732/www/6.732-pt2.

[87] M. A. Ordal, L. L. Long, R. J. Bell, S. E. Bell, R. R. Bell, R. W. Alexander, Jr. and C. A. Ward. Optical properties of the metals Al, Co, Cu, Au, Fe, Pb, Ni, Pd, Pt, Ag, Ti, and W in the infrared and far infrared. Appl. Opt., 7 (1983)1099-1120.

[88] P. G. Balmaz and O. J. F. Martin, Electromagnetic resonances in individual and coupled split-ring resonators, J. Appl. Phys., 92(2002)2929-2936.

[89] M. Clemens and T. Weiland, Discrete electromagnetism with the finite integration technique, Progr. Electromagn. Res., 32(2001)65-87.

[90] T. H. Nguyen, S. T. Bui, T. T. Nguyen, T. T. nguyen, Y. P. Lee, M. A. Nguyen, and D. L. Vu. Metamaterial-based perfect absorber: polarization insensitivity and broadband. Adv. Nat. Nanosci., 5(2014) 025013-7.

[91] Q. Y. Wen, Y. S. Xie, H. W. Zhang, Q. H. Yang, Y. X. Li, Y. L. Liu. Transmission line model and fields analysis of metamaterial absorber in the terahertz band. Opt. Exp., 17(2009) 20256- 20264.

[92] J. Zhou, H. T. Chen, T. Koschny, A. K. Azad, A.J. Taylor, C. M. Soukoulis, and J. F. O'Hara. Application of metasurface description for multilayered metamaterials and an alternative theory for metamaterial perfect absorber. arxiv.org/abs/1111.0343.

[93] H.T. Chen, J. Zhou, J. F. O'Hara, F. Chen, A. K. Azad, and A. J. Taylor. Transmission line model and fields analysis of metamaterial absorber in the terahertz band. Phys. Rev. Lett., 105(2010) 073901-4.

[94] J. W. Park, P.V. Tuong, J. Y. Rhee, K. W. Kim, W. H. Jang, E. H. Choi, L. Y. Chen, and Y. P. Lee. Multi-band metamaterial absorber based on the arrangement of donut-type resonators. Opt. Exp., 21(2013)9691- 9702

[95] X. Shen, Y. Yang, Y. Zang,J. Gu, J. Han, W. Zhang, and T. J. Cui. Triple-band terahertz metamaterial absorber: Design, experiment, and physical interpretation. Appl. Phys. Lett. 101(2012)154102-4.

[96] F.Dincer, M. Karaaslan, E. Unal, K. Delihacioglu, and C. Sabah Polarization angle independent perfect metamaterials absorbers for solar cell applications in the microwave, infrared and visible regime. Prog. Electromagn. Res., 144(2014) 93-101.

[97] T. Wanghuang, W. Chen, Y. Huang, and G. Wen. Analysis of metamaterial absorber in normal and oblique incidence by using interference theory. AIP Advances, 3(2013) 102118-9.

[98] H.T. Chen, W. J. Padilla, J. M. O. Zide, A. C. Gossard, A. J. Taylor & R. D. Averitt. Active terahertz metamaterial devices. Nature, 444(2006)597-600.

[99] J. Zhu, J. Han, Z. Tian , J. Gu , Z. Chen , W. Zhang . Thermal broadband tunable Terahertz metamaterials. Opt. Commun., 284 (2011) 3129–3133.

[100] S. T. Bui, V. D. Nguyen, X. K. Bui,T. T. Nguyen, P. Lievens, Y. P Lee and D. L. Vu. Thermally tunable magnetic metamaterials at THz frequencies. J. Opt. 15 (2013) 075101-5.

[101] A. Minovich,D. N. Neshev, D. A. Powell, I. V. Shadrivov, and Y. S. Kivshar. Tunable fishnet metamaterials infiltrated by liquid crystals. Appl. Phys. Lett., 96 (2010)193103-3.

[102] F. Zhang,Q. Zhao, W. Zhang, J. Sun, J. Zhou,and D. Lippens. Voltage tunable short wire-pair type of metamaterial infiltrated by nematic liquid crystal. Appl. Phys. Lett., 97(2010)134103-3.

[103] Q. Bai, C. Liu, J. Chen, C. Cheng, M. Kang, and H. T. Wang. Tunable slow light in semiconductor metamaterial in a broad terahertz regime. J. Appl. Phys., 107(2010)093104-8.

[104] Q. Y. Wen, H. W. Zhang, Q. H. Yang, Y. S. Xie, K. Chen, and Y. L. Liu. Terahertz metamaterials with VO 2 cut-wires for thermal tunability. Appl. Phys. Lett. 97(2010)021111-3.

[105] R.A Matula. Electric resistivity of Copper, Gold, Palladium and Silver. J.Phys.Chem.Ref.Data, 8(1979)1147-1298.

[106] S. Adachi. Properties of Group IV, III-V and II-VI semiconductors. John Wiley & Sons, 2009.

[107] K.S. Novoselov, A.K. Geim, S.V. Morozov, D. Jiang, Y. Zhang, S.V. Dubonos, I.V.Grigorieva, A.A. Firsov. Electric field in atomically thin carbon films. Science, 306(2004)666–669.

[108] R. Garg, N. K. Dutta and N. Roy Choudhury. Work Function Engineering of Graphene. Nanomaterials, 4(2014)267-300.

[109] C. Zhou, S. Chen, J. Lou, J. Wang, Q. Yang, C. Liu, D. Huang and T. Zhu. Graphene's cousin: the present and future of graphene. Nan. Res. Lett. 2014. http://www.nanoscalereslett.com/content/9/1/26.

[110] A. Plume. Graphene: ten years of the 'gold rush'. Research trends 38 (2015).

http://www.researchtrends.com/issue-38-september-2014/graphene-ten-years-of-the-gold-rush/. Last Accessed June 19, 2015.

[111] A. K. Geim. Graphene: status and prospects. Science 324(2009)1530-1534.

[112] Y. Zhang, Y.W.Tan, H.L.Stormer, P.Kim. Experimental observation of the quantum hall effect and Berry's phase in graphene. Nature, 438 (2005)201–204.

[113] K.S.Novoselov, E. McCann, S.V. Morozov, V.I. Falko,M.I Katsnelson, U. Zeitler, D.Jiang, F.Schedin, A.K.Geim. Unconventional quantum hall effect and Berry's phase of 2pi in bilayer graphene. Nat. Phys. 2(2006) 177–180.

[114] K.S.Novoselov,A.K. Geim, S.V.Morozov, D.Jiang,M.I. Katsnelson,I.V.Grigorieva, S.V.Dubonos,A.A. Firsov Two dimensional gas of massless Dirac fermion in graphene. Nature, 438(2005)197–200.

[115] S.Y. Zhou, G.H. Gweon, J. Graf, A.V.Fedorov. First direct observation of Dirac fermions in graphite. Nat. Phys. 2(2006)595–599.

[116] S. Chen, Q.Wu, C.Mishra. New graphene-related materials on the horizon. Nat. Mater., 11 (2012) 203–207.

[117] R.R.Nair.; P.Blake, A.N.Grigorenko. Fine structure constant defines visual transparency of graphene. Science, 320(2008) 1308.

[118] A.R Oganov, R.J. Hemley, R.M.Hazen. Structure, bonding and mineralogy of carbon at extreme conditions. Rev. Mineral. Geochem. 75(2013) 47–77.

[119] I. A. Ovid'Ko. Mechanical properties of graphene. Rev.Adv. Mater. Sci. 34 (2013) 1-11.

[120] C. Lee,X. Wei, J.W. Kysar, J. Hone. Measurement of the Elastic Properties and Intrinsic Strength of Monolayer Graphene. Science, 321(2008)385-388.

[121] T. K.Das and S.Prusty. Recent advances in applications of graphene. Int. J. Chem. Sc. Appl., 4(2013)39-55.

[122] Y.Zhu , S. Murali , W.Cai , X.Li , J. W. Suk , J. R. Potts , And R. S. Ruoff. Graphene and graphene oxide: synthesis, properties, and applications. Adv. Mater. 2010, XX, 1–19.

[123] K. S. Novoselov , A. K. Geim , S. V. Morozov , D. Jiang , M. I. Katsnelson ,I. V. Grigorieva , S. V. Dubonos , A. A. Firsov ,Two-dimensional gas of massless Dirac fermions in graphene. Nature 438(2005) 197-200.

[124] Y. Zhang, Y .W. Tan, H. L. Stormer, and P.Kim. Experimental observation of quantum hall effect and berry's phase in graphene. Nature, 438 (2005)201-204.

[125] G. Jo, M. Choe, C.Y. Cho, J. H. Kim,W. Park, S. Lee,W.K. Hong,T.W.Kim, S.J. Park, B.H. Hong,Y. H. Kahng, and T. Lee. Large-scale patterned multi-layer graphene films as transparent conducting electrodes for GaN light-emitting diodes. Nanotechnology, 21 (2010) 175201-6.

[126] P. Blake, P.D. Brimicombe, R. R. Nair, T.J. Booth, D.Jiang, F. Schedin, L. A. Ponomarenko, S. V. Morozov, H.F. Gleesn, E.W. Hill, A. K. Geim, K.S. Novoselov. Graphene-based liquid crystal device. Nano Lett., 8 (2008)1704–1708.

[127] J.Wu, M.Agrawal, H.A. Becerril, Z.Bao,Z.Liu, Y. Chen, and P.Peumans. Organic Light-Emitting Diodes on Solution-Processed Graphene Transparent Electrodes. ACS Nano, 4(2010)43–48.

[128] T.H.Han, Y. Lee, M.R.Choi, S.H.Woo,S.H. Bae,B. H.Hong, J.H. Ahn & T.W.Lee. Extremely efficient flexible organic light-emitting diodes with modified graphene anode. Nature Photonics, 6(2012)105-110.

[129] Q.Liu,Z. Liu, X.Zhang,N. Zhang,L.Yang,S. Yin,and Y.Chen. Organic photovoltaic cells based on an acceptor of soluble graphene. Appl. Phys. Lett., 92(2008)223303-3.

[130] Z. Liu, Q. Liu, Y.Huang, Y. Ma, S. Yin, X.Zhang, W.Sun, and Y. Chen. Organic photovoltaic devices based on a novel acceptor material: Graphene. Adv. Mater. 20(2008) 3924–3930.

[131] K.S Novoselov, D. Jiang, F. Schedin, T. J.Booth, V. V. Khotkevich, S. V. Morozov and A.K. Geim, Two-dimensional atomic crystal. Proc. Natl. Acad. Sci. USA. 102(2005)10451-10453.

[132] L. DiCarlo, J. R. Williams, Y.Zhang,D. T. McClure, and C. M. Marcus. Shot noise in graphene. Phys. Rev. Lett. 100 (2008) 156801.

[133] L. H .Tang, Y. Wang, Y. M. Li, H. B. Feng, J.Lu and J. H. Li. Preparation, structure and electrochemical properties of reduced graphene sheet films. Adv. Funct. Mater. 19(2009) 2782-2789.

[134] W.K. Lee, M. Haydell, J.T. Robinson, A.R. Laracuente, E.Cimpoiasu, W. P. King, and P. E. Sheehan. Nanoscale reduction of graphene fluoride via thermochemical nanolithography. ACS Nano, 7 (2013) 6219–6224.

[135] N. L. Rangel,A. Gimenez,A. Sinitskii,and J. M. Seminario. Graphene Signal Mixer for Sensing Applications. J. Phys. Chem. C, 115(2011) 12128–12134.

[136] A. Tamburrano, F. Sarasini, G .De Bellis, A. G. D'Aloia, and M. S. Sarto. The piezoresistive effect in graphene based polymeric composites. Nanotechnology 24 (2013) 465702-10.

[137] N.L. Rangel and J. M. Seminario. Graphene terahertz generators for molecular circuits and sensors. J. Phys. Chem. A, 112(2008) 13699–13705.

[138] Y. Shao,J. Wang,H. Wu, J. Liu, I. A. Aksay,Y.Lin. Graphene based electrochemical sensors and biosensors: a review. Electroanalysis, 22(2010) 1027 – 1036.

[139] L. G. De Arco, Y. Zhang, C. W. Schlenke, K. Ryu, M.E. Thompson,and C. Zhou. Continuous, Highly Flexible, and Transparent Graphene Films by Chemical Vapor Deposition for Organic Photovoltaics. ACSnano., 4(2010)2865-2873.

[140] Y. Zheng, Y. Jiao, L. Ge, M. Jaroniec, and S. Z. Qiao. Two-step boron and nitrogen doping in graphene for enhanced synergistic catalysis. Angew. Chem., 125(2013) 3192 –3198.

[141] L. Qu, Y.Liu, J.B. Baek, and L. Dai. Nitrogen-doped graphene as efficient metal-free electrocatalyst for oxygen reduction in fuel cells. Acs nano, 4(2010)1321-1326.

[142] X. Huang, Z. Zeng, Z. Fan, J. Liu, H. Zhang. Graphene-based electrodes. Adv. Mater. 24(2012)5979–6004.

[143] H. Wang, L.F.Cui , Y. Yang , H.S. Casalongue , J. T. Robinson , Y. Liang, Y. Cui and Hongjie Dai. Mn3O4−graphene hybrid as a high-capacity

anode material for lithium ion batteries. J. Am. Chem. Soc., 132(2010)13978–13980.

[144] M. Liang and L. Zhi. Graphene-based electrode materials for rechargeable lithium batteries. J. Mater. Chem., 19(2009)5871-5878.

[145] I. D. Mery Stoller, S. Park, Y. Zhu, J. An, and R. S. Ruoff. Graphene-based ultracapacitors. Nano Lett., 8 (2008)3498-3502.

[146] Y. Wang, Z. Shi, Y.Huang, Y. Ma, C. Wang, M. Chen, and Y. Chen. Supercapacitor devices based on graphene materials. J. Phys. Chem. C, 113(2009)13103–13107.

[147] W. Zhu, I. D. Rukhlenko, and M.Premaratne. Graphene metamaterial for optical reflection modulation. Appl. Phys. Lett. 102(2013) 241914-4.

[148] R. Alaee, M. Farhat, C. Rockstuhl, and F.Lederer. A perfect absorber made of a graphenemicro-ribbon metamaterial. Opt. Exp., 20(2012)28018-28024.

[149] S. He,and T. Chen. Broadband THz Absorbers with Graphene-Based Anisotropic Metamaterial Films. IEEE transactions on terahertz science and technology, 3(2013) 757-763.

[150] R. Ning, S. Liu, H. Zhang, B. Bian, and X. Kong. A wide-angle broadband absorber in graphene-based hyperbolic metamaterials. Eur. Phys. J. Appl. Phys. 68 (2014) 20401-20407.

[151] Q. Zhang,Q. Ma,S.Yan,F. Wu,X.He , J. Jiang. Tunable terahertz absorption in graphene-based metamaterial. Opt. Commun., 353 (2015)70–7572.

[152] A. Andryieuski, and A. V. Lavrinenko. Graphene metamaterials based tunable terahertz absorber: effective surface Conductivity approach. Opt. Exp., 21 (2013)9144-9155.

[153] Y. Zhang, Y. Feng, B. Zhu, J. Zhao, and T. Jiang. Graphene based tunable metamaterial absorber and polarization modulation in terahertz frequency. Opt. Exp., 22(2014) 22743-22752

[154] H.A. K. Othman, C. Guclu, and F. Capolino. Graphene-based tunable hyperbolic metamaterials and enhanced near-field Absorption. Opt. Exp., 21(2013) 7614-7632.

[155] G. W. Hanson. Dyadic Greens functions and guided surface waves on graphene. J. Appl. Phys. 103(2006)064302-064320.

[156] M. Idrio,S.Boscolo,M. Moresco,M. Romagnoli,C. De Angelis,A. Locatelli,and A. D. Capobianco. Graphene assisted critically coupled optical ring modulator. Opt. Exp., 20(2012) 23144-23155.

[157] A. Vakil, and N. Engheta. Transformation optics using graphene. Science, 32(2011)1291–1294.